A SOIL - VEGETATION - ATMOSPHERE MODEL FOR MICROCLIMATOLOGICAL RESEARCH IN ARID REGIONS

by

MICHEL M. VERSTRAETE

Lic. Physique, Université Catholique de Louvain (1974)
Lic. Sp. Géophysique, Université Libre de Bruxelles (1976)
M. Sc. Meteorology, Massachusetts Institute of Technology (1978)

Submitted to the Department of Earth, Atmosphere and
Planetary Sciences in partial fulfillment of the
requirements for the degree of

Doctor of Science

at the

MASSACHUSETTS INSTITUTE OF TECHNOLOGY

February 1985

Signature of the Author _____
Department of Earth, Atmosphere and Planetary Sciences

Certified by _____
Reginald E. Newell
Thesis Supervisor

Certified by _____
Robert E. Dickinson
Thesis Supervisor

Accepted by _____
Theodore R. Madden
Chairman, Departmental Committee on Graduate Students

A SOIL - VEGETATION - ATMOSPHERE MODEL FOR MICROCLIMATOLOGICAL RESEARCH IN ARID REGIONS

by Michel M. Verstraete

Submitted to the Department of Earth, Atmosphere and
Planetary Sciences in February 1985, in partial
fulfillment of the requirements for the degree of
Doctor of Science

ABSTRACT

A multi-layer one-dimensional vertical model of the upper soil, vegetation and lower atmosphere is developed and implemented. This model includes explicit representations of the heat and moisture diffusion both in the soil and in the atmosphere, and computations of various mass and energy fluxes at the soil-air, vegetation-air and soil-root interfaces.

Four models are run in parallel to compute the fluxes and profiles both under clear and cloudy skies, and over bare and vegetated soil, with otherwise similar forcing. Under specific scaling conditions, environmental profiles are derived from a weighted average of these submodels, where the weights depend on the assumed cloud and vegetation covers. The model is specially designed to describe dry ecosystems where the vegetation cover is discontinuous.

The vegetation component includes explicit parameterizations of the canopy (to intercept both radiation and precipitation), of a root system (able to pump soil water) and of the stomates (to control the transpiration rate). No biochemistry or photosynthesis is included in the current version.

The sensitivity of the model to various parameters is assessed. The surface water and energy fluxes, and the profiles of temperature and specific humidity in the four submodels are compared. This model is currently better suited as a theoretical research tool for sensitivity analyses than for applied research on a specific crop, plant species or environment.

Thesis Supervisors: Robert E. Dickinson (NCAR) and Reginald E. Newell (MIT)

ACKNOWLEDGMENTS

A few sentences cannot properly express my feelings towards the many people who helped me one way or another during the two and a half years this project took to complete. I have tried to thank everybody individually as appropriate, and the following is only for the record.

I would like to thank first Professor R. E. Newell, who guided me while I was in residence at MIT. I have benefited from his exceptional ability to generate new ideas and research topics, as well as from his unconditional support and encouragment to progress in my research interests. Professors P. S. Eagleson and K. A. Emanuel provided me with valuable comments on the various drafts of this Thesis.

I feel very fortunate to have had the opportunity to work with Dr. R. E. Dickinson, who was my principal advisor at NCAR. His mastering of the subject matters and knowledge of the literature, his availability to answer questions, and his remarks and suggestions on my work allowed me to progress quickly. I am very grateful to him for introducing me to this field of research, and for helping me improve the model significantly. I also want to thank Professor D. M. Gates for his many suggestions on the final draft and his genuine interest in this work.

This Thesis was accomplished at the National Center for Atmospheric Research†, in the Advanced Study Program, thanks to Drs. S. H. Schneider and M. H. Glantz who invited me to apply for a Research Assistantship. I have been most privileged to participate in this Program, which provided me with a unique opportunity to work with leading researchers in a very stimulating atmosphere.

† The National Center for Atmospheric Research is operated by the University Corporation for Atmospheric Research and sponsored by the National Science Foundation

It is a pleasure to acknowledge the support and encouragements of many graduate students and post-doctoral fellows of ASP. Drs. N. Dalfes, P. Rasch and S. Thompson, have been particularly helpful to me. I also benefited from occasional help from Drs. V. Ramaswamy and J. Kiehl. Finally, I whould like to thank the administrative staff of ASP for their very efficient support.

I am also very much indebted to another friend and ASP colleague, J.-P. van Ypersele, who helped me in many ways during the last year. His many comments on the draft thesis have been useful in preparing the final version, and his dedicated support, especially during the last phase of this project, is greatly appreciated.

Mrs. M. Krenz revised the entire manuscript in her spare time, and I am very grateful to her for improving the quality of the text, not only by suggesting many modifications, but also by pointing out passages that needed clarification.

Last but not least, there are many other people who made the whole exercise possible by providing the support and encouragements that are often necessary. My wife and children have had much more patience and understanding than could reasonably be expected, and I want to give them a very special *thank you* for accepting the burden of this endeavor.

TABLE OF CONTENTS

PART 2 SENSITIVITY ANALYSES AND MODEL RESULTS

Chapter 1: Introduction

1.1 Background discussion

There is a currently growing interest in the vegetation cover as it interacts with and modifies the environment, especially the atmosphere. This section outlines some of these new developments, and thereby provides the justification for this work.

A number of major environmental issues have been raised over the last two decades. One of them is the problem of desertification, often viewed as a progressive intensification of arid conditions or as an advance of deserts into regions that were not desert-like before.

The nature of the problem and the actual reasons why desertification occurs appear to be very controversial (Verstraete, 1983). The most extreme positions view this phenomenon as either a large-scale and long-term aridification of climate, accompanied by geophysical processes of wind and water erosion (e.g. El-Baz, 1983), or as the result of human activities in the regions concerned, such as overgrazing, wood cutting, agricultural mismanagement, etc. (e.g. United Nations, 1977). A number of authors recognize the importance of both climatic conditions and human influence, but, unable to quantify the environmental effects, presume that human pressure on the land must be the major cause of desertification. This debate is not academic because of its implications in terms of responsibilities and opportunities for action; indeed, desertification is always consid-

ered a harmful process, since it entails a loss or degradation of natural reusable (but not necessarily renewable) resources, whether soils or vegetation.

There is a large body of literature on the issue of desertification, but little evidence on the actual causes of the problem (Warren et al., 1977), often because a number of suspected causal factors are present simultaneously. Nevertheless, there is a general consensus on the central role of the vegetation cover in preserving dry ecosystems from further aridification: overgrazing, wood cutting and other practices that result in partial or complete disappearance of the canopy, especially during drought periods, seem to be associated with one form or another of environmental degradation.

Some experiments have been conducted, but mostly (and understandably) to try to remedy the situation: e.g. reforestation, setting up exclosures, fallowing, etc... While these activities can provide useful information on the recovery from desertification, they do not necessarily clarify the causal factors. Furthermore, since human populations are always involved, there are rather severe limitations on the kind of experimentation that can or should be done. A computer model that would adequately represent an ecosystem would therefore provide an interesting research tool, since it is safe and relatively cheap, compared to the cost of installing and maintaining experimental plots and observation stations.

Major advances have been made over the last few decades in understanding the behavior of the general circulation of the atmosphere as a fluid subjected to differential heating and in motion around a rotating planet. These theoretical advances eventually led to the development of weather prediction by numerical means. This approach currently permits reasonably accurate forecasting at up to a couple of days in advance. The progressive loss of accuracy at longer time scales is thought to be due to one or more of the following factors: inherent limits to the predictability of the system, insufficient accuracy of the initial conditions, or inadequate representation of the ocean-atmosphere interactions, of the cloudiness, precipitation and other sub-grid scale phenomena, or of surface processes.

Since about 70% of the land areas are covered by some form of vegetation, and since a plant canopy has very specific radiative, dynamic and thermodynamic properties, it is expected that such a cover should influence considerably on the weather and climate of this planet. Accordingly, there have been a few attempts recently to incorporate better surface representations (including vegetation) in General Circulation Models (GCMs). Mesoscale models would also benefit from more realistic lower boundaries, but none of these large scale models can afford to include detailed plant models because the computational costs would be prohibitive. There is therefore a need to develop detailed and comprehensive small-scale models that could be used to derive simpler and more appropriate parameterizations for the larger models.

Finally, technological and scientific developments of the last two decades have resulted in the launching of a large number of satellites, many of which are equipped with active or passive sensors looking down at the surface of the Earth. The interpretation of the signals received from such satellites is complex, as they depend often crucially on the radiative properties of the surface. The latter, in turn, depend not only on the nature and structure of the vegetation cover, but also on the type, humidity and temperature of the underlying soil, as well as the physical and chemical properties of the atmosphere. A detailed soil-vegetation-atmosphere model could therefore provide much needed information for the proper analysis of satellite data.

These are but three examples of quite independent fields of research that could benefit from detailed models of the soil-vegetation-atmosphere continuum. This modeling approach is particularly appropriate to study physical interactions, since the models can then be based on well known mathematical and physical laws. Such models are also a very flexible research tool since they can be used to formulate hypotheses and conditions that cannot or should not be attempted in reality.

The work described in this Thesis is a step in that direction: the goal is to provide a comprehensive model from which less sophisticated but also less expensive models could

be derived. At a later stage, this detailed model should be fully validated and become a benchmark for evaluating simpler models, or for studying a particular environment. In the meantime, it should be used only to investigate the sensitivity of the model environment to prescribed perturbations, and to thereby identify the most relevant processes to be included in simpler models.

1.2 Overview

This Thesis describes the design and implementation of a multi-layer, one-dimensional vertical model of the upper soil, vegetation and lower atmosphere. Its vertical extent typically varies from 0.5 to 5 meters below the soil surface, and from 3 to 10 meters above it. The vertical resolution is 1 to 20 cm, and the model is integrated in time over periods of a few hours to a few days, with time steps from a fraction of a minute to a fraction of an hour.

Because this model should (at a later stage) be appropriate to study the issue of desertification, it must be able to deal explicitly with discontinuous vegetation covers. Furthermore, the large radiative effects of a broken cloud cover on the surface fluxes of heat and moisture suggested the consideration of four separate cases: bare ground under clear sky, complete canopy cover under clear sky, bare ground under cloudy sky and complete canopy cover under cloudy sky. The model therefore consists of four separate *submodels*, all running in parallel. Each one of these is subjected to the same external forcing (described below).

Each of these submodels is represented by a set of differential equations which are discretized in both space and time. The resulting finite difference equations are then integrated to yield the time evolution of the system, given initial and boundary conditions. By analogy with the terminology of Energy Balance Models (EBMs), this model could

be considered to be of dimension 1.5 (e.g. Schneider and Dickinson, 1974). Strictly speaking, a one-dimensional vertical model does not have any horizontal resolution: the "half" dimension refers to the four submodels included in this model to represent different horizontal situations simultaneously.

The relative effect of a cloud or vegetation cover on the surface fluxes of water or energy, or on the profiles of temperature and humidity in the environment, can therefore begin to be assessed by comparing the results of these submodels. Furthermore, to the extent that the fluxes and profiles in these four submodels are independent (i.e. that advection has had less influence on the characteristics of the air than the surface itself), the surface heat and moisture fluxes, as well as the profiles of specific humidity and air temperature for the whole environment, where these four conditions co-exist, can be computed as weighted averages of the fluxes and profiles of these four submodels. Since these environmental profiles are then explicitly dependent on the cloud and vegetation covers, the influence of imposed variations of the latter, representing the effect of drought or overgrazing situations, can be studied.

This averaging procedure implies the statistical independence of the four submodels, and this, in turn, is valid only for certain space scales. At the continental scale, there is an obvious correlation between the average location of the cloud and vegetation bands. At the other extreme, it is clear that the characteristics of the atmosphere above an isolated bush are the same as those above the adjacent bare ground. The averaging scheme suggested here is therefore appropriate for *patches* of vegetation or bare ground that are large enough that the advection effects in the transition zones are small compared to the local processes in each submodel. Typical horizontal dimensions of 1 to 10 kilometers are probably reasonable. (Remember that only the first few meters of the atmosphere are considered here.) Munn (1966, p. 107 ff.) reviews briefly the problem of finding the fetch or distance in the field after which the air flow has adjusted to new surface conditions.

For mechanical perturbations to the air flow, the fetch is found to be 50 to 100 times the height of the obstacle.

The role of the various physical and biological processes included in this model is to transport vertically water and energy between the atmosphere, the vegetation and the soil. Both liquid water and water vapor are present (no snow or ice), and energy can take the form of radiation, latent or sensible heat.

The amount of solar radiation available at the top of the atmosphere is computed from the location and time of year. This radiation then interacts with a partly cloudy atmosphere. The latter is not explicitly modeled, but the model computes the net downward solar radiation arriving at the surface, based on prescribed cloud and atmospheric characteristics, for each of the four submodels described above. This radiation is reflected and absorbed by the surface and/or the canopy, and provides a major heating term for the system.

The surface water and energy balance equations are then used to compute the humidity and temperature of the top soil layer, which, in turn, are used as boundary conditions for the diffusion equations for heat and moisture into the ground. The surface fluxes of heat and moisture are also used to determine the profiles of specific humidity and temperature in the atmosphere.

The vegetation canopy alters significantly the transfers of water and energy in the environment. The canopy intercepts visible and infrared radiation, and these processes depend, among other things, on the nature and structure of the canopy, and the size and orientation of the leaves. Plants also intercept precipitation; in doing so, they reduce the precipitation rate on the soil surface, and allow water to be stored on the leaves. This reduces the transpiration rate since some of the stomates are now covered with free water, but increases evaporation. The actual rate of transpiration may be controlled by the ability of the root system to pick up water in the soil, a process which depends on the

characteristics of the root system, on the soil type, and on the availability of water in the soil. The latter is of course influenced by the water balance at the surface.

A typical run of this model simulates a diurnal cycle. By comparing the results from the four submodels, one can get an idea of the role and influence of a complete canopy or cloud cover on the micro-climate, and by comparing different runs, one can assess the sensitivity of this micro-climate to changes in the canopy and cloud covers, to differences in soil composition, etc.

1.3 Original contributions

A number of atmospheric scientists have devoted their professional life to the study of micro-climatology, and many of their contributions are used in this work. The vast majority of these works, however, apply to bare ground, or horizontally uniform surfaces (such as infinite crop fields or forests). Micro-meteorologists are often concerned with the estimation of the fluxes of heat and moisture at the surface, either to describe the local climate itself, or to specify the surface forcing of the atmospheric general circulation. When they are concerned with the detailed biological processes responsible for these fluxes, it is almost always in connection to a particular crop or plant species of economic importance.

Similarly, numerous agronomists have developed crop models to predict the yield of specific cereals or other agricultural products. While they also assume horizontal uniformity, such models are usually fine tuned to specific plant species or agricultural regions. Some agro-meteorological models have been developed to investigate the micro-climate in the crop canopy, but these often avoid the complications associated with a discontinuous canopy cover, or the soil and atmospheric processes outside the canopy.

The diffusion of heat and moisture in the soil has been the subject of intense research over the last fifty years, but has rarely been incorporated into larger models that also try to represent plant and atmospheric processes with comparable detail.

The design of this model presents the following original aspects:

1. First of all, it provides an unusual degree of detail about and integration between physical and biological processes in the lower atmosphere, the vegetation (both the canopy and the root zone) and the soil.
2. The model actually contains four submodels that are integrated in time simultaneously, each representing a different combination of vegetation and cloud cover.
3. The model addresses directly the complex problem of estimating the actual fluxes and profiles in the environment in the case of a non-continuous cover, both in the vegetation canopy and in cloudiness, at least within certain space scales.
4. Each submodel contains multiple layers, both in the vegetation canopy, the root system, the atmosphere, and the soil.
5. Although the usual logarithmic wind profile has been used, a scheme has been derived for computing the roughness length as a function of the "thickness" of the canopy. In particular, the roughness length presents a unimodal distribution, which peaks for specific values of the leaf area index and wind speed, as has been observed.
6. The model includes a number of physical and physiological processes relative to the plant cover, and the parameterizations are general and flexible enough to be able to represent any vegetation, from grass to trees.
7. A new and relatively simple scheme has been developed to compute the exchanges of infrared radiation between the various leaf layers in the canopy, as well as to compute the net infrared radiation at the soil surface under the canopy, or at the top of the canopy. This scheme is based only on the fluxes emitted by each leaf layer and the geometry of their overlap.
8. The vegetation canopy is allowed to intercept radiation, and the temperature of the leaves in each layer is computed from an energy balance equation that accounts for radiation absorption and exchanges of heat with the atmosphere.

9. Similarly, the canopy intercepts precipitation and the model keeps track of a separate water budget equation for each leaf layer. Furthermore, transpiration is only allowed from those parts of the leaves not covered by rain water, and is subject to the availability of water picked up by the roots in the soil.

Although there have been recent efforts to integrate two or more of the soil, vegetation, and atmospheric components into single models (e.g. Sellers and Lockwood, 1981a, b; Federer, 1979, 1982), the present model represents a step forward in complexity and integration. This increase in complexity of theoretical investigations is made at a cost: Federer wrote (1979, p. 555)

> "[Simulation models] divide either the root zone of the soil or the canopy-atmosphere zone into several layers. Layered canopy models assume either that the soil is continuously wet or that it dries uniformly with depth. Layered soil models assume that the canopy-atmosphere interaction can be represented either by the Penman-Monteith combination equation or by a single leaf-air humidity gradient. Combined layered canopy and layered soil models do not seem to exist, perhaps because they require too many unmeasurable parameters."

These comments are still applicable, and the model described in this work is therefore mainly useful for sensitivity analyses, rather than for modeling concrete situations. This drawback will exist for all such theoretical investigations, until new and better measurements are made on a routine basis. In the meantime, this detailed model could be used to try to identify the most important parameters for which measurements are needed.

PART 1: DESCRIPTION OF THE MODEL COMPONENTS

This first part describes the various equations that constitute the model. Chapter 2 provides a general discussion of the model and its major components. Chapter 3 describes the computation of the incoming solar radiation at the top of this micro-meteorological model while Chapter 4 shows how this radiation interacts with the soil and vegetation. It also covers the exchanges of infrared radiation between the soil surface, the vegetation and the lower atmosphere. The derivation of the wind profiles is covered in Chapter 5, and Chapter 6 describes the water and energy balance equations used to derive the temperature and humidity of the top soil layer. Chapter 7 shows how the specific humidity and temperature profiles are computed in the lower atmosphere, and Chapter 8 does the same thing for heat and moisture diffusion in the soil. The second part of the dissertation presents the results of runs made under different initial or boundary conditions, and discusses the sensitivity of the model to these conditions and to variations in some of the forced variables.

In any large and complex model such as the one described in this work, all the parts are integrated and depend on each other. On the other hand, since the written description is necessarily linear, it is occasionally necessary to refer the reader to a later chapter or section, because the needed information fits better in another context. To the extent possible, however, I have tried to follow a logical progression in the order of presentation, from topics that stand alone to those that are best approached after the rest of the model has been described.

Chapter 2: Generalities

The first three Sections of this Chapter provide some general information on the main components and assumptions of the model, namely the atmosphere, the vegetation canopy and the soil. Section 4 covers some additional major hypotheses included in the design of the model, and Section 5 describes the input (forcing) and output (results) of the model.

As was stated in the previous Chapter, the model really consists of four *submodels*, each with a different combination of vegetation and cloudiness cover. Each of these submodels, however, covers both the soil, the vegetation (if appropriate) and the atmosphere; these are called model *components*. (See Figure 2.1 below).

2.1 Atmosphere

This multi-layer model covers explicitly only the lowest few meters of the atmosphere, a region Brutsaert (1982, p. 54) calls the dynamic sublayer. In this layer, the profiles of atmospheric pressure, specific humidity, temperature and wind are computed at each grid point. The wind speed at any level depends on the imposed wind speed at the top of the model, and on the roughness of the surface, itself a function of the vegetation. The profiles of temperature and specific humidity are computed from the surface fluxes of water vapor and sensible heat, accounting for the sources and sinks of water vapor and heat in the canopy. No attempt has been made to model the bulk of the atmospheric boundary layer.

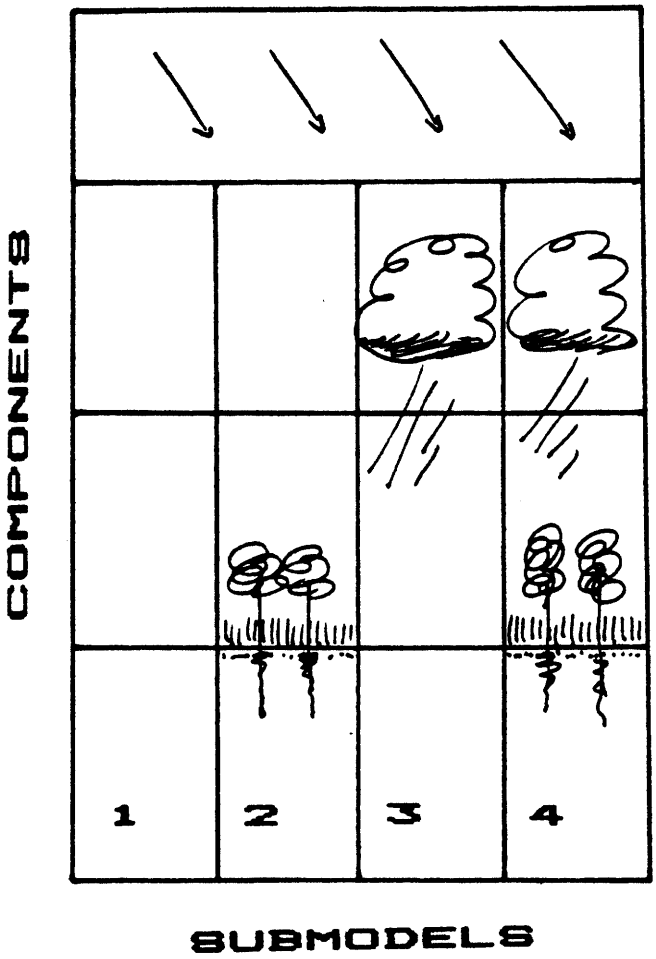

Figure 2.1 Model components and submodels.

Clearly, the radiation, water and heat balances at the surface require information on processes that occur above the dynamic sublayer. Many of these are not included in the current version of this model, and could conceivably be provided by a larger scale model in which this one could be embedded. Alternatively, the vertical extent of the current model could be increased to cover the whole boundary layer. (The effect of atmospheric stability on the fluxes and profiles should then be included.) This would certainly improve the ability of the model to duplicate actual conditions, but may also require the inclusion of other processes, such as the radiative flux divergence or the thermodynamics of water phase changes. For the purpose of this Thesis, I have concentrated on the physical processes

very close to the surface, particularly in the vegetation canopy, rather than on the better known atmospheric processes.

The solar radiation outside the atmosphere is computed directly from latitude and time. The flux densities of solar radiation (both visible and near-infrared) at the top of this model are computed as a function of ozone, water vapor, and cloudiness. Specific assumptions are made concerning the vertical profiles of these atmospheric constituents, since they lie outside the multi-layer model itself. No further absorption of radiation takes place in the model atmosphere, that is, between the top of the model and the soil surface.

The atmosphere interacts with the soil surface and the vegetation by exchanging water vapor and heat, and these exchanges are computed from balance equations. Precipitation is allowed to occur, but since it originates above the top of the model, the rate of precipitation is prescribed rather than computed or predicted. The role of CO_2 variations is not explicitly included because both the radiation and physiological schemes of the model should be more complex to take it into consideration. The effect of atmospheric stability is not taken into account, mostly because it is negligible in the first few meters of the atmosphere.

2.2 Vegetation

A plant is a complex system in itself, so that the representation of vegetation in any soil-vegetation-atmosphere model has to be simplified. An effort has been made to incorporate in the model the major physical and physiological processes that affect the flow of water and energy in the environment. No attempt has been made to include the numerous chemical and bio-chemical cycles that take place in these plants.

The first task is to describe the vegetation from the geometrical point of view. As mentioned before, I assume a discontinuous canopy cover and call *patch of vegetation*, or

simply *patch*, a volume of vegetation separated from all others by bare ground. Such a patch is characterized by two linear dimensions: an horizontal radius r_v and a vertical height h_v, both in m.

The actual shape of the patches is irrelevant to this discussion, only the two characteristic dimensions, r_v and h_v, are used. It is also assumed that all patches have the same characteristic dimensions, which can be selected as the mean radius and mean height of the actual vegetation patches in the environment.

A third parameter is then introduced, namely the number, N_v, of such patches of vegetation per unit surface (e.g. 100 square kilometers). The radius r_v, the height h_v and the number N_v of vegetation patches are specified by the user, and may include a seasonal cycle. The fractional vegetation cover is then computed from N_v and r_v as follows:

$$V = (N_v \pi r_v^2)/10^8.$$

Obviously, N_v and r_v must be chosen so that V never exceeds 1.0.

One very important geometrical characteristic of the vegetation is the *Leaf Area Density*, often denoted LAD. It is the total area of one side of all leaves per unit bulk volume (air and vegetation). This parameter is expressed in $m^2\,m^{-3}$, and in a way represents a "density" of leaves. This function can be integrated vertically to yield

$$L(z) = \int_z^{h_v} LAD(z)dz, \tag{2.1}$$

where $L(z)$ represents the amount of leaf area above level z per unit area of ground surface. Obviously, $L(z > h_v) = 0.0$. When the integration is taken over the whole depth of the canopy, one obtains the better known *Leaf Area Index*, abbreviated *LAI*:

$$LAI = L(z = 0). \tag{2.2}$$

The Leaf Area Index (*LAI*) is therefore the total area of one side of all leaves per unit surface of ground. It is usually expressed in $m^2\,m^{-2}$, meaning m^2 of leaf material per m^2

of soil surface. The *LAI* is variable from one type of vegetation to another and also from one season to the next, as can be seen from Table 2.1.

Table 2.1: Typical Leaf Area Indexes for various vegetation types and seasons

Vegetation type	LAI_{Max}	LAI_{Min}
Arable / mixed farming	6	0.5
Grazing land	2	0.5
Coniferous forest	6	5
Mixed deciduous / coniferous forest	6	3
Deciduous forest	6	1
Equatorial forest	6	0.5
Tropical woodland/grassland	6	0.5
Desert / no vegetation	6	0.5
Tundra or high altitude	6	0.5
Rice / irrigated land	6	0.5

Source: Dickinson et al. (1981, p. 46).

In this context, a "leaf" is any part of the plant able to interact with the environment: no formal distinction is made between a leaf area index and a stem area index. In arid regions, however, a significant part of the plant may be dry or dead, especially during the dry season. To account for this, the fraction of the total leaf area that is actually green (i.e. transpiring) can be specified for each leaf layer. All model plant processes (such as radiation and precipitation interception) depend on the *LAI*, except that the transpiration computations are based on this reduced or "green *LAI*."

The next task is to describe the vegetation in morphological terms. Plants are made of leaves, stems, branches and roots. For the purpose of this model, these elements are incorporated only insofar as they affect the flow of water or energy in the ecosystem. As a result, the only role of stems and branches is to allow water to circulate from the root system to the leaves, and not much code is actually devoted to these elements. In contrast, leaves are modeled in much greater detail, as will be seen below.

From a morphological point of view, leaves are assumed to have an average area and a typical linear dimension. Their thickness, together with the transpiring ("green") fraction

of the *LAI*, is used to compute the mass of biological material that is of importance in heat exchanges. (The specific heat of dry or dead tissues is smaller than that of water, so that heat storage can occur only in the wet parts of the plant, which are also assumed to have the same heat capacity as water.) The interaction between the radiation field and the canopy also depends on the structure of the canopy, and the orientation of the leaves. The latter is assumed to be random, but input parameters to the model allow some flexibility in specifying the type of canopy.

In addition to areal parts, a plant must also have a root system to acquire in the soil the water needed for transpiration. Roots are characterized by the vertical distribution of their length density and average radius. These characteristics, together with those of the soil (including the volumetric soil water content) determine the rate at which the plants can extract water from the various soil layers. This water is transported upward in the plant under the action of a water potential gradient, which ultimately forces the water to exit the plants through the stomates. (The water potential depends on its chemical potential, i.e. on how the Gibbs free energy of the system changes as water is added or removed while all other parameters and constituents remain constant (Jones, 1983, p. 64 ff.). A water potential may be defined in the atmosphere also, and it is usually much lower than the water potential in the soil.)

Since a plant is a living organism, it can also be described in physiological terms. In particular, each plant regulates the rate of transpiration from its leaves by controlling the stomatal aperture. Stomates are little openings at the surface of leaves in which most of the water and CO_2 exchanges take place. In this model, the resistance offered by the stomates to the flow of water depends on the plant species, solar radiation, temperature, humidity of the air and water potential in the leaves. The stomatal resistance is also adjusted to reduce transpiration if the roots have difficulty extracting water from the soil.

Some other leaf characteristics will be needed later on: for example, the interception of radiation by the canopy depends on the leaf single scattering coefficient, and on whether

the plants have small vertical or large horizontal leaves. The parameters needed for such specific purposes will be introduced as and when appropriate.

There is no explicit chemistry or bio-chemistry in this model: photosynthesis is not included, although a fraction of the solar radiation absorbed in the canopy does not enter the leaf energy balance used for computing the leaf temperature (since this energy is stored in chemical bonds.) Similarly, there is no attempt to track the flow of CO_2 in this model. Consequently, the model currently does not attempt to predict growth (increase in total biomass) or development (succession of stages from seeds to flowering) of plants as a result of soil and atmospheric conditions.

2.3 Soil

The next component of this model is a multi-layer soil model. A soil layer is represented by a grid point, located inside the layer. All computations are relative to that location. The vertical distribution of these grid points is arbitrary; they can be equally spaced or distributed in such a way as to provide a greater density near the surface. Of course, the selection of a time step for the integration must be made in accordance with the selected spatial distances between grid points: the closer the latter, the shorter the time step.

A soil type can be assigned to each soil layer. This soil type can be selected among a set of 11 possible soils, from sand to clay. The soil type itself determines the following soil characteristics: the soil density, in $kg\,m^{-3}$, the relative content of the soil in quartz and clay material, the saturated soil water content, in $m^3\,m^{-3}$, and the saturated soil matric potential, in m. (The matric potential is a negative pressure potential resulting from the capillary and adsorptive forces due to the soil matrix (Hillel, 1982, p. 69). For all practical purposes, water moves in the soil under the combined influence of the gravitational potential and of this matric potential.)

The soil type also specifies a parameter that enters the computation of the moisture characteristic (the relation between the soil moisture content and the matric potential), and the dependency on the soil water content of the soil hydraulic diffusivity and conductivity. The latter imposes a constraint on the maximum evaporation rate that the soil can support. The soil type also affects directly the soil heat capacity, diffusivity and conductivity, and the rate at which the roots of the plants can extract water from the soil.

2.4 Design hypotheses and limitations

Some additional fundamental assumptions have been made at the outset, and these are described here, together with the limitations they impose on the results or applicability of the model:

1. Although all real systems occur in a three-dimensional world, a one-dimensional vertical model is constructed. Aside from being a more tractable problem mathematically, this approach is customary in micro-climatology, because the vertical gradients of temperature and humidity (the two most important micro-climatological variables as far as plants are concerned), both in the atmosphere and in the soil, are much larger than the horizontal ones. Nevertheless, by its nature, this model will not be able to describe explicitly local horizontal advection.
2. A representation of the vegetation cover is of course necessary, but the model must also clearly be applicable to areas where the vegetation cover is not continuous. As discussed above, it is assumed that the average fluxes and profiles of such an environment may be derived from a weighted average of the fluxes and profiles that would occur in the absence of vegetation or in the presence of a complete canopy cover. The same applies to the cloud cover. Furthermore, it is also assumed that there is no statistical correlation between the cloud and vegetation covers. This would not be true on a large scale, but is probably correct on the space scales considered here.

Accordingly, the weight given to each submodel in the computation of environmental conditions is simply the product of the appropriate fractional covers:

Table 2.2: Weight of submodels

	Sub-model	Weight
1	Bare ground under clear sky	$(1-C)(1-V)$
2	Canopy under clear sky	$(1-C)V$
3	Bare ground under cloudy sky	$C(1-V)$
4	Canopy under cloudy sky	CV

where C is the fractional cloud cover and V is the fractional vegetation canopy cover. Such a scheme provides an explicit means of identifying the environmental consequences of changing the vegetation cover, for example, by overgrazing.

3. The multi-layer model attempts to describe in detail the processes in the first few meters of the soil and the atmosphere, and not the dynamics of the atmosphere above this level, nor the ground water flow under the deepest model layer. This implies, for example, that the cloudiness and precipitation will be forced and not computed interactively within the model. This is necessary at this stage to keep the complexity of the model within reasonable bounds, but it prevents the study of the influence of changes of vegetation on the macroclimate.

4. In order to study desertification, it will be important to develop models that can be integrated over multiple seasons, but this detailed model is designed and implemented with a daily time scale in mind. An accurate representation of the daily cycle appears to be a prerequisite before attempting longer time scale integrations. Furthermore, the space and time increments must be chosen in a consistent manner: a typical run of this model will have grid points separated by 1 to 10 cm, while the integration time step is of the order of a few seconds to a few minutes. Integration of such a model over longer time scales may require some simplifications to keep the computer costs within reasonable bounds.

2.5 Input to and output from the model

This model requires two types of input: initial values for numerous parameters and variables (space, time, type of soil and vegetation, etc.), and values of the forcings (cloudiness, precipitation, etc.); the most important elements are listed below:

1. Location: It includes the latitude, longitude and altitude of the ecosystem. The latitude enters directly in the computation of the solar radiation available at the top of the atmosphere. The longitude and altitude are not currently used but are included for completeness.
2. Time: It includes the year, month, day, hour, minute, and second. The initial value of these variables specify the starting time of the integration. At each time step, they are incremented as needed. Some of the forced variables are computed as single valued functions of time, for example, when a daily or seasonal cycle is imposed.
3. Grids: The location of the grid points, both in the soil and the atmosphere, can be specified. It should be noted that the grid points in the vegetation (both the canopy and the roots) occur at the place they would occur in the absence of vegetation.
4. Stepping: This is the time interval at which all computations are done for the four submodels. This time step of integration, together with the number of time steps to be executed and the initial time, defines the time at the end of the run and the duration of the run.
5. Soil characteristics: As mentioned above, each soil layer can be assigned a soil type, and initial moisture content and temperature. A number of specific parameters are also needed: for example, the thermal conductivity of the soil depends on the shape of the grains of soil. This and other parameters will be introduced when appropriate. For the purpose of this thesis (sensitivity analyses), the soil type has always been the same for all layers, and the initial profiles of soil moisture and temperature were

constant with depth; but there is no inherent restrictions on this. The soil surface can also be characterized by a slope angle and azimuth, and an initial profile of organic matter content can be specified.

6. Atmospheric characteristics: Similarly, the initial profiles of specific humidity and temperature in the air can be specified. Usually, profiles constant with height were selected initially, and the model integrated for a few days.
7. Wind: The wind speed at the top of the model is forced as a daily cycle superimposed on a seasonal cycle. If and when this model is coupled to a larger scale model, this wind speed will be provided by the dynamics of the larger model.
8. Cloudiness: The clouds in this model are characterized by a number of parameters, such as the cloud cover, the height of the base and the depth of the cloud. In order to compute radiative properties, it is also possible to specify such micro-physical quantities as the number density of droplets, together with their average radius. The rate of precipitation and its time evolution are forcing parameters.
9. Vegetation: Quite a few parameters are provided to describe the canopy and the root system. These include the vertical distribution of the leaf area density, and of the root length density, as well as of the initial temperature of the leaves. Additional input parameters are available to describe the thickness and dimension of the leaves, the maximum and minimum stomatal resistance, the structure of the canopy, the coefficient of absorption of radiation in the canopy, the extent of the vegetation cover, the biomass above the ground and the maximum precipitation collection efficiency. The root mean diameter can also be selected, as can be the thickness of the film of water deposited on the leaves when it rains, and the maximum fractional area of these leaves that can be wetted in such a case.

The output of the model consists essentially of the profiles of temperature and humidity in the atmosphere, the canopy and the soil, the fluxes of heat and moisture at the surface or at the top of the canopy. Of course, the values of most model variables are

output at periodic intervals during the run. Various kinds of diagnostic information can also be output at pre-assigned times.

The final profiles of temperature and moisture (i.e., the profiles at the end of the run), both in the soil and the air, can be saved for each submodel individually and re-used as input for the next run (provided the location, time, and soil and vegetation distributions are also preserved). The results presented in this Thesis do not normally refer to the first day of integration because it takes some time for the model to "settle" after being started from arbitrary initial conditions.

Chapter 3: Solar Radiation in the Atmosphere

This chapter describes the computation of the amount of solar radiation incoming at the "top" of the atmosphere, and the absorption and transmission of that radiation, both in the visible and near-infrared parts of the spectrum, inside the atmosphere. The interaction of the incoming solar radiation with the surface, as well as the radiative budget in the infrared are covered in the next chapter.

3.1 Solar radiation at the top of the atmosphere

Various formulae are available to compute the solar radiation reaching the Earth outside the atmosphere, ranging from simple approximate equations to complex computations based on the astronomical relations describing the motion of this planet around the Sun. At a later stage, this model may be applied to other geological periods, in which case an accurate computation of all elements of the orbit of the Earth must be done (Berger, 1978.) But for the present purpose, the basic astronomical variables are computed with reasonably accurate parameterizations for current conditions.

The computation of the solar radiant energy flux density reaching the Earth is detailed in a number of textbooks, and will not be repeated here. We follow the derivation of Sellers (1965, p. 13 ff.):

$$R_0 = S_0(\bar{d}/d)^2 \cos Z, \tag{3.1}$$

where R_0 is the solar radiation flux density, in $\mathrm{W\,m^{-2}}$; S_0 is the so-called *Solar constant*, taken to be 1367 $\mathrm{W\,m^{-2}}$; d is the actual distance between the Earth and the Sun, in m; $\bar{d}$ is the average distance d over a period of one year, in m; and Z is the solar zenith angle, in radians, defined as the angle between the local vertical and the direction of the Sun. The solar zenith angle varies between $-\pi$ and π.

Parameterizations have been developed for the two main variables of this equation, namely the ratio of the distances and the solar zenith angle. We adopted a popular formulation, as given, for example, in Knapp et al. (1980, p. 252 ff.) or Paltridge and Platt (1977):

$$(\bar{d}/d)^2 = 1.00011 + 0.00128\sin\beta + 0.034221\cos\beta + 0.000077\sin(2\beta) + 0.000719\cos(2\beta) \tag{3.2}$$

where $\beta = 2\pi D/N_y$, a non-dimensional number, D is the *relative Julian day* or the number of that day in the year minus one (0 to $N_y - 1$), and N_y is the number of days in the year (365 or 366). This ratio of distances varies from 1.0344 on January 3 to 0.9674 on July 5 (Sellers, 1965, p. 16). The upper part of Figure 3.1 shows the seasonal variation of this "distance factor": the Earth receives somewhat more solar radiation in January than in July, because it is closer to the Sun.

The cosine of the solar zenith angle is given by

$$\cos Z = \sin\phi\sin\delta + \cos\phi\cos\delta\cos h = \mu_0,$$

where ϕ is the latitude of the location, in radians; δ is the solar declination for that particular time, in radians; h is the hour angle, in radians; and μ_0 is another notation for $\cos Z$.

Finally, the solar declination is computed from

$$\delta = 0.006918 + 0.070257\sin\beta - 0.3999912\cos\beta + 0.000907\sin(2\beta) - 0.006758\cos(2\beta) + 0.00148\sin(3\beta) - 0.002697\cos(3\beta) \tag{3.3}$$

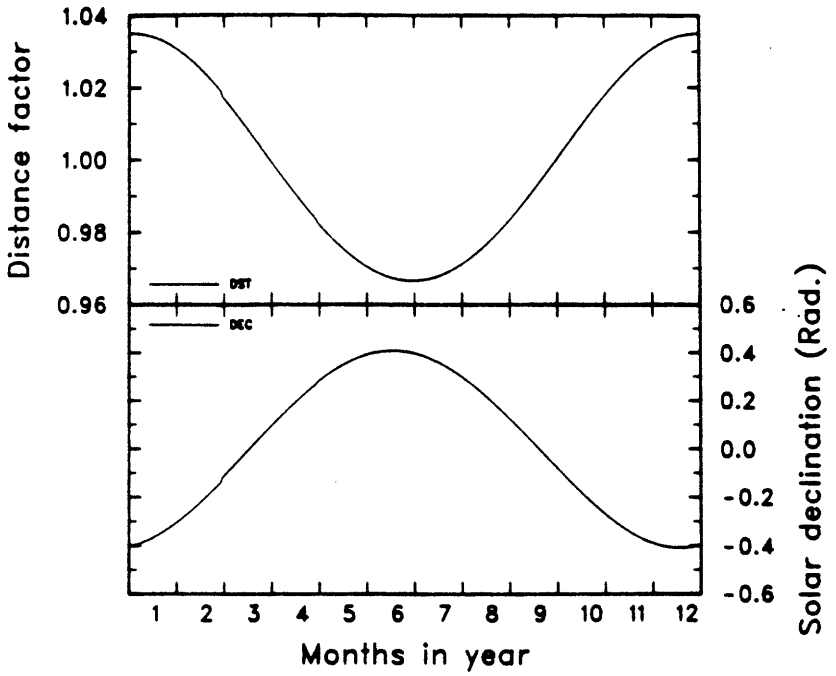

Figure 3.1: Seasonal cycles in distance and declination.

The lower part of Figure 3.1 shows the seasonal variation of the solar declination, for the current period. If this model is to be applied to a different geological era, this formulation should be replaced by a more appropriate one; and other parameters, such as the eccentricity or the longitude of the perihelion of the orbit of the Earth, should also be computed.

This system of equations completely determines the solar radiation flux density at the top of the atmosphere. Note that in this model the solar declination changes only every day, due to the "resolution" of Equation 3.3.

The upper part of Figure 3.2 displays the seasonal evolution of the solar radiation flux density at noon, for a latitude of 12° North. A double maximum is clearly visible and typical of these latitudes. The lower part of the same figure shows how the mean daily solar radiation flux density varies over the year.

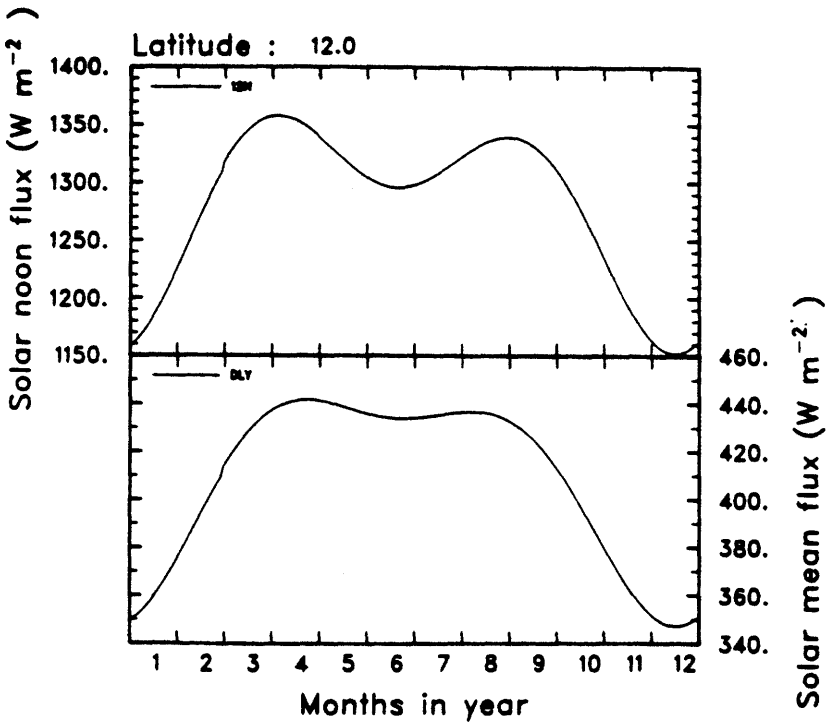

Figure 3.2: Noon and daily mean solar flux density.

3.2 Absorption of solar radiation in the atmosphere

As soon as the solar radiation flux enters the atmosphere, it interacts with the various atmospheric constituents, most notably ozone (in the stratosphere), water vapor (including clouds) and carbon dioxide (both in the troposphere), as well as other aerosols. Depending on the complexity of the model and of the problem of interest, some or all of these interactions must be taken into account.

Since this model is primarily concerned with the microclimate near the ground, no radiative transfer equation is solved: instead, I will follow the leading work of Lacis and Hansen (1974) who designed a very comprehensive model of solar radiation transfer through the atmosphere, in the presence of ozone and water vapor. These authors suggest physically based formulae to be used to compute surface fluxes when detailed information on the atmospheric profiles of water vapor and temperature are not available.

First of all, the amount of atmospheric ozone, expressed in m (STP), in a vertical column above a level H relative to sea level, is taken to be given by (Lacis and Hansen, 1974, p. 123)

$$O_3(H) = \frac{a + a\exp(-b/c)}{1 + \exp[(H-b)/c]},$$

where a is the total amount of ozone above sea level, in m (STP); b is the altitude of the maximum ozone concentration, in m; and c is a parameter related to the maximum concentration, in m. H is also expressed in m. For the purpose of this work, the following values have been selected:

$$a = 0.0028 \text{ m, STP}$$

$$b = 20000 \text{ m}$$

$$c = 5000 \text{ m}$$

These are representative of the ozone quantities found at 12° North, such as over the Sahel. No attempt has been made to vary these parameters, as the influence of slight changes in ozone amount is assumed to be negligible compared to the other changes or forcings imposed.

Since the direct solar radiation usually penetrates in the atmosphere at an angle with respect to the local vertical, the amount of ozone on the radiation path is generally higher than the amount in a vertical column. This is taken into account by multiplying $O_3(H)$ by a non-dimensional magnification factor, M, defined as (Lacis and Hansen, 1974, p. 122)

$$M = \frac{35}{(1224\mu_0^2 + 1)^{1/2}}, \tag{3.4}$$

where μ_0 is the cosine of the solar zenith angle, defined above.

Ozone absorbs mainly in two regions of the solar spectrum, the ultraviolet and the visible. The absorption coefficients for each of these bands are given by (Lacis and Hansen, 1974, p. 122)

$$\begin{aligned} A_{oz}(x) &= A_{oz1}(x) + A_{oz2}(x) \\ A_{oz1}(x) &= \frac{108.2x}{(1 + 13,860x)^{0.805}} + \frac{6.58x}{1 + (10,360x)^3} \\ A_{oz2}(x) &= \frac{2.118x}{1 + 4.2x + 3.23x^2} \end{aligned} \tag{3.5}$$

where A_{oz1} and A_{oz2} are the absorptions in the ultraviolet and visible bands, respectively, and where $x = MO_3$ is the effective ozone amount along the radiation path. These absorption coefficients are non-dimensional. One advantage of this parameterization is its simple representation in terms of polynomials of the ozone amount. The accuracy is remarkable.

Since the top of the model lies at a height of a few meters, the amount of water vapor in the bulk of the atmosphere is computed by assuming an exponential profile (Brutsaert, 1982, p. 139)

$$\rho_v(z) = \frac{0.622 e_a}{R_d T_a} \exp[-z/H_v],$$

where $\rho_v(z)$ is the density of water vapor at level z, in $\mathrm{kg\,m^{-3}}$; e_a is the surface water vapor pressure, in Pa; R_d is the gas constant for dry air, in $\mathrm{J\,kg^{-1}\,K^{-1}}$; T_a is the surface air temperature, in K; z is the altitude above the reference surface, in m; and H_v is the scale height for water vapor, also in m. The constant 0.622 is the ratio of the molecular weight of water vapor to that of dry air. All these "surface" values are taken at the top of the dynamic sublayer, which is also the top layer of the model. The water vapor scale height is assumed to be 2500 m, and is kept constant in space and time in this model, although it is actually somewhat variable in reality.

Only the total amount of water vapor in the column is of importance for the computation of the resulting radiative flux at the surface; therefore, this equation can be integrated vertically to give the total amount of precipitable water in the column:

$$W = \int_0^{Top} \rho_v(z) dz = \rho_{vs} H_v,$$

where W is the amount of precipitable water, in $\mathrm{kg\,m^{-2}}$; ρ_{vs} is the surface water vapor density, in $\mathrm{kg\,m^{-3}}$; and H_v is the water vapor scale height defined above.

The actual amount of water vapor interacting with the incoming solar radiation beam is larger than W if the beam is not vertical. The same correcting factor M derived for ozone is used again. However, the formula to compute the absorption coefficient for water vapor uses the precipitable water, y, in units of length, and MW is therefore multiplied

by the specific volume of water to derive the proper quantity y defined as $y = 10^{-3}MW$, in m. The absorption coefficient itself is given by (Lacis and Hansen, 1974, p. 126)

$$A_{H_2O}(y) = \frac{290.0y}{(1 + 14,150y)^{0.635} + 592.5y}, \tag{3.6}$$

where all symbols have been defined above.

The current version of this model does not include the effects of atmospheric carbon dioxide on the radiation balance because a better infrared radiation scheme and a more detailed photosynthesis model would be required to take these variations into consideration. As for the dust, it would be very interesting to include its effect, but this will require a better representation of the lower troposphere than is presently available.

3.3 Cloud parameters

Since the model does not include the bulk of the atmosphere, clouds are included only insofar as they influence the radiation balance at the surface, or the rate of precipitation. Five parameters are imposed: the cloud fractional cover C, non-dimensional; the cloud depth H_d and the height of the base of the cloud H_b, both in m; the cloud droplet number density N_d, in m^{-3}; and the cloud droplet radius r_d, in m. They allow a fair amount of flexibility in determining the radiative properties of the cloud layer. These five basic cloud parameters are kept constant for the duration of one run of the model, but could be specified at each time step, if desired.

From these parameters, it is possible to compute three more variables of importance for the radiation balance: the cloud droplet scattering cross-section, in m^2; the cloud optical thickness and the cloud albedo, both non-dimensional.

Following Houghton (1977, p. 73), the cloud droplet scattering cross-section is given by

$$\sigma = 2\pi r_d^2.$$

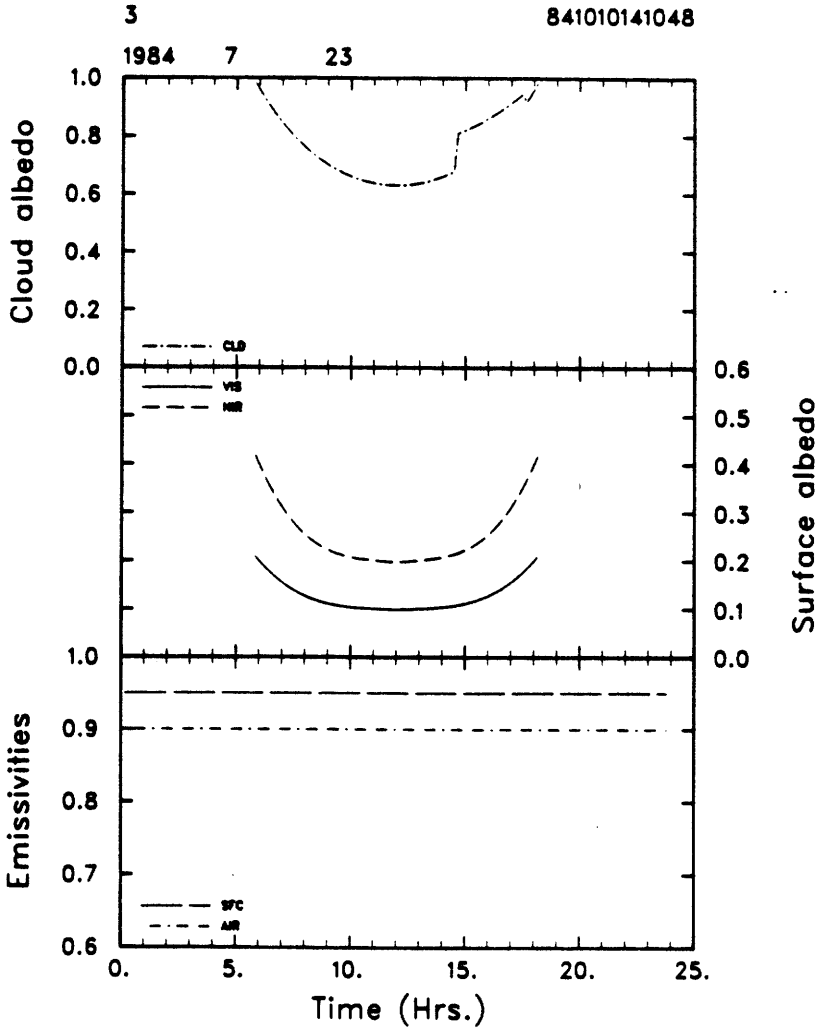

Figure 3.3: Cloud and surface albedos.

It is assumed that $2\pi r_d \gg \lambda$, where λ is the wavelength of the solar radiation. From this cross-section, we compute the cloud optical thickness as

$$\tau = N_d \sigma H_d \mu_0^{-1}$$

and the cloud albedo from Lacis and Hansen (1974, p. 124), as

$$\overline{R}_a(\mu_0) = \frac{0.13\tau}{1 + 0.13\tau}.$$

The top part of Figure 3.3 shows the daily evolution of the cloud albedo. Notice the increase in albedo when the depth of the cloud is suddenly increased from 800 to 2000 m. The other two frames of this figure will be covered in the next chapter.

All these parameters will now be used to compute the incoming solar radiation flux density at the surface.

3.4 Transmission of solar radiation under clear skies

From their detailed model, Lacis and Hansen (1974, p. 131) derive the following formula for the visible part of the spectrum, defined as the region $\lambda = 0.3$ to 0.9μm:

$$T_{v1} = R_0[0.647 - \overline{R}_r(\mu_0) - A_{oz}(x)]/(1 - \overline{\overline{R}}^*_r \alpha_s), \tag{3.6}$$

where T_{v1} is the visible solar radiation flux density at the surface, in $\mathrm{W\,m^{-2}}$; R_0 is the solar radiation flux density at the top of the atmosphere, in $\mathrm{W\,m^{-2}}$; $R_r(\mu_0)$ is the reduction of radiation due to Rayleigh scattering; and A_{oz} is the reduction due to ozone absorption, both non-dimensional. The constant 0.647 represents the fraction of the total solar radiation flux density in that spectral region. The denominator in this equation takes into account the multiple reflection of radiation between the atmosphere and the surface: its last term is the product of the atmospheric albedo for upward radiation ($\overline{\overline{R}}^*_r$) and the surface albedo α_s. (It should be noted also that this formulation does not distinguish between direct and diffuse radiation: only the total is provided.)

The non-dimensional Rayleigh scattering coefficient is a function only of the solar zenith angle (Lacis and Hansen, 1974, p. 131):

$$\overline{R}_r(\mu_0) = \frac{0.28}{1 + 6.43\mu_0}$$

and the spherical albedo of the Rayleigh atmosphere for illumination from below is taken as a constant:

$$\overline{\overline{R}}^*_r = 0.0685.$$

The computation of the surface albedo is explained in the next chapter.

As for the near-infrared part of the spectrum, defined as the region $0.9\,\mu\text{m} < \lambda < 5.0\,\mu\text{m}$, the same authors derive the following formula (Lacis and Hansen, 1974, p. 131):

$$T_{n1} = R_0[0.353 - A_{\text{H}_2\text{O}}(y)],$$

where the non-dimensional water vapor coefficient $A_{\text{H}_2\text{O}}(y)$ is that derived earlier. No corrections for ozone absorption or Rayleigh scattering are applicable in this spectral region.

3.5 Transmission of solar radiation under cloudy skies

Lacis and Hansen (1974, p. 131) have similarly derived a scheme to compute the solar radiation at the surface under cloudy skies.

The corresponding formula for visible radiation is now

$$T_{v2} = R_0[0.647 - A_{\text{oz}}(x)][1 - \overline{R}_a(\mu_0)](1 - \overline{\overline{R}}^*_a\alpha_s),$$

where all symbols have been defined previously, except for $\overline{\overline{R}}^*_a$, which is the cloud albedo for diffuse upward radiation, assumed to be equal to the cloud albedo for direct downward radiation, $\overline{R}_a$.

The computation of the surface solar radiation flux density in the near-infrared is somewhat more complex because of the nature of the absorption by water vapor. Instead of computing the transmission by lines or narrow bands, Lacis and Hansen (1974, p. 128 ff.) have derived a scheme whereby the total transmitted radiation is taken to be a weighted average of the transmissions at specified wavelengths. The full scheme is detailed in their publication; only the relevant equations have been reproduced below for reference:

$$T_{n2} = R_0 \sum_{n=2}^{8} T_n p(k_n),$$

where T_{n2} is in $\mathrm{W\,m^{-2}}$; and $p(k_n)$ is a discrete probability distribution for the absorption coefficient. (In the continuous case, the expression $p(k)dk$ represents the fraction of the incident flux associated with an absorption coefficient between k and $k + dk$.) In this equation,

$$T_n = \frac{4u}{(u+1)^2 e^t - (u-1)^2 e^{-t}}.$$

The various variables in these equations are defined as follows:

$$u = \left[\frac{1-g\omega}{1-\omega}\right]^{1/2},$$

$$t = [3(1-\omega)(1-g\omega)]^{1/2}\,\tau,$$

$$\omega = \tau/T,$$

$$T = \tau + k_n w,$$

where w is the effective water vapor amount, expressed as a quantity of precipitable water, in m; g is the cloud asymmetry factor (0.85); and τ is the cloud optical thickness. The values of k_n, in m, and $p(k_n)$ are tabulated in Table 3.1.

Table 3.1: Values of k_n and $p(k_n)$

n	k_n	$p(k_n)$
1	$4.0\,10^{-3}$	0.6470
2	0.20	0.0698
3	3.50	0.1443
4	37.70	0.0584
5	195.00	0.0335
6	940.00	0.0225
7	4460.00	0.0158
8	19000.00	0.0087

Source: Lacis and Hansen (1974, p. 129).

In summary, the variables T_{v1}, T_{v2}, T_{n1} and T_{n2} are computed from assumed or imposed values of atmospheric constituents (ozone and water vapor), and include corrections for Rayleigh scattering, cloudiness and multiple reflections between the atmosphere and the surface. This is probably the best estimate that can be reached without requiring more

knowledge on the vertical profiles of temperature and specific humidity in the bulk of the atmosphere.

One more correction must be applied: Lacis and Hansen (1974, p. 131) selected 0.9 μm as the threshold wavelength between visible and near-infrared radiation. With this threshold, the proportions of solar radiation in the visible and near-infrared portions of the spectrum are 0.647 and 0.353 respectively. This is somewhat inconvenient here because the spectral reflectance of the vegetation often shows a sharp increase for wavelengths longer than 0.7 μm (as will be seen in the next chapter). Fortunately, there is only very weak absorption by the water vapor in the interval 0.7 to 0.9 μm, and a linear correction is therefore applied as follows.

Based on the tables of energy flux densities in various spectral intervals given by Houghton (1977, p. 177), the following percentages of the total amount of solar radiation contained in the visible (V_R) and in the near-infrared (N_R) spectral intervals are derived:

$$0.3 < \lambda < 0.7\,\mu\text{m} \qquad V_R = 0.4646,$$

$$0.7 < \lambda < 5.0\,\mu\text{m} \qquad N_R = 0.5354.$$

The total energy flux density $(T_{vi} + T_{ni})$ as computed with the above scheme is then redistributed as follows:

$$T^*_{vi} = (T_{vi} + T_{ni})V_R$$

$$T^*_{ni} = (T_{vi} + T_{ni})N_R, \qquad \text{for i} = 1, 2$$

where T_{vi} and T_{ni} are the transmitted flux densities computed earlier for clear skies ($i = 1$) and cloudy skies ($i = 2$). T^*_{vi} and T^*_{ni} are the new values, and the asterisk will be dropped since the old values are not needed anymore.

Chapter 4: Radiation Balance at the Surface

This chapter starts by deriving the parameterizations of the albedos and emissivities for bare ground and for a vegetation canopy, and then proceeds to describe the interactions between the radiation fields and the surface, namely the absorption of visible and near-infrared radiation, both by the soil and by the vegetation canopy. The chapter ends with a description of the handling of the absorption and emission of infrared radiation by the same surfaces.

4.1 Soil albedo and absorption of radiation by the surface

Solar radiation penetrates into the soil, but is very quickly absorbed. The balance of radiation is therefore such that the incoming radiation is either reflected or absorbed. The fraction of the incoming radiation reflected by the surface is called the albedo; it depends on the radiative properties of the surface, on the spectral characteristics of the incoming radiation, and on the solar zenith angle. Since the model distinguishes only two bands of solar radiation, only averages of the albedo in the visible and the near-infrared regions of the spectrum need be specified, respectively.

There is only limited information on the actual albedos of most soils. Condit (1970) studied a large number of soil samples from the United States, but it is not clear whether

the results are applicable to other continents or latitudes. Furthermore, the spectral reflectance of many soils is very variable, especially at wavelengths larger than 600 nm.

Dickinson (1983) reviewed the literature on this subject from a more analytical point of view. While it is possible to derive a theory of the dependency of soil albedo on the nature and structure of the soil particles, observations tend to show a lower dependency of soil albedo on solar zenith angle than that predicted by such a theory. For the purpose of this research, the soil albedo is considered to depend on the soil type, the volumetric soil moisture content of the top soil layer, and the solar zenith angle. It is further assumed that the soil albedo in the near-infrared part of the spectrum is twice as high as in the visible part (Condit, 1970).

An observational study of soil albedo by Idso et al. (1975) suggests the following behavior for the albedo of an Avondale loam soil in the visible part of the spectrum:

$$\alpha_s = [[\alpha_{s0} f(\theta)] + g(Z)]\ h(\nu),$$

where α_s is the actual soil albedo, α_{s0} is the surface albedo for dry soil and for an incoming radiation beam perpendicular to the surface, $f(\theta)$ is the soil moisture dependency, $g(Z)$ is the zenith angle dependency, and $h(\nu)$ is the spectral dependency.

The limited available evidence (e.g. Idso et al., 1975; Condit, 1970) suggests that the soil albedo (for a generic soil) depends on soil moisture as follows:

1. the albedo of dry soil is twice larger than that of wet soil;
2. the decrease in albedo is proportional to the increase in soil water content of the first soil layer (normally between a few millimeters and a couple of centimeters deep), up to the field capacity;
3. the soil albedo is constant for all soil moisture contents equal or larger than the field capacity.

The field capacity is loosely defined as the volumetric water content of a soil that has been allowed to dry for a few days after it has been saturated. Hillel (1982, p. 243 ff.) discusses the history of this expression; it is used here only as a threshold value.

These statements can be formalized as follows:

$$f(\theta) = 1 - (\theta / 2\theta_{FC}) \qquad \text{for } 0.0 < \theta < \theta_{FC}$$

$$f(\theta) = 1/2 \qquad \text{for } \theta_{FC} < \theta < \theta_s,$$

where θ is the volumetric soil moisture content, θ_{FC} the volumetric soil moisture content at field capacity, and θ_s the saturated volumetric soil moisture content, all in $m^3\,m^{-3}$.

The data of Idso et al. for the Avondale soil suggests the following dependency of soil albedo on solar zenith angle:

$$g(Z) = -3.48\,10^{-4} + 2.14\,10^{-2} Z - 3.84\,10^{-2} Z^2 + 4.65\,10^{-2} Z^3,$$

where Z is the solar zenith angle in radians, as before. Figure 4.1 shows the daily cycle of soil albedo for a sandy loam; notice that the correction is always small except for large zenith angles. The lower part of this Figure shows the emissivities of the soil surface and the air, but this is discussed in greater detail later.

In the absence of detailed and comparable observational data on various soils, it is assumed that all soils behave in a similar manner. This is certainly not the case in reality, but we also note that the solar zenith angle dependency of soil albedo depends on soil structure, a parameter not included in the present model. Furthermore, the albedo increase due to large zenith angles is often short-lived in tropical regions since the Sun rises quickly above the horizon. For these reasons, this simplification should not affect very long the results of the model.

One further simplification is introduced: in the two *cloudy* submodels, the surface solar radiation is mostly diffuse, while in the two *clear sky* cases, most of the solar radiation is in the direct beam. The solar zenith angle used in the above formula is computed at each time step in the last two cases, but is set to 60° for the cloudy cases. This customary

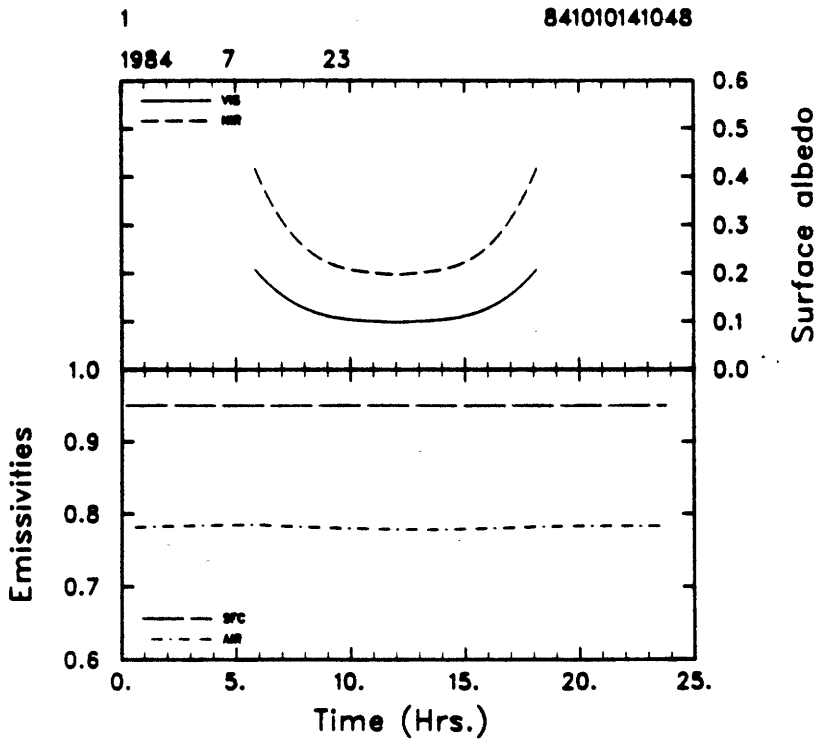

Figure 4.1: Soil albedos and emissivities.

value underestimates the influence at high zenith angles, and underestimates it at lower angles. The soil albedo therefore does not present any zenith angle dependency under cloudy skies. The model could be improved a little by distinguishing between the direct and diffuse radiation transmissions in the atmosphere.

Finally, the spectral dependency is given by

$$h(\nu) = 1.0, \text{ for visible radiation } (\nu < 0.7\mu\text{m})$$

$$h(\nu) = 2.0, \text{ for near} - \text{infrared radiation } (\nu > 0.7\mu\text{m})$$

The amount of solar radiation absorbed at the soil surface is then easily computed from

$$\begin{aligned} A_{vi} &= T_{vi}(1-\alpha_v) \\ & \qquad \text{for i} = 1, 2, \\ A_{ni} &= T_{ni}(1-\alpha_n) \end{aligned} \tag{4.1}$$

where A and T represent the absorption and transmission of radiation, in W m^{-2}, the indexes v and n stand for visible and near-infrared bands, the index i stands for clear skies ($i = 1$) or cloudy skies ($i = 2$), and α_v and α_n are the surface albedo for the visible and near-infrared parts of the spectrum, respectively.

This absorption of solar radiation is deemed to occur in the first soil layer, and provides one of its main heating terms.

4.2 Vegetation albedo and absorption of radiation by the canopy

The transfer of radiation inside plant canopies is very complex because of the number, size, shape, orientation, and radiative characteristics of the leaves. Each leaf, in turn, reflects, absorbs and transmits solar radiation, in proportions that depend on the spectral characteristics and angle of incidence of the incoming radiation.

Dickinson (1983) reviewed the mathematical theory of radiative transfer in plant canopies, and his results are used here. The vegetation canopy is modeled as a "medium" composed of a large number of scattering elements (leaves), randomly distributed in space and orientation. With these assumptions, Dickinson and Hansen (1984) derived the following formula for the albedo of a deep canopy as a whole:

$$\alpha_c = \frac{\omega_\ell \kappa}{(a+\kappa)(1+a)}$$

where α_c is the non-dimensional canopy albedo, κ is a canopy structure parameter ($\kappa = 0.5/\mu$ for a canopy where all leaves have arbitrary orientations, μ is the cosine of the solar zenith angle, as before); and $a = (1-\omega_\ell)^{1/2}$, where ω_ℓ is the single scattering albedo of a single leaf, typically 0.10 in the visible and 0.50 in the near-infrared regions, respectively.

The albedo of a vegetation canopy is almost half as large as the reflectance of an individual leaf, mostly due to light trapping inside the canopy. This formulation correctly represents this fact, and also includes a dependency on the solar zenith angle, so that the albedo of a given canopy is time dependent.

Since this model is applied to arid and semiarid regions where the vegetation canopies are rather shallow, this formulation may not be totally appropriate. Indeed, with sparse low vegetation, a significant fraction of the solar radiation may reach the ground under

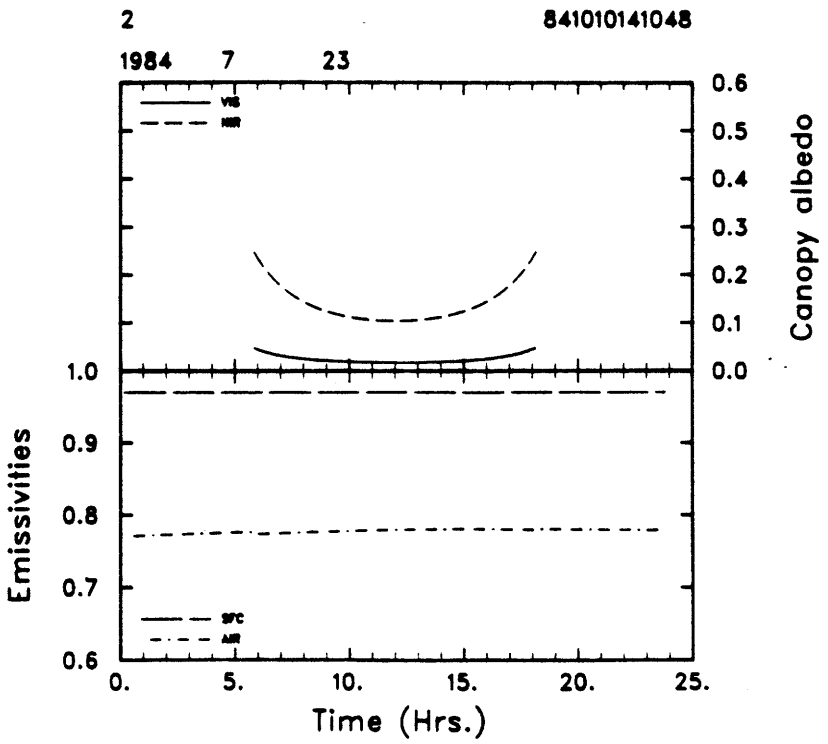

Figure 4.2: Deep canopy albedos and emissivities.

the plant, and be reflected there also. To take this effect into account, the albedo of the vegetated surface is computed as a weighted average of the deep canopy albedo and of the bare soil albedo, with the weights calculated as follows.

First, a canopy is assumed to be deep if its leaf area index is equal to or larger than 3. The selection of this particular value is based on the fact that the absorption of solar radiation in the canopy follows an exponential profile (see below). For such a leaf area index, the solar radiation at the surface under the plant would be reduced to approximately 5% of the flux density at the top of the canopy, and no correction is therefore required.

For canopies with a leaf area index (LAI) of less than 3, the weights are $LAI/3$ and $(3 - LAI)/3$ for the canopy and soil albedos respectively. In this way, the albedo of a canopy converges towards the soil albedo when the leaf area index decreases, and towards the albedo of a deep canopy when the leaf area increases. The top part of Figure 4.2 shows the daily cycle of the vegetation albedo, both for the visible and near-infrared radiation, for a case where the leaf area index is larger than 3. (A case where the LAI is less than

3 will be shown in Chapter 9.) This approximation may not be very accurate, but it is probably not justified to develop a much more elaborate scheme.

The radiation not reflected by the canopy must then be absorbed by the canopy or the underlying ground. The complete theory mentioned above computes the layer absorption explicitly in order to derive the canopy albedo, but as the latter has been determined, the total solar radiation absorbed in the whole canopy and the underlying surface is known to be given by

$$A_{vi} = T_{vi}(1 - \alpha_v)$$
$$A_{ni} = T_{ni}(1 - \alpha_n) \qquad \text{for i} = 1, 2,$$

where α_v and α_n are now the combined albedos for vegetation and soil in the visible and near-infrared radiation, respectively. The only problem left is to distribute this absorbed flux among the leaf layers and the top soil layer.

It has been found experimentally that the absorption of solar radiation inside the canopy follows an exponential law, such as (Ross, 1975, p. 37)

$$T(z) = T(h)\tau(L)$$
$$\tau(L) = \exp(-kL),$$

where $T(z)$ is the transmitted solar radiation flux density, in $\mathrm{W\,m^{-2}}$, at level z inside the canopy; $T(h)$ is the solar radiation flux transmitted at the top of the canopy, also in $\mathrm{W\,m^{-2}}$; $\tau(L)$ is the transmission function for radiation in the foliage; k is the non-dimensional extinction coefficient; and the function $L(z)$ represents the amount of leaf area above level z per unit area of ground surface, as defined in Chapter 2.

These equations can be applied to compute the transmitted radiation flux density at the bottom of each vegetation layer in the model, and the net layer absorption is then derived from the difference between the incoming and outgoing fluxes. Finally, the transmitted radiative flux density at the bottom of the last (deepest) vegetation layer is assumed to be absorbed in the first soil layer. In this model, no distinction is made between the photosynthetically active radiation and the visible radiation.

The value of the extinction coefficient k varies with the type of plant and the structure of the canopy, with typical values ranging from 0.3 for plants with small vertical leaves to 1.5 for canopies with large horizontal leaves (Ross, 1975, p. 37.)

4.3 Infrared radiation balance at the surface

One of the main cooling mechanisms of the atmosphere is through radiative emission in the infrared part of the spectrum. Such emission takes place in all directions, and in particular downwards, therefore contributing an additional heating term for the surface. The latter also emits infrared radiation, and the net balance is usually negative for the surface because it emits more infrared radiation than it receives.

In principle, the computation of the downward infrared radiation from the atmosphere requires detailed knowledge of the vertical profiles of water vapor concentration and temperature in the atmosphere. This information is not available in the current version of the model, since the topmost layer is located at a level of 10 m or less. One way to compute this flux would have been to adopt one or another of the many empirical equations which have been derived from observational data for particular locations or uses. Instead, I decided to use a more physical approach and compute the downward radiation on the basis of the air temperature and specific humidity at the top of the dynamic sublayer. This method has been used by other authors, and Brutsaert (1982, p. 138 ff.) discusses it in detail.

The infrared radiation flux density from the atmosphere to the surface is given by the usual fourth power law (Brutsaert, 1982, p. 138)

$$I^d = \epsilon_a \sigma T_a^4,$$

where I^d is the infrared *back-radiation* flux density from the sky, in $\mathrm{W\,m^{-2}}$; ϵ_a is the emissivity of the atmosphere, a non-dimensional number; and T_a is the air temperature, in K, at the top of the model.

The emissivity ϵ_a must still be computed. Assuming exponential profiles of atmospheric pressure, temperature and water vapor, Brutsaert (1982, p. 139) analytically derives the following formula for the sky emissivity:

$$\epsilon_a = 0.642 \left(\frac{e_a}{T_a}\right)^{1/7} \qquad \text{under clear skies,}$$

where e_a is the water vapor pressure of the topmost layer of the model, in Pa; and T_a is the air temperature at the same level, in K. As was explained earlier, this model integrates four submodels in parallel, two of which are characterized by cloudy conditions. In these cases, a somewhat higher sky emissivity must be selected to account for the increased downward infrared radiation, and the emissivity is arbitrarily set to 0.9.

The ratio e_a/T_a, itself, is computed from the thermodynamical identity (Brutsaert, 1982, p. 37):

$$\frac{e_a}{T_a} = \frac{\rho_v R_d}{0.622},$$

where ρ_v is the water vapor density in the air at the top of the model, in $\mathrm{kg\,m^{-3}}$, and R_d is the gas constant for dry air.

It is seen that clouds will influence the infrared radiation balance mainly through the change in emissivity. It should be remembered also that the environmental conditions are defined as a weighted average of the four individual profiles, and that the cloud cover will play a major role in this respect.

Of course, a fraction $(1-\epsilon_s)$ of the incident infrared flux is reflected back to the atmosphere (ϵ_s is the surface emissivity), but since no infrared radiation divergence calculations are made in the atmosphere, and since this reflected flux does not enter the surface energy balance, this flux component is not computed or carried in the model.

The soil surface also emits infrared radiation, at a rate governed by its temperature:

$$I^u = \epsilon_s \sigma T_s^4,$$

where I^u is the infrared radiation flux density emitted by the surface to the atmosphere, in $\mathrm{W\,m^{-2}}$, ϵ_s is the emissivity of the radiating surface, σ is the Stefan-Boltzmann constant, and T_s is the temperature of the surface, in K. The latter is derived from an energy budget equation, as explained in the next chapter.

The emissivity of the surface is assumed constant in this model; in particular, no spectral dependency is included since the thermal infrared radiation is treated as one radiation band. Following Brutsaert (1982, p. 137), the emissivities of bare ground and vegetation are taken to be

$$\epsilon_s = 0.95 \qquad \text{for bare ground,}$$

$$\epsilon_s = 0.97 \qquad \text{for vegetation.}$$

4.4 Infrared radiation inside the canopy

For the two submodels that include a canopy, infrared radiation exchanges between the leaf layers, and between the canopy and the soil or the atmosphere must be estimated. A special scheme, based only on the geometry of the canopy and the emitted flux densities, has been designed and is described next.

At the outset, it is recognized that the exchanges of infrared radiation between leaf layers are rather limited, mostly due to the fact that their temperatures are not very different. It is again assumed that the leaves are distributed randomly in the canopy, and that infrared radiation is either absorbed or transmitted through a leaf layer. Furthermore, the flux of infrared radiation emitted by one leaf layer is assumed to be absorbed by or transmitted through the adjacent layers in proportion to the product of the appropriate fractional leaf areas of these layers. Since the emission of infrared radiation is also proportional to the fractional area, it is expected that the infrared radiation emitted in one layer and absorbed in an adjacent layer will be proportional to the product of the fractional

areas of the emitting and absorbing leaf layers. If these interacting layers are not adjacent, they can only exchange infrared radiation through the "holes" of the intervening layers.

Let L_i be the fractional leaf area of the ith leaf layer, and let i be the index of the leaf layer for which the infrared radiation balance is sought. Let j be a running index to designate leaf layers that are j layers away from the ith leaf layer, either above or below. Finally, let I^d_{i+j} be the infrared radiation flux density emitted downward by the leaf layer $(i+j)$. The product $L_{i+j}I^d_{i+j}$ is then the actual flux emitted by the leaf layer $i+j$, of which a fraction,

$$\prod_{k=1}^{j-1}(1-L_{i+k})L_{i+j}I^d_{i+j},$$

is transmitted to layer i through the intervening leaf layers. A fraction L_i of this flux will be absorbed by the the ith leaf layer, and the rest will be transmitted downward to interact with deeper layers. A similar scheme is developed for the infrared radiation emitted upward from leaf layers below layer i. These expressions must then be summed over all leaf layers above and below the ith one, and the contributions from the atmosphere above the canopy and from the soil surface must also be taken into account.

The resulting infrared energy balance of the ith leaf layer can then be written as follows:

$$\begin{aligned} I^n_i = &- L_i I^u_i + \sum_{j=1}^{N-i} L_i \prod_{k=1}^{j-1}(1-L_{i+k})L_{i+j}I^d_{i+j} \\ &- L_i I^d_i + \sum_{j=1}^{i-1} L_i \prod_{k=1}^{j-1}(1-L_{i-k})L_{i-j}I^u_{i-j} \\ &+ L_i \prod_{j=i+1}^{N}(1-L_j)L_{N+1}I^d_{N+1} \\ &+ L_i \prod_{j=1}^{i-1}(1-L_j)L_0 I^u_0, \end{aligned}$$

where I^n_i is the net infrared radiation balance for the ith leaf layer; N is the number of leaf layers; k is another running index, usually designating intermediate layers between i and j; and the indices 0 and $N+1$ represent the soil surface and the atmosphere, respectively.

I^d_{N+1} is the sky irradiance, and I^u_0 is the emitted flux density from the soil surface. This equation can be applied for $i = 0, 1, ..., N, N+1$; provided $L_0 = L_{N+1} = 1$.

All variables I on the right hand side of this equation are positive, since the signs are explicit. The net balance I^n_i is positive if the layer gains more than it emits, and negative otherwise.

Chapter 5: Wind Profiles

This small chapter describes how the wind profiles are computed in the submodels, since these will be needed in further computations. As before, two cases must be distinguished, depending on whether there is vegetation or not (the wind profiles are assumed to be independent of the cloud cover).

Again, the model only covers the first few meters of the atmosphere. In order to concentrate on the physical processes at and near the surface, a simple logarithmic scheme has been selected. In principle, such a formulation applies only to a neutrally stable atmosphere. A deeper boundary layer parameterization would be desirable: it would allow a better representation of dynamic processes. Such models have been investigated by others, however, and this was not a priority objective in this work.

5.1 The wind profile outside the vegetation

The first and simplest case is the one without vegetation (submodels 1 and 3): the wind profile in the dynamic sublayer is assumed to be logarithmic. This type of profile is well known, and a derivation of the mathematical expressions can be found in numerous textbooks, such as Brutsaert (1982), Oke (1978) or Sellers (1965). The relevant equations are reproduced here for easy reference.

The mean wind speed profile, in $\mathrm{m\,s^{-1}}$, is given by (Brutsaert, 1982, p. 59)

$$u = \frac{u_*}{k} \ln\left(\frac{z-d}{z_0}\right) \qquad z \gg z_0, \tag{5.1}$$

where u_* is the friction wind velocity, in $\mathrm{m\,s^{-1}}$; k is the non-dimensional von Karman constant (equal to 0.4), z is the altitude of the level above the ground surface, d is the displacement height, and z_0 is the roughness length, all in m.

Three parameters must be specified in this equation: u_*, d, and z_0. These three variables are not independent since they all relate to the surface roughness. The friction wind velocity is directly linked to the surface drag coefficient, and the other two parameters are dependent upon the sizes of the obstacles responsible for the roughness. In addition, I wanted to keep a way to influence the wind profile with an external forcing, namely the wind speed at the top of the dynamic sublayer u_T. This forcing variable was selected because this model may become coupled with or embedded into larger scale models which could predict the geostrophic wind or some equivalent wind speed at a level z_T of around 10 m.

The vegetation patches are assumed to represent the major cause of surface roughness in the model, and the displacement height, d, in the bare ground patches is therefore nul or very close to zero. The roughness length, z_0, is similarly assigned a constant value of 0.01 m, to account for stones and other debris that occur over bare ground. For typical values of z_0 in various environments, see Brutsaert (1982, p. 114), Sellers (1965, p. 150), or Oke (1978, p. 48).

Imposing the mean wind speed, u_T, at the top of the dynamic sublayer in Equation (5.1) leads to the computation of the friction wind speed, u_*:

$$u_* = \frac{k u_T}{\ln((z_T - d)/z_0)}.$$

This wind speed, u_T, can be set constant or given a daily and seasonal cycle, as is done in the current implementation of the model.

Finally, the non-dimensional drag coefficient C_D can be computed from this friction wind velocity using the classical formula (Brutsaert, 1982, p. 88)

$$C_D = u_*^2/u_T^2.$$

These equations completely determine the wind profile in the two non-vegetated submodels, and these profiles can be modified externally (forcing), using the wind speed at the top of the model.

Of course, the logarithmic profile is valid only for heights z much larger than the roughness length z_0. It is therefore stipulated that the wind profile is logarithmic at heights z larger than ten times z_0. Below that height, the wind speed is simply interpolated linearly to zero at the soil surface.

5.2 The parameters d and z_0 in the canopy

The variables d and z_0 must also be parameterized for the two other submodels. Experimental results reviewed by Brutsaert (1982, p. 116) suggest that the displacement height, d, for fully vegetated surfaces, is variable but can be approximated with reasonable accuracy by $d = (2/3)h_v$, where h_v is the height of the vegetation. Compared to z_0 (see below), this parameter is relatively less sensitive to the nature of the underlying surface.

The situation is not as simple for the roughness length, z_0, which is observed to depend not only on the size of the roughness elements but also on their distribution in space. Various authors have attempted to relate z_0 to the height of the plants, and Brutsaert (1982, p. 113) suggests that, within the limitations of such an approach,

$$z_0 = h_v/7.5 \tag{5.2}$$

should be a reasonable estimate for fully vegetated surfaces.

However, experimental data also shows that the roughness actually increases when the canopy cover decreases from complete to sparse. This is due to the fact that a full canopy presents less roughness to the air flow than a broken canopy, up to a point. Following the works of Thom (1971, 1972) and Seginer (1974), it appears that the roughness length can be meaningfully computed in terms of a non-dimensional parameter, $Cd_f A_f h_v$, where Cd_f is a foliage drag coefficient and A_f is the vertically-averaged leaf area (both sides) per unit volume of air.

In terms of the variables of this model, $A_f = 2\,LAI/h_v$, and is therefore readily available. Thom (among others) has investigated the nature of Cd_f, and derived the following dependency for a bean crop (Thom, 1971, p. 426):

$$Cd_f = c_f u^{-1/2}$$

where u is the wind speed inside the canopy, in $\mathrm{m\,s^{-1}}$; and c_f is a plant-specific coefficient equal to 0.108 for beans. Assuming the dependency on the inverse square root of the wind speed holds for various types of canopies (Brutsaert, 1982, p. 100), we have adopted a value of 0.1 for the coefficient c_f in this model.

Data collected by Seginer (1974, p. 384) indicates that the ratio $z_f = z_0/h_v$ depends piecewise linearly on $l_f = \ln(Cd_f A_f h_v) = \ln(2Cd_f LAI)$, the logarithm of the non-dimensional coefficient defined above. Brutsaert (1982, p. 114) suggests that the maximum roughness length could be taken as 1.5 to 2 times that given by Equation (5.2).

Taking the other values from Seginer's figure, the adopted parameterization is as follows:

$$z_f = 0.02 + (z_t - 0.02)(l_f - 0.02)/0.18 \qquad 0.02 < l_f < 0.2$$

$$z_f = z_t + (0.02 - z_t)(l_f - 0.2)/1.8 \qquad 0.2 < l_f < 2.0,$$

where $z_t = (1.75/7.5)$.

Now that the displacement height is not zero, the logarithm in Equation (5.1) may become undefined if z becomes equal to or less than d. However, since the wind speed inside the canopy is computed from another formula (see below), and since d is always smaller than the height of the canopy, this condition never occurs.

5.3 The wind profile inside the vegetation

In a manner similar to the bare ground cases, a wind profile can be derived from these parameterizations, since the wind speed at the top of the model is imposed. The roughness length and displacement height are different, however. The logarithmic profile is used as is from the top of the canopy to the top of the model. Another formulation must however be applied to compute the wind speed inside the canopy, to account for the absorption of momentum by the leaves.

Inside a complete canopy cover, the wind speed has been observed to follow an exponentially decreasing profile from the top of the vegetation, corresponding to the absorption of momentum by the leaves and stems. Brutsaert (1982, p. 97 ff.) reviews this subject in greater detail, and suggests that the following formulation is applicable for a complete canopy cover:

$$u_c(z) = u(h_v) \exp[-a(h_v - z)/h_v],$$

where u_c is the horizontal wind speed inside the canopy, in $\mathrm{m\,s^{-1}}$; $u(h_v)$ is the wind speed just above the top of the canopy, also in $\mathrm{m\,s^{-1}}$ (as computed earlier); and a is an extinction coefficient given by

$$a = \frac{A_k h_v}{h_v - d},$$

where A_k is a constant slightly smaller than or equal to unity.

These equations may be appropriate for tall vegetation canopies, but because of the nature of the exponential function, the wind speed never reaches zero close to or at the surface. To remedy this situation, a linear correction is applied throughout the canopy, and the wind profile for a complete cover is now given by

$$u_c(z) = u(h_v)\,[\exp[-a(h_v - z)/h_v] - [(h_v - z)/h_v]\exp(-a)]\,.$$

This profile approaches $u(h_v)$ when z tends to the top of the canopy, and approaches zero at the surface.

Figure 5.1 shows two typical wind profiles: the continuous line applies outside the vegetation (this is a usual logarithmic profile), and the dashed line is representative of the wind profile inside the canopy. The latter presents a linear section near the top of the canopy: this is an artifact of the graphic routine that plots curves by joining points, not a part of the algorithm.

In summary, the wind profile is logarithmic over bare ground and above the vegetation canopy, although with slightly different parameters (displacement height and roughness length). Inside the canopy, momentum is absorbed by the stems and leaves, resulting in a somewhat faster decrease of wind speed. In both cases, the wind speed approaches zero near the ground.

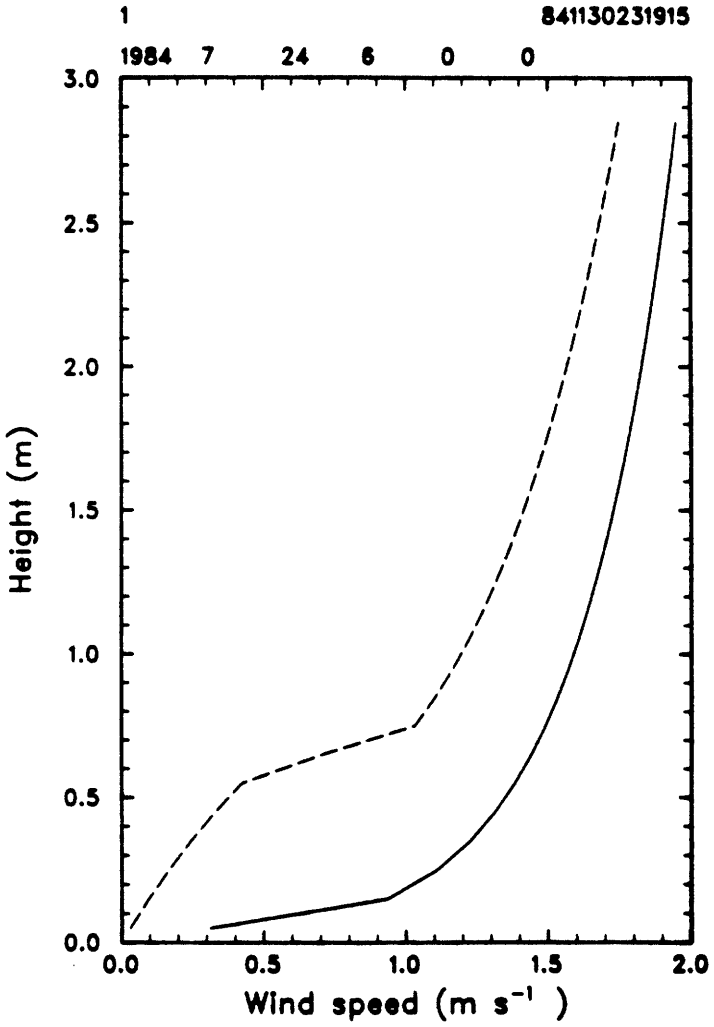

Figure 5.1: Wind profiles inside (– –) and outside (—) the canopy.

Chapter 6: Water and Energy Balances at the Surface

The volumetric soil water content and the temperature of the first soil layer are obtained by solving a water and an energy balance equation, respectively. These values will later be used as boundary conditions for the integration of diffusion equations for heat and water in the soil.

6.1 The surface water balance

The surface water balance is an equation expressing the conservation of the mass of water: the sum of all fluxes of water in the specified volume must equal the net change in soil water content. Such an equation can be written (Sellers, 1965, p. 82) as

$$P - E - R_f - G_w - S_w = 0, \tag{6.1}$$

where P is the precipitation rate, E the evaporation rate, R_f the runoff rate, G_w the infiltration rate into the next soil layer, and S_w the storage rate of water in the top soil layer. All these rates are expressed in $\mathrm{kg\,m^{-2}\,s^{-1}}$. The precipitation rate is one of the forcing parameters of this model (see Part 2); all other terms are computed as explained below. Note that when there is a vegetation cover, part of the precipitation is intercepted by the canopy. This topic is covered in Chapter 7.

At the outset, it is recognized that all the terms of this equation, except the precipitation rate, depend on the new value of the volumetric water content that the top soil layer

will take at the end of the current time step (this will become clearer later in this section). A Newton-Raphson scheme is therefore applied, where the soil moisture content of the top soil layer is varied until the water balance Equation (6.1) is satisfied. This is possible because the soil moisture content at the previous time step, and the variables necessary to evaluate the various fluxes, are known or can be computed, as explained below.

6.1.1 Evaporation: demand and supply

The rate of evaporation is one of the most significant micro-meteorological variables, because of its implications not only for the climate near the ground but also for the rest of the atmosphere. Unfortunately, it is also a very difficult flux to measure accurately. There are many ways to estimate it from available meteorological and hydrological data (Miller, 1977, p. 251–344). In this particular model, the actual evaporation rate is computed as the minimum of two fluxes; the potential evaporation rate or atmospheric demand for water vapor, and the maximum rate of water transfer that can be supported by upward diffusion of liquid water in the soil. If the demand from the atmosphere is larger than the supply from the soil, the rate of evaporation is limited by soil diffusion processes, a common situation in arid regions (Hillel, 1980, p. 275 ff.).

The evaporative demand from the atmosphere is estimated as (Brutsaert, 1982, p. 88)

$$E = Ce_r \rho_a \overline{u}_r (\overline{q}_s - \overline{q}_r) \tag{6.2}$$

where Ce_r is a non-dimensional water vapor transfer coefficient, to be defined below; ρ_a is the air density at the top of the model, in $\mathrm{kg\,m^{-3}}$; $\overline{u}_r$ is the wind speed at the top of the model, in $\mathrm{m\,s^{-1}}$; $\overline{q}_s$ is the specific humidity of the air at the surface, in $\mathrm{kg\,kg^{-1}}$; and $\overline{q}_r$ is the specific humidity of the air at the top of the model, in $\mathrm{kg\,kg^{-1}}$. The top of the model is typically 3 to 10 meters high. The horizontal bars on top of some of these symbols mean that a time average value should be taken: this equation does not apply to instantaneous

deviations from the average. It should be noted that the rate of evaporation vanishes when the wind speed tends to zero.

Each of the variables in Equation (6.2) must now be given a numerical value. The wind speed at the top of the dynamic sublayer u_r is one of the forcing parameters of the model (see the previous chapter). The density ρ_a is derived from the atmospheric pressure and temperature at that same level, using the perfect gas law. The specific humidity $\bar{q}_r$ is obtained from the model, as explained in the next chapter, so that $\bar{q}_s$ and Ce_r remain to be determined.

The value of $\bar{q}_s$ is assumed to be the specific humidity of the air inside the top soil layer, and is computed from (e.g. Milly and Eagleson, 1980, p. 27; or Hillel, 1980, p. 85)

$$\bar{q}_s = q_* \exp[(g\psi)/(R_v T)],$$

where q_* is the specific humidity at saturation, in $\mathrm{kg\,kg^{-1}}$, corresponding to the soil temperature T, in K; g is the acceleration of gravity, in $\mathrm{m\,s^{-2}}$; ψ is the matric potential of the water in the soil, in m; and R_v is the gas constant for water vapor, in $\mathrm{J\,kg^{-1}\,K^{-1}}$.

The transfer coefficient Ce_r in Equation (6.2) could be taken as constant; it is of the order of $2.5\,10^{-3}$, but since it depends only on the the wind speed in the dynamic sublayer, and since this information is available in the model, it is computed explicitly.

Following Brutsaert (1982, p. 88),

$$Ce_r = \frac{Cd_r^{1/2}}{(Da_0^{-1} - a_v^{-1} Cd_0^{-1/2} + a_v^{-1} Cd_r^{-1/2})},$$

where

$$\begin{aligned} Cd_r &= \frac{u_*^2}{u_r^2} \\ Cd_0 &= \frac{u_*^2}{u_h^2} \\ a_v &= \frac{k_v}{k} \simeq 1.0 \\ Da_0^{-1} - a_v^{-1} Cd_0^{-1/2} &= 7.3 z_{0+}^{1/4} Sc^{1/2} - 5.0, \end{aligned} \tag{6.3}$$

where Da_0 and Sc are the Dalton and Schmidt numbers, respectively, k_v is the von Karman constant for water vapor, and k is the von Karman constant (0.4). All these numbers are

non-dimensional. u_* is the friction velocity, in $\mathrm{m\,s^{-1}}$; and u_h is the wind speed at the level where the profile formulations for the dynamic sublayer and the interfacial sublayers are joined, in $\mathrm{m\,s^{-1}}$. For reference, the Dalton number Da_0 is defined as (Brutsaert, 1982, p. 88):

$$Da_0 = \frac{E}{\rho_a u_* (q_s - q_h)},$$

where q_h is the specific humidity at the top of the canopy.

It should be noted that the actual value of u_h is not required because of Equation (6.3). Finally, z_{0+} is the roughness Reynolds number defined by

$$z_{0+} = \frac{u_* z_0}{\nu},$$

where z_0 is the roughness length for the wind profile (see Chapter 5), and ν is the kinematic viscosity of the air, in $\mathrm{m^2\,s^{-1}}$, computed as

$$\nu = (-1.13092 + 0.00902\,T)10^{-5}. \tag{6.4}$$

The Schmidt number is simply the ratio of the kinematic viscosity of the air over the water vapor diffusivity in air, κ_v, expressed in $\mathrm{m^2\,s^{-1}}$ and computed as

$$\kappa_v = (-1.91401 + 0.01519\,T)10^{-5}.$$

In these equations, T is the air temperature, in K.

This completely determines the atmospheric evaporative demand. The water vapor supply from the soil is itself limited by the rate at which the water can diffuse upward in the soil and reach the surface. This rate is computed from the water diffusion equation in the soil (Hillel, 1980, p. 113):

$$E_{soil} = -K(\psi)\rho_w \frac{\partial \psi}{\partial z},$$

which is the product of the soil water conductivity $K(\psi)$, in $\mathrm{m\,s^{-1}}$, the density ρ_w of water, and the soil water matric potential gradient between the top two soil layers. When the

water balance equation is solved, the water potential in the top soil layer is automatically adjusted in such a way that the demand from the atmosphere is equal to the actual supply from the soil.

It should be stressed that these expressions apply only to the evaporation from the soil surface to the atmosphere. If there is a vegetation canopy, the flux of water vapor at the top of the canopy would be increased by the transpiration from the leaves (and possibly by the evaporation of liquid water that may have been intercepted by these leaves during a previous rain event), but this would not affect the water balance at the soil surface.

6.1.2 Runoff, infiltration and storage

In this model, runoff only occurs when there is an excess of incoming water (from precipitation) that cannot be absorbed in the top soil, nor evaporated. This simple parameterization is customary in meteorological models (Němec, 1983).

The next term in the balance equation is the infiltration rate, G_w, in $\mathrm{kg\,m^{-2}\,s^{-1}}$. The theory of water infiltration into the soil will be covered in greater detail in a later chapter. For the present purpose, it will be sufficient to recall that at $z = 0$ (Milly and Eagleson, 1980, p. 24):

$$G_w = -\rho_w K_w \nabla[\psi + z],$$

where ρ_w is the liquid water density, in $\mathrm{kg\,m^{-3}}$; K_w is the soil water conductivity, in $\mathrm{m\,s^{-1}}$; ψ is the matric water potential, in m; and the additional z term represents the gravitational potential, also in m.

The last term of the water balance equation is simply the storage term, i.e. the accumulation or diminution of water in the top soil layer during the current time step:

$$S_w = \frac{\partial \theta}{\partial t} \Delta z,$$

where θ is the volumetric soil water content, in $\mathrm{m^3\,m^{-3}}$; and Δz is the thickness of the top soil layer, in m.

6.2 The surface heat balance

The surface heat balance is a mathematical statement for the fact that the sum of all energy fluxes into or out of the volume representing the first soil layer must balance any change in the temperature of that layer. This fact is expressed mathematically by (Brutsaert, 1982, p. 128)

$$R_n - LE - H - G_h - S_h = 0, \tag{6.5}$$

where R_n is the net radiation balance at the air/soil interface, as computed in Chapter 4, LE is the latent heat flux, H is the sensible heat flux from the surface to the atmosphere, G_h is the heat flux into the ground, and S_h is the storage term, corresponding to the temperature change of the layer. All terms in this equation are in $\mathrm{W\,m^{-2}}$.

The formulae used to estimate the last four terms of this equation will now be reviewed. It will be seen that all terms of Equation (6.5) are dependent on the temperature of the surface, which can therefore be obtained by applying a Newton-Raphson iterative scheme. This method, in effect, searches what value of the soil surface temperature will satisfy Equation (6.5), given all other parameters and variables. And since the latter vary during the day, this scheme, applied at each time step, will yield the time evolution of the soil surface temperature.

The latent heat flux from the surface to the atmosphere is derived as the product of the water vapor flux density E, computed as described in the previous section, by the latent heat of vaporization L:

$$LE = L\ E,$$

where the latent heat of vaporization L, in $\mathrm{J\,kg^{-1}}$, is also a function of the air temperature, in K (Dufour and Van Mieghem, 1975, p. 124):

$$L = (3.14003 - 0.00234\,T)10^6.$$

6.2.1 Sensible heat flux

To compute the sensible heat flux from the soil surface to the atmosphere, an approach similar to that taken to compute the rate of potential evaporation is chosen. Again following the notations of Brutsaert (1982, p. 89):

$$H = Ch_r \rho_a \overline{u}_r c_p (\overline{T}_s - \overline{T}_r), \tag{6.7}$$

where Ch_r is a non-dimensional sensible heat transfer coefficient, to be defined below; ρ_a is the air density, in $\mathrm{kg\,m^{-3}}$; $\overline{u}_r$ is the wind speed, in $\mathrm{m\,s^{-1}}$; $\overline{T}_s$ is the temperature of the soil surface, in K; and $\overline{T}_r$ is the temperature of the air, in K, evaluated at some reference level r, inside the dynamic sublayer. The variables Ch_r, ρ, $\overline{u}_r$ and $\overline{T}_r$ are all evaluated at this same level, taken here as the topmost layer of the model. The remarks made concerning Ce_r in the previous subsection also apply here for Ch_r. Here also, the horizontal bars signify time averages of the appropriate quantities. As for the evaporation rate, the sensible heat flux vanishes when the wind speed tends to zero.

The derivation of the coefficient Ch_r is very similar to that of Ce_r above:

$$Ch_r = \frac{Cd_r^{1/2}}{\left(St_0^{-1} - a_h^{-1} Cd_0^{-1/2} + a_h^{-1} Cd_r^{-1/2}\right)},$$

where

$$\begin{aligned} Cd_r &= \frac{u_*^2}{u_r^2} \\ Cd_0 &= \frac{u_*^2}{u_h^2} \\ a_h &= \frac{k_h}{k} \simeq 1.0 \end{aligned} \tag{6.6}$$

$$St_0^{-1} - a_h^{-1} Cd_0^{-1/2} = 7.3 z_{0+}^{1/4} Pr^{1/2} - 5.0,$$

where St_0 and Pr are now the Stanton and Prandtl numbers, respectively, and k_h is the von Karman constant for sensible heat. The Stanton number is defined as (Brutsaert, 1982, p. 88):

$$St_0 = \frac{H}{\rho_a u_* c_p (T_s - T_h)},$$

where c_p is the specific heat of dry air at constant pressure, and T_h is the air temperature at the top of the canopy. Strictly speaking, this equation should be formulated in terms of the potential temperature, but within the limits of applicability of this model, the actual and the potential temperature do not differ appreciably.

The Prandtl number is the ratio of the kinematic viscosity of the air, ν, computed in Equation (6.4), over the thermal diffusivity of air, κ_h, expressed in $\mathrm{m^2\,s^{-1}}$ and computed as

$$\kappa_h = (-1.58384 + 0.01265\,T)10^{-5}.$$

In this equation, T is the air temperature, in K, as before.

Here also, these expressions apply only to the sensible heat flux from the soil surface to the atmosphere, and do not include any contribution from the vegetation. The above formulations for the latent and sensible heat flux computations apply whether or not there are clouds.

The theory of heat transfer into the ground will be covered in more detail in a later chapter, it will suffice here to recall that this flux can be computed from

$$G_h = -K_h \nabla T,$$

where K_h is the soil thermal conductivity, in $\mathrm{W\,m^{-1}\,K^{-1}}$, and T is the soil temperature, in K.

Finally, the term S_h represents a flux of energy that is stored in the top soil layer as a result of a change in soil temperature:

$$S_h = C_s \frac{\partial T}{\partial t} \Delta z,$$

where C_s is the soil heat capacity, in $\mathrm{J\,m^{-3}\,K^{-1}}$, and Δz is the thickness of the first soil layer, in m.

As mentioned before, the temperature that satisfies the energy conservation Equation (6.5) above is found iteratively.

Chapter 7: Water and Heat Diffusion in the Air

Water is being evaporated at the soil surface and transpired from the vegetation canopy, and carried upward by vertical turbulent diffusion. Similarly, sensible heat is exchanged at the soil surface and between the plants and the atmosphere. This chapter describes the equations used to derive the profiles of specific humidity and temperature in the first few meters above the ground, both inside and outside the canopy.

7.1 Turbulent diffusion of scalar quantities

Since moisture and heat are both scalar and inert quantities (they do not interact with the dynamics of the flow on the space and time scales considered here), their transfer upward may be described by similar differential equations, the general form of which is presented in this section.

The turbulent transport of a scalar inert quantity is assumed to be given by an equation relating the divergence of the vertical flux to the sources or sinks (Brutsaert, 1982, p. 104):

$$\frac{\partial F}{\partial z} = S_f, \tag{7.1}$$

where F is the vertical flux density of that scalar quantity, in Stuff $\mathrm{m}^{-2}\,\mathrm{s}^{-1}$, and S_f is a source or sink term, in Stuff $\mathrm{m}^{-3}\,\mathrm{s}^{-1}$. Obviously, if there are no sources or sinks the flux

F will be constant with height. In this context, the quantity being transported could be either water vapor or sensible heat.

The flux itself is also related to the vertical gradient of the quantity being transported, and to a diffusion coefficient. This is expressed as (Brutsaert, 1982, p. 104)

$$F = -\rho K \frac{\partial c}{\partial z} \tag{7.2}$$

where ρ is the air density, in $\mathrm{kg\,m^{-3}}$; K is the appropriate diffusion coefficient, in $\mathrm{m^2\,s^{-1}}$; and c is the concentration of the quantity transported, in $\mathrm{Stuff\,m^{-3}}$. In the case of water vapor, $c = q$, the specific humidity, and in the case of sensible heat, $c = c_p T$, where T is the air temperature.

The vertical profiles are then computed by integrating these equations, and a boundary condition is needed to specify which solution is to be selected. The boundary condition for the first equation is provided by the surface flux, as computed above. Assuming that there is no accumulation of the transported quantity in the atmosphere, it is logical to impose that the total amount of that quantity in the model be conserved. In other words, the surface flux, possibly increased by the source term, must equal the net flux at the top of the model. This condition completely specifies the profile.

The assumption that the flux (of water vapor or heat) is constant with height in the first few meters of the atmosphere has been the subject of much debate. In the case of heat, a vertical flux divergence calculation would make sense only if other terms were also allowed to play a role, such as the infrared radiation flux divergence. This approximation is probably justified within the context of this model.

Only the diffusion coefficient remains to be specified. Although there is observational evidence that the diffusion coefficients for momentum, heat and water may not be exactly the same, there does not seem to be a consensus on a general formulation. We have assumed that the three coefficient are indeed the same, although their common value is different inside the canopy than outside of it.

The diffusion coefficient K is computed as follows. First of all, outside or above the canopy, the turbulent diffusion coefficient is given by (e.g. Sutton, 1953, p. 81, Sellers, 1965, p. 151, or Brutsaert, 1982, p. 103)

$$K(z) = ku_*(z - d),$$

where z is the altitude above the ground, in m, k is the von Karman constant, and d is the displacement height defined in Chapter 5. K is expressed in $m^2 s^{-1}$.

Brutsaert (1982, p. 106) suggests that within a uniform canopy, the diffusivity at any level z inside the vegetation can be computed from

$$K_v(z) = K(h_v) \exp(-a\xi),$$

where $K(h_v)$ is the diffusion coefficient defined above at a height h_v corresponding to the top of the canopy, in m, $a = h_v/(h_v - d)$ and $\xi = (h_v - z)/h_v$.

This completely determines the profile of an arbitrary scalar inert quantity, both inside and outside the vegetation canopy, provided the vertical distributions of the sources and sinks are defined. This is the subject of the next sections.

7.2 Evapotranspiration from the canopy

The net flux of water from the leaves to the atmosphere may be attributed to two factors: the transpiration of the leaves, a necessary by-product of the process of photosynthesis, and the evaporation of water that may be standing on the leaves after precipitation has been intercepted. The rate of transpiration, in turn, depends on various soil, plant and atmospheric factors, and is controlled by the stomatal aperture. These stomates are explicitly represented in this model, and they react to light, temperature, atmospheric humidity, and, through the plant water potential, to the ability of the root system to pick

up water in the various soil layers. Not unexpectedly, this part of the model is one of the most complex ones.

7.2.1 Interception of precipitation

The amount of water intercepted by the leaves depends on past precipitation and on the structure of the canopy, as well as on the ability of the leaves to store water on their upper surfaces. Since the leaves get wetter and drier with the passage of rain events, the contributions of the transpiration and evaporation to the net flux of water (from the dry and wet parts of the canopy to the atmosphere, respectively) are time dependent.

In order to compute the actual water fluxes from transpiration and evaporation, it is necessary to estimate the proportions of leaves which are dry and wet in each leaf layer. Indeed, it is assumed that no transpiration can take place from the wet parts of the leaves and no evaporation takes place from their dry parts. This new parameter (the fractional area of wet leaves ϵ_e) is obtained from the following system of equations, applied to each canopy layer:

$$\begin{aligned} \frac{\partial P_i}{\partial z} &= \frac{\partial W}{\partial t} && \text{if } W < W_m \\ \frac{\partial P_i}{\partial z} &= 0 && \text{if } W = W_m \end{aligned} \tag{7.3}$$

where P_i, a function of both z and t, is the rate of precipitation, in $\mathrm{kg\,m^{-2}\,s^{-1}}$; W is the actual storage of water on the foliage of this particular canopy layer, in $\mathrm{kg\,m^{-3}}$; and W_m is the maximum amount of water that can be stored in that layer, also in $\mathrm{kg\,m^{-3}}$. This maximum value is computed below.

Equation (7.3) means that whenever the rate of precipitation varies with height in the canopy, there must be some accumulation of water on the leaves, and the rate of this accumulation is, in fact, equal to the divergence of the precipitation flux. This occurs in particular during the first stages of a precipitation event that follows a dry period. Such a process cannot obviously continue indefinitely, since the leaves have only a finite capacity to hold water. So when the maximum storage W_m is achieved, there cannot be anymore

accumulation and the precipitation flux cannot experience any more divergence. This is the role of the second part of Equation (7.3).

The time variation of the amount of water stored on a leaf layer is in turn described by

$$\frac{\partial W}{\partial t} = LAD[\epsilon_r P - \epsilon_e E_*],$$

where LAD is the leaf area density defined in Chapter 2, in $\mathrm{m^2\,m^{-3}}$, ϵ_r is a non-dimensional rainfall collection efficiency coefficient, ϵ_e is the fractional area of wet leaves, and E_* is the rate of evaporation from the wet parts of the leaves, in $\mathrm{kg\,m^{-2}\,s^{-1}}$.

The coefficient ϵ_r is there because there cannot be any increase in the water storage beyond the maximum allowed:

$$\epsilon_r = 1 \qquad \text{if } W < W_m$$

$$\epsilon_r = 0 \qquad \text{if } W \geq W_m$$

while the fractional area of wet leaves is assumed to be proportional to the amount of water actually stored in this layer:

$$\epsilon_e = \epsilon_e^{Max}(W/W_m).$$

The value of ϵ_e^{Max} is taken to be 0.8 (the same value was selected by Sellers and Lockwood, 1981a, p. 402 ff.), and could be decreased for grassy plants or cacti. This scheme implies that the thickness d, in m, of the film of water on the wet parts of the leaves is constant. The maximum amount of water that can be stored on the leaves of a given canopy layer is then given by

$$W_m(z,t) = LAD(z,t)\epsilon_e^{Max}\rho_w d,$$

where ρ_w is the density of liquid water, in $\mathrm{kg\,m^{-3}}$.

Since the rate of precipitation is one of the forcing parameters of this model, and since the rate of evaporation is computed (as will be described below), these equations can be

solved to estimate the amount of water stored on the leaves, as a function of height in the canopy and of time.

7.2.2 Transpiration and stomatal response

In order to compute the transpiration rate from the leaves, the stomatal resistance to the flow of water will be required. This topic is dealt with separately here to unclutter the discussion. The stomates are the little openings in the leaf through which the plant exchanges water vapor and carbon dioxide with the atmosphere; water vapor exits the plant while CO_2 enters the stomates. Carbon dioxide is an essential ingredient of the process of photosynthesis, and the evaporation of water in the stomates and its subsequent transpiration may represent a significant cooling mechanism for the leaves.

Different plant species have different "strategies" to control their rate of transpiration; for example, some peculiar desert species can open their stomates only at night when there is less atmospheric evaporative demand. But in most cases, a plant opens its stomates during the day to obtain its carbon dioxide when the solar radiation also allows photosynthesis to take place. For the purpose of this model, the vegetation is assumed to be photosynthetically active during the day.

Since plants cannot acquire CO_2 without losing water, they must manage their water supply to ensure survival: they must open the stomates during the day to get CO_2, but excessive losses of water may generate a water stress which will affect the process of tissue formation. Worse, the reduced effectiveness or lack of cooling through transpiration could also threaten the physical integrity of the plant due to excessive temperatures (denaturation).

Observations have shown that the opening and closing of the stomates depend on the plant species, the level of (photosynthetically active) solar radiation, the difference of humidity across the opening of the stomate, the leaf temperature and the water potential inside the plant (Jones, 1983, p.104 ff.). By analogy to the flow of electricity through a

resistor, the flow of water through the stomates is often parameterized as the product of a *stomatal resistance* and the gradient of specific humidity across the stomatal aperture, among other factors (See below.) In this model, the stomatal conductance g_S (the inverse of the stomatal resistance) is computed as follows (Jones, 1983, p. 123):

$$g_S = g_0 + g_r F_R F_S F_P F_T S, \tag{7.4}$$

where g_0 is the minimum conductance, in $\mathrm{m\,s^{-1}}$, a characteristic of the plant species, and g_r is the maximum range of conductance (maximum less minimum) for the same species. The correcting factor S will be explained later. Each of the following F factors have values between 0.0 and 1.0. F_R represents the influence of solar radiation, F_S is the specific humidity factor, F_P is the water potential factor and F_T is the temperature factor. These are computed with

$$F_R = 1 - \exp(-k_1 R) \qquad \text{if } 0 < R$$

$$F_R = 0 \qquad \text{if } R < 0$$

$$F_S = 1 - (G/k_2) \qquad \text{if } 0 < G < k_2$$

$$F_S = 0 \qquad \text{if } G < 0 \text{ or } k_2 < G$$

$$F_P = a + k_3 \psi_p \qquad \text{if } -2.53\,10^6 < \psi_p$$

$$F_P = 0 \qquad \text{if } \psi_p < -2.53\,10^6$$

$$F_T = 1 - k_4 (T - T_m)^2 \qquad \text{if } 273 < T < 333$$

$$F_T = 0 \qquad \text{if } T < 273 \text{ or } 333 < T$$

where R is the flux density of solar radiation, in $\mathrm{W\,m^{-2}}$; G is the specific humidity difference between the stomate and the atmosphere, in $\mathrm{kg\,kg^{-1}}$; ψ_p is the plant water potential in the leaf, in Pa; T is the leaf temperature and T_m a maximum temperature, both in K. The various k coefficients and the constant a are species-specific; in the current version of this model, $k_1 = 0.02$, $k_2 = 6000$, $k_3 = 0.4348\,10^{-6}$, $k_4 = 6.9388\,10^{-4}$, $a = 1.1$, and $T_m = 308\,\mathrm{K}$.

Since these correcting factors enter a product, they must all have relatively large values for the conductance to increase, and even if only one of these factors is comparatively low,

the conductivity will be low irrespective of the other factors. For example, at night there is no solar radiation and $F_R = 0$ implies a minimum conductance (maximum resistance). The stress factor, S, in Equation (7.4), is a further coefficient to account for the ability of the root system to supply the water the leaves would want to evaporate. If the root system has difficulty extracting water from the soil, the value of S is decreased from 1 so that the opening of the stomates is always consistent with the supply of water by the roots.

The computation of the potential transpiration rate from the leaf layers to the atmosphere starts by estimating the evaporative demand from the atmosphere. This is the flux density of water, in $\mathrm{kg\,m^{-2}\,s^{-1}}$, from the leaf to the atmosphere, that would occur if the root system were able to supply the water to the plant at the same rate. Following Jones (1983, p. 114), this is given by

$$T_r = 2.17\,10^{-3}(g_S + g_a)GL_i/T_\ell,$$

where T_r is the actual rate of transpiration from a leaf layer to the atmosphere, in $\mathrm{kg\,m^{-2}\,s^{-1}}$; g_S and g_a are the stomatal and boundary layer conductances, in $\mathrm{m\,s^{-1}}$, respectively; G is the difference of water vapor pressure between the stomate and the atmosphere, in Pa; L_i is the leaf area index in that particular leaf layer (i.e., the product of the leaf area density by the thickness of that layer), in $\mathrm{m^2\,m^{-2}}$; and T_ℓ is the leaf temperature, in K. The factor $2.17\,10^{-3}$ and the leaf temperature dependency enter this equation in order to convert the vapor pressure difference into a specific humidity difference (Jones, 1983, p. 88).

The conductance g_a is a function of the size and shape of the leaf, as well as of the wind speed. Empirical studies have shown that the boundary layer conductance for heat transfer for flat plates in laminar forced convection is (Jones, 1983, p. 53):

$$g_a = k\,6.62\,10^{-3}(u/d_\ell)^{1/2},$$

where u is the wind speed, in $\mathrm{m\,s^{-1}}$; d_ℓ is a typical linear dimension of the leaves, in m; and k is a constant defined below. In fully turbulent air, the boundary layer conductance for heat and for water vapor are the same. When the air flow becomes laminar, or stops altogether, the conductance for water vapor may be a few percent higher than that for heat, because the transport processes become purely diffusive and the diffusion coefficients for heat and moisture are somewhat different (Jones, 1983, p. 48–55). In the current version of the model, the two boundary resistances have been assumed the same.

According to Jones, this equation (which applies to laminar flow conditions) underestimates the boundary layer conductance of actual leaves in turbulent flow by a factor 1 to 2. For this reason, the conductance has been increased by a factor $k = 1.5$ in this model. (The boundary layer conductance has also been shown to depend on the presence of hair on the surface of the leaves.)

7.2.3 Water supply by the roots

The next step involves computing the water potential in the root system, since the gradient between this value and the water potential in the soil will determine the rate of extraction of water by the roots. The water potential in the roots is derived from the water potential in the leaves, assuming that the stem resistance is small relative to the gravitational potential difference.

The model of roots adopted here follows closely that developed by Federer (1979, p. 556 ff.). Using his notations, the rate of transfer E_r of water from the soil to the roots is given by

$$E_r = \frac{(\psi_s - \psi_r)}{(\eta\chi/(\Delta z\,\varsigma))},$$

where E_r is expressed in $\mathrm{kg\,m^{-2}\,s^{-1}}$; ψ_s and ψ_r are the soil and root water potential respectively, in m; η is a conversion factor equal to 9807 $\mathrm{Pa\,m^{-1}}$; Δz is the thickness of the soil layer, in m; and ς is the geometric mean potential $(\psi_s\psi_r)^{1/2}$.

The function χ is defined by

$$\chi = (1/(8\pi L_r))[\delta - 3 - 2\ln\delta/(1-\delta)],$$

where L_r is the length of root per unit volume of soil, in $\mathrm{m\,m^{-3}}$.

If the roots are uniformly spaced in that soil layer, $L_r = 1/(\pi R_2^2)$, where R_2 is half the mean distance between the roots, in m; and $\delta = \pi R_1^2 L_r = R_1^2/R_2^2$, where R_1 is the mean root radius, in m. R_1 and R_2 are, of course, different for different plant species and/or environments; the constant values taken in this model are $R_1 = 10^{-3}$m, and $R_2 = 10^{-1}$m (Federer, 1979, p. 557).

These equations allow the estimation of the theoretical fluxes of water required by each leaf layer, and supplied by each root layer. The total supply can then be compared to the total demand, and since they do not generally match, the actual rate of transpiration must be taken as the minimum of these two fluxes. If the supply exceeds the demand, the root resistance is artificially increased; and if the demand exceeds the supply the stomatal resistance is increased, until the supply and the demand match. Of course, the rate of water extraction by the roots is a sink for the soil water diffusion Equation (8.1).

It may be of interest to note here that since the stomatal resistance of each leaf layer is dependent on the temperature of the leaves, and since the latter is obtained by solving iteratively an energy balance equation, these computations may have to be repeated more than once for any given time step. The derivation of the leaf temperatures is explained in the next section.

7.3 Sensible heat exchanges in the canopy

The canopy can also be a source or sink of heat for the atmosphere, since sensible heat exchanges occur between the air and the leaves. These, in turn, depend on the

leaf temperature. The temperature of each leaf layer is obtained from an energy balance equation similar to the one used above for the top soil layer:

$$R_n - LE - H - S_p = 0, \tag{7.5}$$

where R_n is the net radiation balance for the leaf layer, LE is the latent heat flux, H is the sensible heat flux and S_p is the storage term. All terms of Equation (7.5) are expressed in $\mathrm{W\,m^{-2}}$.

This equation can be solved iteratively with a Newton-Raphson scheme to yield the temperature of the leaves in that particular leaf layer. First, a radiation balance is computed, to estimate the net radiative absorption in the layer, which provides a major heating term (see Chapter 4). The loss of energy due to latent heat release is a direct function of the evapotranspiration loss computed in the preceding section. The sensible heat flux and the change in internal energy of the leaves corresponding to their change in temperature are the last two subtopics of this section.

Following Jones (1983, p. 187), the sensible heat flux between a leaf and the air is given by

$$H = \rho_a c_p (T_\ell - T_a) g_a,$$

where ρ_a is the air density, in $\mathrm{kg\,m^{-3}}$; c_p is the specific heat of dry air at constant pressure, in $\mathrm{J\,kg^{-1}\,K^{-1}}$; T_ℓ and T_a are the leaf and air temperatures, respectively, in K; and g_a is the leaf boundary layer conductance, in $\mathrm{m\,s^{-1}}$, as computed above.

The last term in Equation (7.5) is the storage term, evaluated as follows:

$$S_p = c\, m_\ell \frac{\partial T_\ell}{\partial t}$$

where c is the heat capacity of the green plant material, in $\mathrm{J\,kg^{-1}\,K^{-1}}$ (taken to be the same as that of water); and where m_ℓ is the mass of green leaves in the particular leaf layer, in $\mathrm{kg\,m^{-2}}$.

Chapter 8: Water and Heat Diffusion in the Soil

Water in the soil moves continually, albeit slowly, in response to gravitational and matric potential gradients. To some extent, soil water may move horizontally, but in this model only vertical diffusion is allowed. Apart from the initial soil water profile, water is supplied at the soil surface from precipitation, and removed from the soil by surface evaporation and root extraction. Similarly, heat diffuses in the soil because the net absorption of solar and infrared radiation heats up the top soil layer during the day and cools it down during the night, thereby creating a vertical gradient of temperature.

Both of these processes are included in this model because they influence the volumetric soil moisture content and the temperature of the top soil layer, whose values are computed from water and energy balance equations, as was seen in Chapter 6. In addition, it is important to model the downward diffusion of soil water so that the plants can extract it with their root systems and transpire it through their leaves.

8.1 Diffusion of water in the soil

The theory of soil water infiltration was pioneered and developed by Philip (1957a, 1957b, 1957c, 1975) among others, and is systematically presented in a number of textbooks; for example Eagleson (1970). It will therefore be sufficient to briefly describe the equations and parameterizations used.

In this model, soil water exists in two phases: liquid and vapor. Both phases are combined as far as the diffusion is concerned, and the amount of water vapor is computed diagnostically from the water potential and soil temperature.

The dynamics of the motion of liquid water in the soil can be derived from the conservation of mass equation, the momentum equation (the Navier-Stokes equations of fluid mechanics, or equations derived from them), and an equation of state relating the local pressure to the volumetric water content of the soil and the density of water (Eagleson, 1970, p. 261 ff.).

Following Milly and Eagleson (1980, p. 24), the flow of liquid water inside an unsaturated soil is described by

$$F_w = -\rho_w K_w \nabla[\psi + z],$$

where ρ_w is the liquid water density, in $\mathrm{kg\,m^{-3}}$; K_w is the soil water conductivity, in $\mathrm{m\,s^{-1}}$; ψ is the pressure or matric water potential, in m; and the additional z term represents the gravitational drainage. For both the water and the heat diffusion equations, the running coordinate z increases downward from an origin located at the interface between the soil and the atmosphere. F_w is expressed in $\mathrm{kg\,m^{-2}\,s^{-1}}$. This equation is combined with the equation for the conservation of mass to yield the diffusion equation for liquid water in the soil. The details of the derivation are standard and can be found in a number of textbooks, they will not be repeated here. It should also be mentioned that the model may be made more accurate by including the flux of water vapor in the soil, and this is done by considering a combined liquid and vapor conductivity, as shown below.

The movement of water in the soil can be expressed in terms of the soil water content θ, in $\mathrm{m^3\,m^{-3}}$, or in terms of the soil water pressure or matric potential ψ, in m. We have adopted a mixed formulation, where the diffusion equation is expressed in terms of the water potential (ψ remains continuous even when adjacent soil layers are characterized by different soil types), and where the hydraulic conductivities and diffusivities are computed

in terms of the soil water content, as usual. Following Milly and Eagleson (1982, p. 132), the equation for the diffusion of water in the soil can be written:

$$\frac{d\theta}{d\psi}\frac{\partial\psi}{\partial t} = \frac{\partial}{\partial z}\left[[K(\theta) + D_{\psi v}(\psi,\theta)]\frac{\partial\psi}{\partial z} + K(\theta)\right] + S(\theta) \tag{8.1}$$

where ψ is the soil water pressure (matric) potential, in m; a measure of the local energy level of the water. $K(\theta)$ is the liquid water conductivity, in $\mathrm{m\,s^{-1}}$; and $D_{\psi v}$ is the water vapor conductivity, also in $\mathrm{m\,s^{-1}}$. The last term on the right hand side, $S(\theta)$, is a source and sink term, expressed in $\mathrm{m\,s^{-1}}$, to account, for example, for the extraction of soil water by the roots of the plants. The first factor on the left hand side is a scale or conversion factor between the two formulations of soil water.

In arid regions, the transport of water vapor inside the soil may be important with respect to the diffusion of liquid water, and this process may be accounted for separately. Equation (8.1), however, represents the combined flux of liquid water and water vapor, thereby avoiding the need for an additional equation.

8.1.1 Hydraulic properties of the soil

In order to integrate this diffusion equation, both the conductivity and diffusivity coefficients of water in the soil must be available. It turns out that these coefficients are very much dependent on the volumetric soil water content θ, and, of course, on the nature of the soil.

No general theory has been developed yet to compute these coefficients from the physical, chemical and structural characteristics of the soil. The problem is further complicated by the fact that water diffuses more readily into a dry soil than it diffuses out of a wet soil (a phenomenon known as hysteresis). The diffusivity coefficient therefore depends also on the past wetting and drying history of the soil. Hysteresis has not been included in the current version of the model, however, mainly because the level of sophistication and

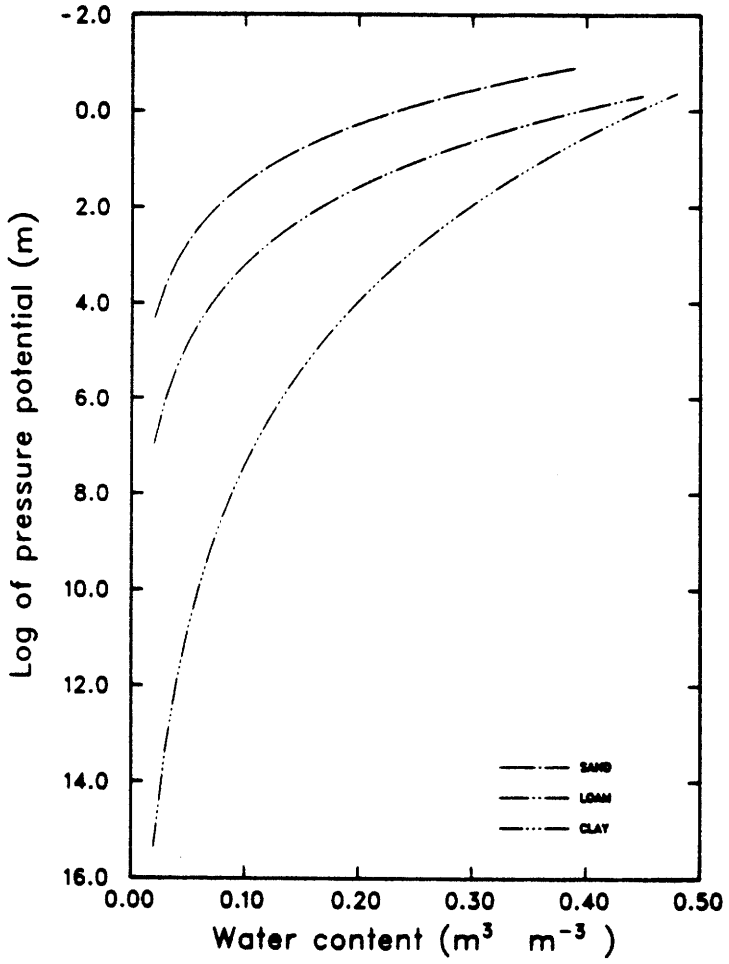

Figure 8.1: Moisture characteristic $\psi = \psi(\theta)$ for sand (– · –), loam (– · · –), clay (– · · · –)

accuracy of the other components of this model, notably the vegetation parameterization, do not warrant an overly complex soil model.

In order to specify the various terms of equation (8.1), we must first adopt a functional relationship between the soil water content θ, in $m^3 m^{-3}$, and the soil water potential ψ, in m. We follow the dependency derived by Campbell (1974) and developed further by Clapp and Hornberger (1978, p. 601):

$$\psi = \psi_s(\theta/\theta_s)^{-b},$$

where the subscript s indicates a saturated value, and the exponent b is a parameter characteristic of the soil type. This functional relationship is shown in Figure 8.1. The

following table lists the values of the exponent b for various soils, together with other soil-dependent parameters.

Table 8.1: Soil dependent parameters

Soil texture	b	ψ_s	θ_s	K_s	clay	θ_{FC}	θ_{WP}
Sand	4.05	-0.121	0.395	$1.76\,10^{-4}$	0.03	0.103	0.040
Loamy sand	4.38	-0.090	0.410	$1.56\,10^{-4}$	0.06	0.144	0.062
Sandy loam	4.90	-0.218	0.435	$3.47\,10^{-5}$	0.09	0.187	0.083
Silt loam	5.30	-0.786	0.485	$7.20\,10^{-6}$	0.14	0.320	0.146
Loam	5.39	-0.478	0.451	$6.95\,10^{-6}$	0.19	0.253	0.113
Sandy clay loam	7.12	-0.299	0.420	$6.30\,10^{-6}$	0.28	0.246	0.107
Silty clay loam	7.75	-0.356	0.477	$1.70\,10^{-6}$	0.34	0.343	0.172
Clay loam	8.52	-0.630	0.476	$2.45\,10^{-6}$	0.34	0.352	0.152
Sandy clay	10.40	-0.153	0.426	$2.17\,10^{-6}$	0.43	0.332	0.170
Silty clay	10.40	-0.490	0.492	$1.03\,10^{-6}$	0.49	0.458	0.231
Clay	11.40	-0.405	0.482	$1.28\,10^{-6}$	0.63	0.448	0.231

Source: Clapp and Hornberger (1978, p. 604); Sellers (1965, p. 133).

In this table, K_s is the saturated hydraulic conductivity; the "clay" column represents the clay fraction in the soil; θ_{FC} is the volumetric soil water content, in $\mathrm{m}^3\,\mathrm{m}^{-3}$, when the soil is at field capacity; and θ_{WP} is the so-called wilting point, the volumetric soil water content at which the plants cannot extract any more water from the soil, also in $\mathrm{m}^3\,\mathrm{m}^{-3}$.

In some cases, it may be possible to derive simplified analytical expressions for both the conductivity and diffusivity coefficients of liquid water in the soil, but for most practical purposes, a parameterization is required. Again following Clapp and Hornberger (1978, p. 601), the soil water conductivity is parameterized as

$$K_\theta = K_s[\theta/\theta_s]^{2b+3},$$

where K_s is the saturated (maximum) soil water conductivity, in $\mathrm{m\,s}^{-1}$; θ_s is the saturated (maximum) volumetric soil water content, in $\mathrm{m}^3\,\mathrm{m}^{-3}$; and b is the same soil-dependent empirical exponent as above.

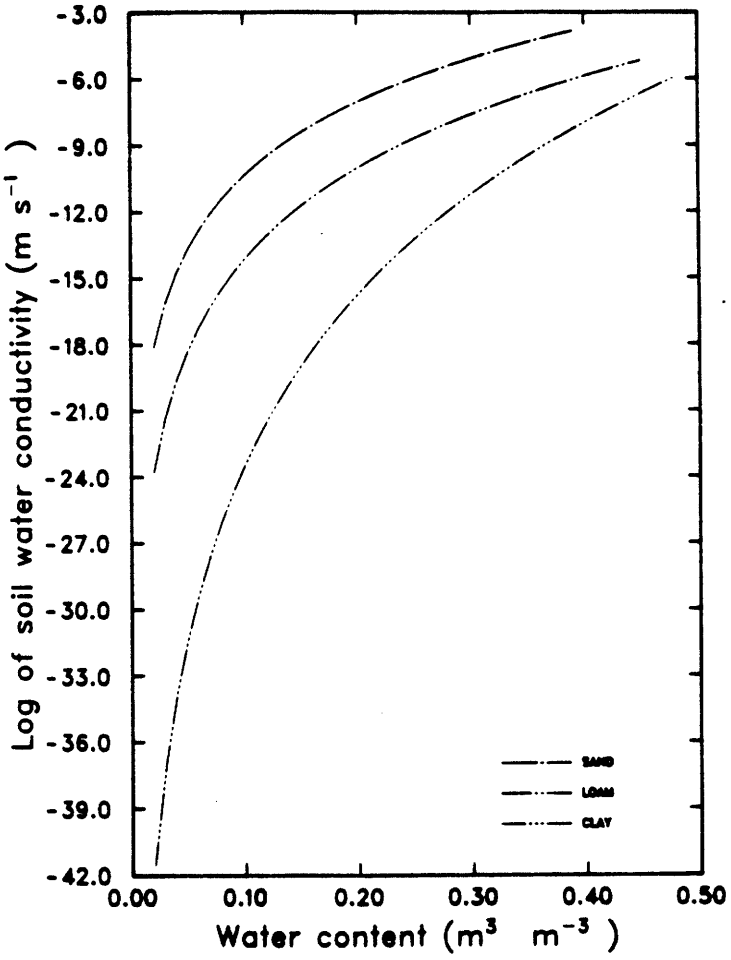

Figure 8.2: Soil water conductivity for sand (– · –), loam (– · · –), and clay (– · · · –)

Figure 8.2 shows this very strong dependency of the soil hydraulic conductivity on the volumetric soil moisture content. Saturated values of the soil water potential, the soil moisture content and the hydraulic conductivity, as well as the value of b have to be determined from laboratory experiments. Clapp and Hornberger (1978, p. 604) compiled the results of a study of 1446 soil samples from 34 locations in the United States into eleven soil types, from sand to clay, and the four first columns of Table 8.1 show the values used in this model.

Initial and boundary conditions are needed to integrate this partial differential equation in time. The initial conditions can be selected in a number of ways. Most of the

time, constant initial soil moisture profiles were selected, and the model was integrated for two to four days. By that time, the soil moisture of the top soil layers seemed to have stabilized. It should be remembered that the profiles at the end of a run can be saved to serve as initial conditions for a subsequent run, and this facility was often used.

In order to solve the diffusion equation, two boundary conditions must be specified as functions of time, one at each end of the soil column. The volumetric soil water content of the top soil layer, which was derived from a water budget equation, as explained in Chapter 6, is used as the top boundary condition. A very simple condition has been selected at the bottom of the soil column, namely that no flux of water leaks in or out of the column. More sophisticated lower boundary conditions, such as a gravitational drainage at the bottom of the column, could be included at a later stage, or for investigating specific issues, but this was not considered a priority in view of the very short time scales studied here.

There are no sources of water in the soil of the model, but there is an important sink, namely the extraction of water by the roots of the plants, whose vertical distribution can be specified. The rate of water extraction depends on the evaporative demand of the atmosphere and the availability of water in the soil, as explained in the previous chapter.

The diffusion equation is discretized and integrated in time using a classical Crank-Nicolson scheme (see Gerald, 1978, p. 400 ff.) This involves solving a three-diagonal matrix equation. Standard routines are available at NCAR to perform the necessary manipulations in an optimal way on the Cray computers.

8.2 Diffusion of heat in the soil

The theory of soil heat diffusion was pioneered and developed by de Vries (1963, 1975), among others, and is also presented in a number of textbooks (e.g., Sellers, 1965). It will therefore be sufficient to briefly describe the equations and parameterizations used.

Energy exchanges within the soil take place under the form of radiation, latent or sensible heat. The latter is by far the most important and is the only mechanism included in the current version of the model.

Empirical evidence shows that the sensible heat flux through a given surface is proportional to the gradient of temperature across the same surface:

$$F_h = -K_h \nabla T,$$

where F_h is the heat flux, in $\mathrm{W\,m^{-2}}$; K_h is the heat conductivity, in $\mathrm{W\,m^{-1}\,K^{-1}}$; and T is the temperature, in K.

Combining this equation with the continuity equation for heat and assuming an isotropic medium, one can derive the following diffusion equation:

$$C_s \frac{\partial T}{\partial t} = \frac{\partial}{\partial z}\left[K_h \frac{\partial T}{\partial z}\right] + S_h, \tag{8.2}$$

where T is the temperature of the soil, in K; t is the time, in s; z is the vertical coordinate, in m; C_s is the soil specific heat, in $\mathrm{J\,m^{-3}\,K^{-1}}$; K_h is the soil heat conductivity coefficient, in $\mathrm{W\,m^{-1}\,K^{-1}}$; and S_h represents the sources and sinks of heat in the column, in $\mathrm{J\,m^{-3}\,s^{-1}}$. No sources or sinks of heat have been implemented in the current version of the soil model.

8.2.1 Thermal properties of the soil

In order to integrate the soil heat diffusion equation developed above, both the conductivity and diffusivity coefficients of heat in the soil must be available. It turns out that these coefficients are very much dependent on the volumetric soil water content, and, of course, on the nature of the soil.

de Vries (1975) developed a theory to compute these coefficients on the basis of a conceptual model of the soil. It is recognized that the agreement between this theory and the measurements made on specific soils is not better than 10%, but this model will be followed in the absence of a better scheme (Kimball et al., 1976). In any case, the accuracy

of other parts of this model, notably the representation of plant processes, do not warrant a better parameterization of the thermal coefficients.

The soil is conceptualized as a collectionof *grains* embedded in a continuous *medium*; water in a saturated soil, or air in a completely dry soil. Since the heat conductivities of the various constituents of the soil are quite different, it is expected that the least conductive constituent will determine the bulk conductivity of the soil.

It turns out that, in relative terms, the mineral constituents are good heat conductors, water is moderately good, and organic matter and air are poor conductors, as shown in the Table 8.2 (de Vries, 1975, p. 9).

Table 8.2: Thermal properties of soil components

Substance	ρ	C_s	λ
Quartz	$2.66\ 10^3$	$2.00\ 10^6$	8.80
Other Minerals	$2.65\ 10^3$	$2.00\ 10^6$	2.90
Organic Matter	$1.30\ 10^3$	$2.50\ 10^6$	0.25
Liquid Water	$1.00\ 10^3$	$4.20\ 10^6$	0.57
Air	1.25	$1.25\ 10^6$	0.025

Source: de Vries (1975, p. 9).

The volume fraction of each soil constituent is computed as follows: first, the organic matter content is given (this parameter is currently kept constant, but could conceivably be a function of time), and the porosity or maximum volumetric soil water content is obtained as a function of soil type only. The mineral soil fraction is then computed as that fraction of the bulk volume not used by organic matter or by the water when the soil is saturated. Finally, the actual water fraction is computed, and the fraction of air is the residual. This implies that the organic matter is part of the solid soil fraction: it "encroaches" on the mineral fraction rather than on the soil water fraction.

The theory developed by de Vries for computing the soil heat conductivity can be summarized as follows: the thermal conductivity coefficient K_h of the previous section is

parameterized as (de Vries, 1975, p. 10 ff.)

$$K_h = \frac{\sum_i k_i x_i \lambda_i}{\sum_i k_i x_i},$$

where the summations are taken over all constituents i; k_i is a non-dimensional proportionality coefficient that is assumed to depend on the shape and the orientation (but not the size) of the grains of soil; x_i is the volume fraction of the i^{th} constituent, in $m^3\,m^{-3}$; and λ_i is the thermal conductivity of the same constituent, in $W\,m^{-1}\,K^{-1}$. The soil constituents are the various mineral soil components, water, air, and organic matter.

For randomly distributed ellipsoidal constituent "particules", these coefficients k_i can, in turn, be estimated as follows:

$$k_i = (1/3) \sum_j \left[1 + (\frac{\lambda_i}{\lambda_0} - 1) g_i \right]^{-1},$$

where g_i can be interpreted as a shape factor for each constituent, depending only on the relative sizes of the principal axes of the ellipsoid. The factor λ_0 is the thermal conductivity of the medium, usually taken to be water.

It is seen that the shape factor of the water ($i = 0$) does not have to be computed, since it is always multiplied by zero. Furthermore, the shape factors of mineral and organic matter particles are assumed constant in space and time: at present, they are fixed at 0.15 and 0.50 respectively (Milly and Eagleson, 1982, p. 64). Consequently, only the shape factor of air pores must be recomputed when the amount of liquid water changes in the soil.

At very low liquid water content, the medium should be air instead of water, but it has been suggested that water could be taken as the medium over all ranges of the actual water content, provided that some correction to the air shape factor was introduced (Kimball et al, 1976).

The procedure for introducing this correction has been extensively discussed by de Vries and Kimball, and reduces to a piecewise interpolation between the cases of saturation

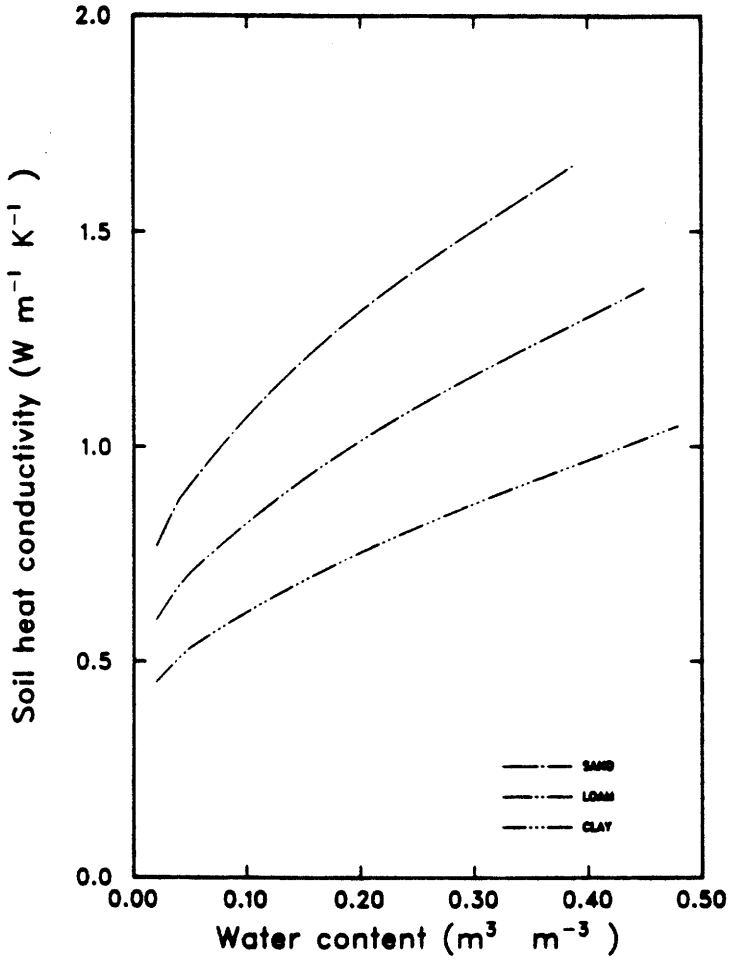

Figure 8.3: Soil heat conductivity for sand (– · –), loam (– · · –), and clay (– · · · –)

and oven dryness. In this work, the following scheme has been implemented:

$$g_a = 0.013 + 0.518\,W \qquad \text{for } W < 0.10$$

$$g_a = 0.035 + 0.298\,W \qquad \text{for } W > 0.10,$$

where $W = \theta/\theta_s$ is the ratio of the actual over the saturated (maximum) soil water content at that location and time. Figure 8.3 shows the dependency of the soil heat conductivity on the volumetric soil water content.

The next step is to compute the heat capacity of the soil, but this is straightforward:

$$C_s = \sum_i x_{si} C_{si} + x_w C_w + x_a C_a,$$

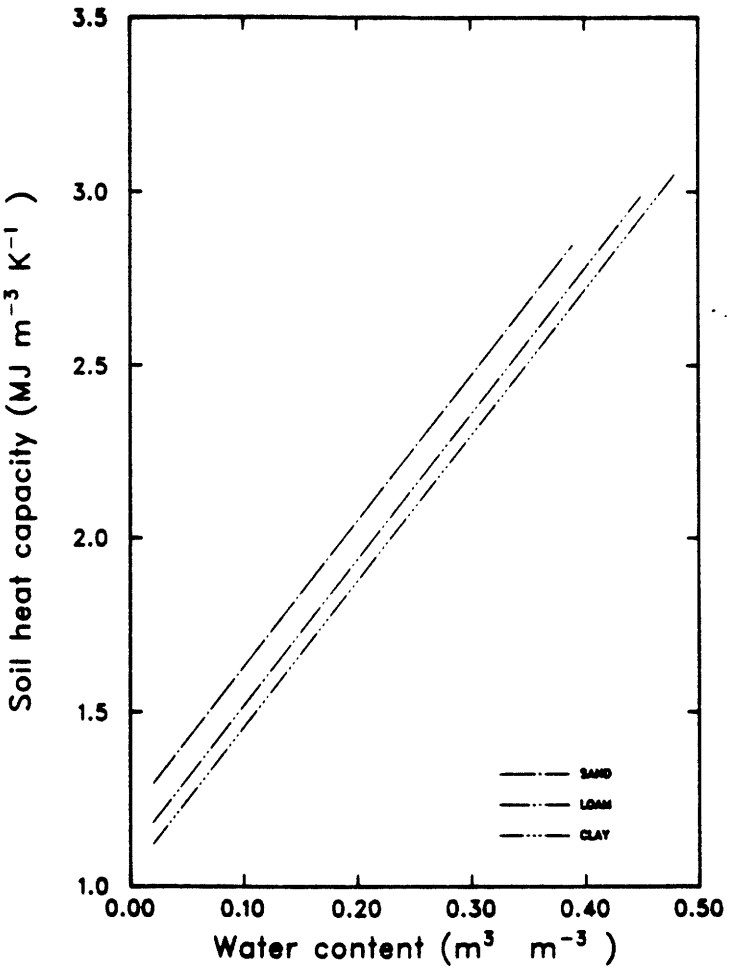

Figure 8.4: Soil heat capacity for sand (– · –), loam (– · · –), and clay (– · · · –)

where C_s denotes the bulk heat capacity of the soil, and the summation is over all mineral and organic soil components. The subscript si refers to the ith soil component (mineral or organic matter), w to the water component, and a to the air component. In practice, since all mineral components of the soil have the same specific heat, this equation reduces to four terms: those corresponding to the mineral component, organic matter, water, and air. The latter may even be discarded in view of its minuscule contribution. As can be seen from Figure 8.4, the soil heat capacity varies by a factor 2 over the range of possible soil moistures.

Finally, the thermal diffusivity is the ratio of the thermal conductivity over the heat

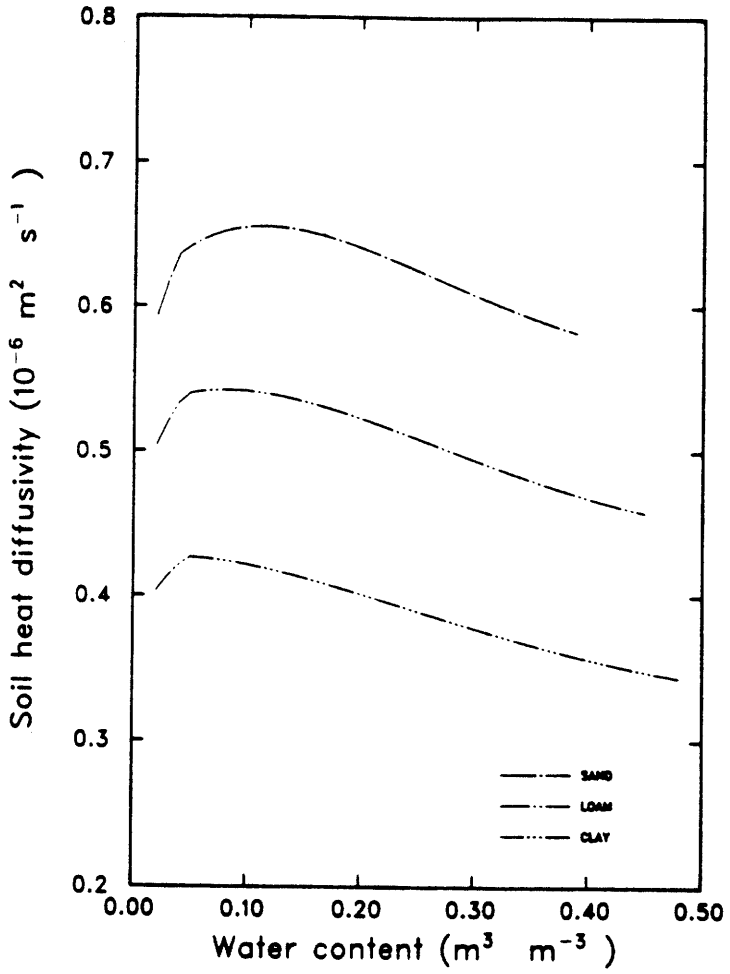

Figure 8.5: Soil heat diffusivity for sand (– · –), loam (– · · –), and clay (– · · · –)

capacity, and its dependency on the volumetric soil moisture content is shown in Figure 8.5. This parameter enters the computations only after both sides of Equation (8.2) have been divided by the soil specific heat.

As for the soil water diffusion equation, initial and boundary conditions are needed to integrate this partial differential equation in time. Constant profiles of temperature were usually taken as initial conditions, and when the model is integrated over two to three days, the well known thermal waves have established themselves in the soil. As for the case of soil water, the temperature profiles in the soil at the end of a run can be preserved and used as initial condition for a later run.

The top boundary condition is given by the surface temperature computed in Chapter 6, and the lower boundary condition is that there is no heat flux at the bottom of the soil column.

The numerical procedure to integrate the heat diffusion equation follows a Crank-Nicolson scheme very similar to the one used for the water diffusion.

PART 2: SENSITIVITY ANALYSES AND MODEL RESULTS

The model described in the first part of this thesis is now applied to a few special case studies to identify its sensitivity to differences in forcing. As was mentioned earlier, no attempt was made to try to design a model applicable to a specific situation. Rather, the goal was to develop a generic research tool that could provide as much flexibility and detail as possible.

Chapter 9 describes in detail the results of a particular run of this model, taken as reference, and compares the simulated micro-climate of the four submodels integral to the overall model. Chapter 10 presents selected results from additional runs, where one parameter or forcing has been changed. Finally, Chapter 11 discusses the work done from a more general point of view, and suggests improvements and applications that would be of interest.

Chapter 9: Results from the Base Run

As mentioned in Chapters 1 and 2, this model is really a composite of four submodels which all run in parallel (see Figure 2.1). These four submodels are all forced identically. This setup is particularly convenient for sensitivity analyses, since it automatically provides four comparable cases.

9.1 Background information

The model currently uses 0.3 seconds of computer time per step of integration on the NCAR Cray-1 super-computer. This includes all computations for the four submodels, as well as the necessary input and output operations. A graphics post-processor has been implemented to read the model results and generate figures that can be better analyzed. In high-quality mode, the graphics post-processor takes about 0.3 to 1.2 seconds Cray computer time per frame, depending on the amount of text written. At a later stage, it will be interesting to produce animated movies: this would allow one to visualize in a few minutes the output of the model.

This chapter will describe a large part of the figures and results generated by a particular run of this model. In the next chapter, selected results from additional runs will be compared with those shown here.

A few simple graphic conventions have been followed in the figures that follow, and should help interpret them:

1. First of all, the number above the top left corner of most figures indicates for which submodel the graph applies. A value of 1 stands for *bare ground under clear sky*, 2 for *canopy under clear sky*, 3 for *bare ground under cloud cover*, and 4 for *canopy under cloud cover*. Occasionally, the value 5 will be seen: the figure then represents a weighted average profile or time series, as discussed in Chapter 2; and the values 2.1 and 4.1 refer to cases 2 and 4, but at the top of the canopy, instead of the soil surface.
2. The three or six numbers that follow immediately below this submodel indicator, but also above the top left corner, are the date and time at which the figure applies. The format is year, month, day, hours, minutes, seconds. The 12-digit number at the top right corner can be discarded: it is used only for organizational purposes.
3. All time series cover a whole day of integration, and all vertical profiles have the dependent variable in abscissa and height in ordinate, increasing upward.
4. The units are indicated after the legend on the axis, unless the variable is non-dimensional.

It would be difficult to specify, and hard to read, the values of all initial parameters and forcing variables for each figure discussed below and in the next chapter. To a large extent, I have attempted to indicate the relevant conditions that produced the particular graph, and to group the information that pertains to more than one figure before the first one of the group. Following is a list of information items, input and forcing data that applies to all the figures in this chapter, until further notice:

1. The latitude of the location for which the computations are made is set at 12° North. The longitude is 0° (Greenwich meridian), and the altitude is 300 m.
2. The model is started at 00:00 on the 21th July 1984, and run for four consecutive days. All results shown here refer to this last day of integration. The time step of integration is 5 minutes for the first three days and 30 seconds for the last one.

3. The 30 grid points in the atmospheric component of the model are equally spaced at 10 cm from each other, the first one being 5 cm above the soil surface. The 20 grid points in the soil component are also equally spaced, but at 2 cm from each other, the first one being at a depth of 1 cm below the soil surface.
4. Both the cloud cover and the vegetation cover are 0.2, the plants have a height of about 80 cm, and the leaf area index is 1.6 $m^2\,m^{-2}$. This leaf area is equally distributed among the different leaf layers.
5. The initial profiles of temperature are constant with height, the soil temperature is 310 K and the air temperature is 300 K. The initial profiles of moisture are also constant with height, and $q = 8\,g\,kg^{-1}$ in the air while $\theta = 0.33\,m^3\,m^{-3}$.
6. The soil type of all layers is loam, the organic matter content of the soil is 5% per volume and constant in time.
7. A precipitation event is started at 14:30 and stopped at 17:30, as can be seen in graphs for submodels 3 and 4. Of course, it never rains in submodels 1 and 2, since they are characterized by clear sky. The cloud is 800 m deep, with a base at 2000 m.

9.2 Albedos and emissivities

The first three figures (9.1 – 9.3) show the diurnal evolution of the surface albedos and emissivities, and of the cloud albedo, for the submodels 1, 2, and 3 respectively.

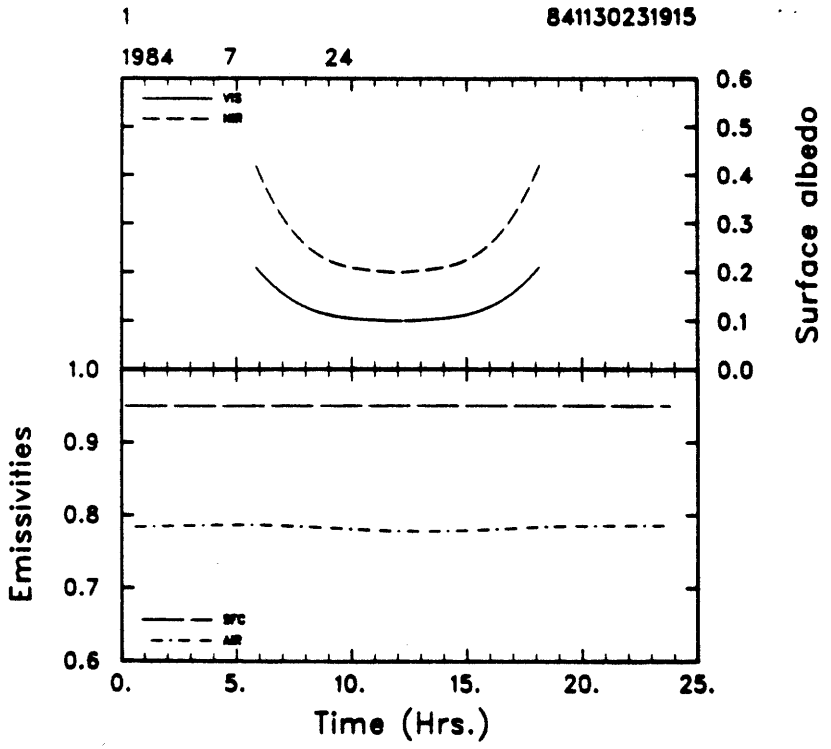

Figure 9.1: Albedos and emissivities, bare ground under clear sky

The top part of Figure 9.1 shows the evolution of the soil surface albedo, both in the visible (VIS: —) and in the near-infrared (NIR: – –). The zenith angle dependency is clearly visible. The lower part of the same figure depicts the simultaneous evolution of the surface (SFC: — —) and atmospheric (AIR: – · –) emissivities. The small variations of the latter are due to changes in specific humidity and temperature at the top of the model (See below).

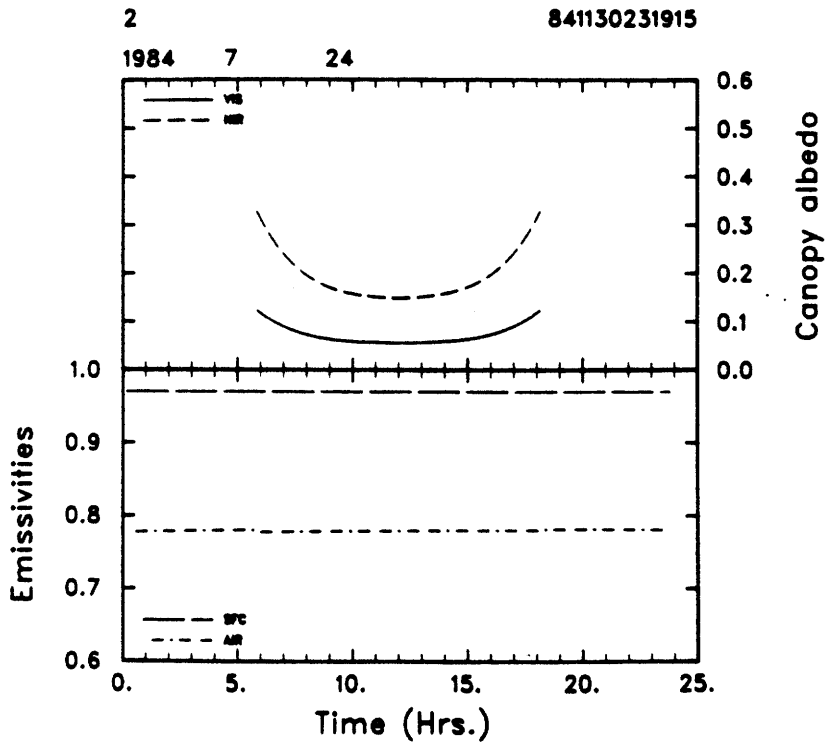

Figure 9.2: Albedos and emissivities, canopy under clear sky

Figure 9.2 presents essentially the same information for the vegetation canopy under clear sky. It is seen that both the visible and the near-infrared albedos are relatively higher than those shown in Figure 4.2 earlier: in the previous case, the canopy had a leaf area index larger than 3, while here a significant part of the canopy albedo comes from the soil albedo.

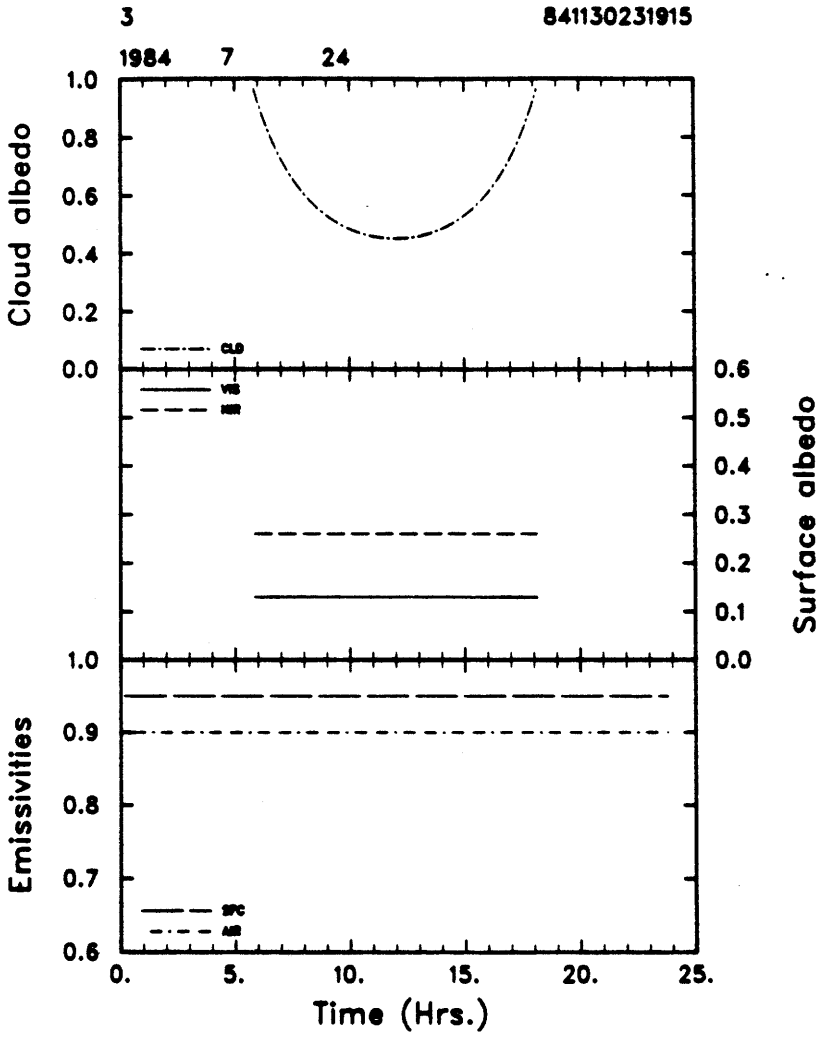

Figure 9.3: Albedos and emissivities, bare ground under cloudy sky

The top part of Figure 9.3 shows the cloud albedo and its dependency on the solar zenith angle. In this case, the depth of the cloud was constant in time, and this figure should be compared with Figure 3.3 where the cloud depth was suddenly increased at the time the precipitation started. Notice also the constant surface albedo, since all the solar radiation is now deemed to be diffuse, coming at a zenith angle of 60°. The albedos and emissivities in the fourth submodel are very similar.

9.3 Radiation

The next four figures (9.4 – 9.7) show the diurnal evolution of the radiative fluxes at the soil surface. The top frame of each graph shows the incoming solar radiation flux transmitted through the atmosphere (submodels 1 and 3), or through both the atmosphere and the canopy (submodels 2 and 4). The middle frames show the infrared fluxes, and the lower frame shows the net surface absorption for each spectral band.

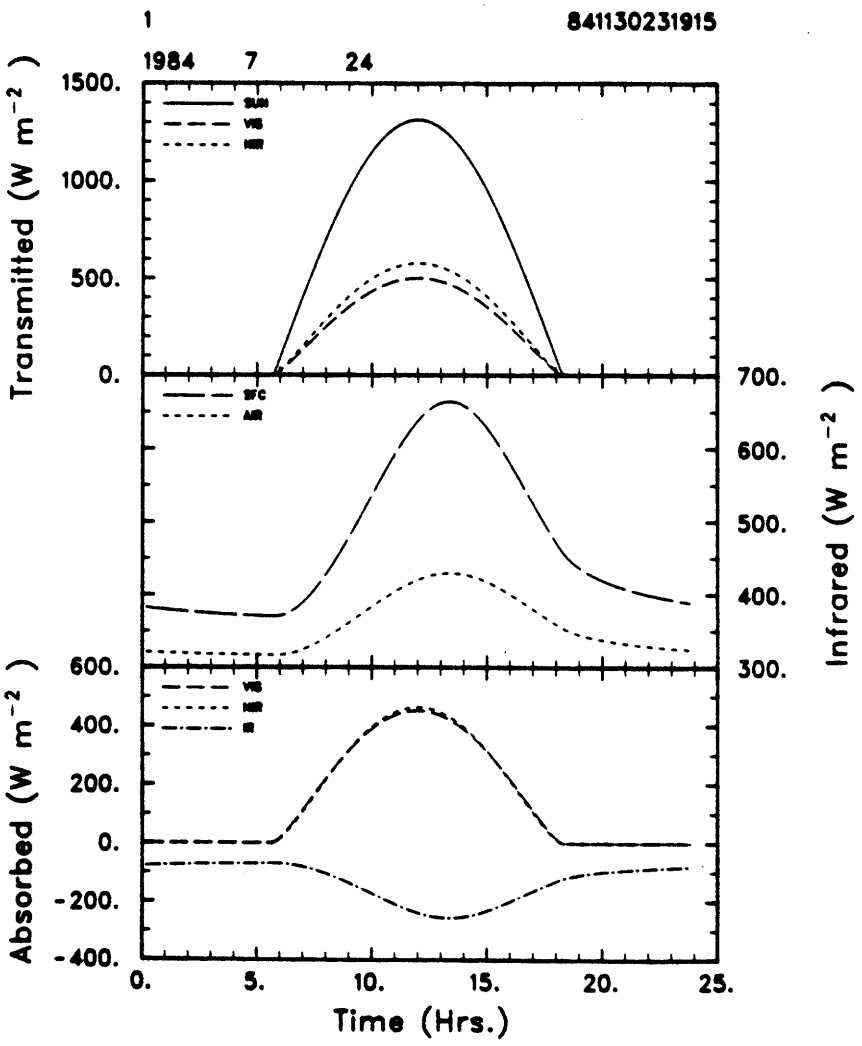

Figure 9.4: Surface radiative fluxes, bare ground under clear sky

In the top frame of Figure 9.4, the continuous line (SUN: —) shows the solar radiation level at the top of the atmosphere, while the two broken lines (VIS: -- and NIR: ---) show the visible and near-infrared fluxes transmitted to the surface. These almost overlap because the selected threshold (0.7 μm) between these two radiation "windows" is very close to the median of the solar energy distribution curve. The middle frame shows the emission of infrared radiation by the soil surface (SFC: ——) and the back radiation from the sky (AIR: --). The lower frame shows the corresponding net absorptions at the surface, in the visible (VIS: --), near-infrared (NIR: ---), and infrared (IR: -·-), respectively.

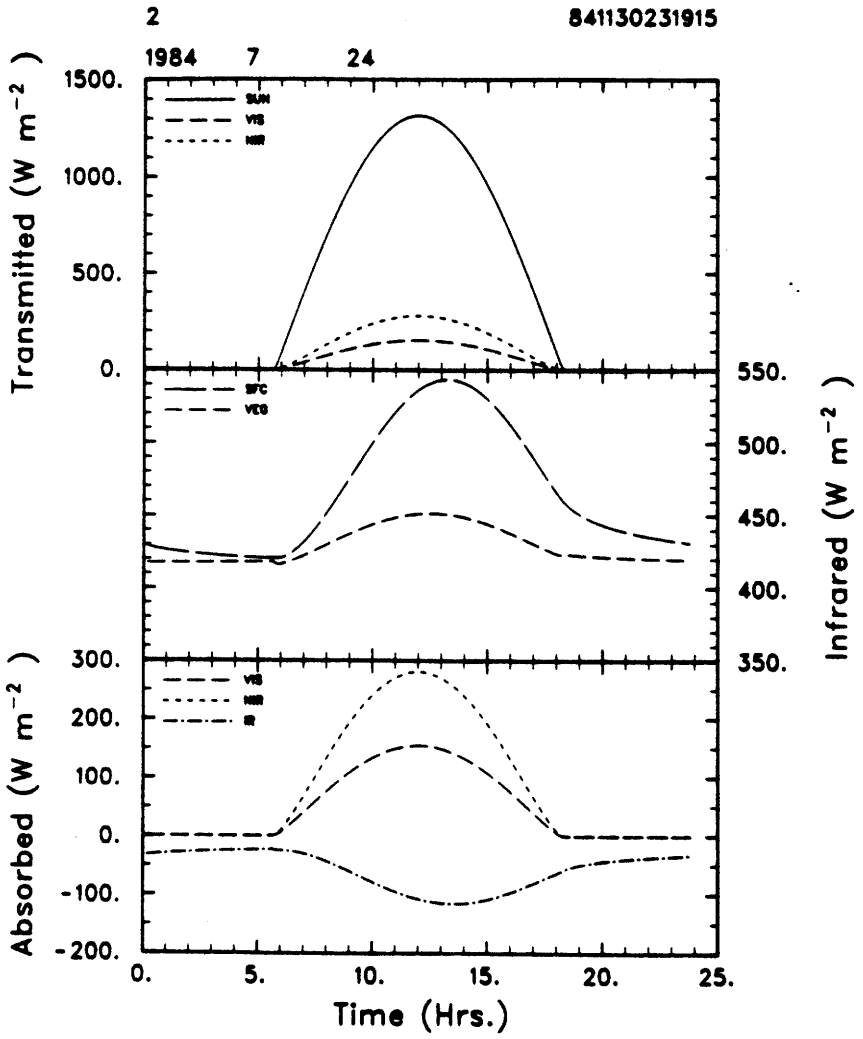

Figure 9.5: Surface radiative fluxes, canopy under clear sky

Figure 9.5 displays the same information but under the canopy. It is seen that the solar radiation levels transmitted to the surface are now reduced due to the interception by the canopy. The infrared flux emitted by the soil surface (SFC: ——) follows a diurnal wave of smaller amplitude than in the bare ground case, showing the protecting effect of the plants. The back radiation (VEG: ---) is somewhat higher and less variable also due to the moderating influence of the canopy.

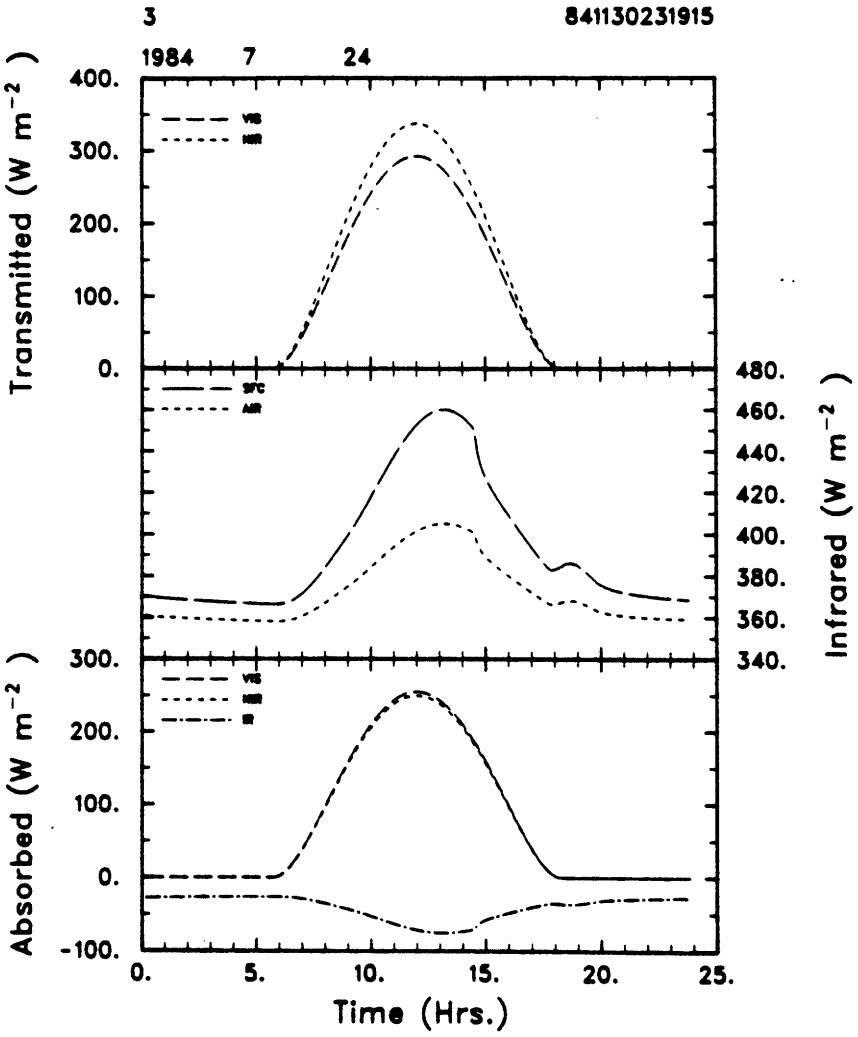

Figure 9.6: Surface radiative fluxes, bare ground under cloudy sky

The solar radiation flux outside the atmosphere has not been drawn in the next two figures, for scaling reasons. The sharp drop in surface infrared emission (SFC: $--$, in the middle frame of Figure 9.6) indicates a soil temperature drop, it will be seen shortly that this is coincident with the onset of a precipitation event.

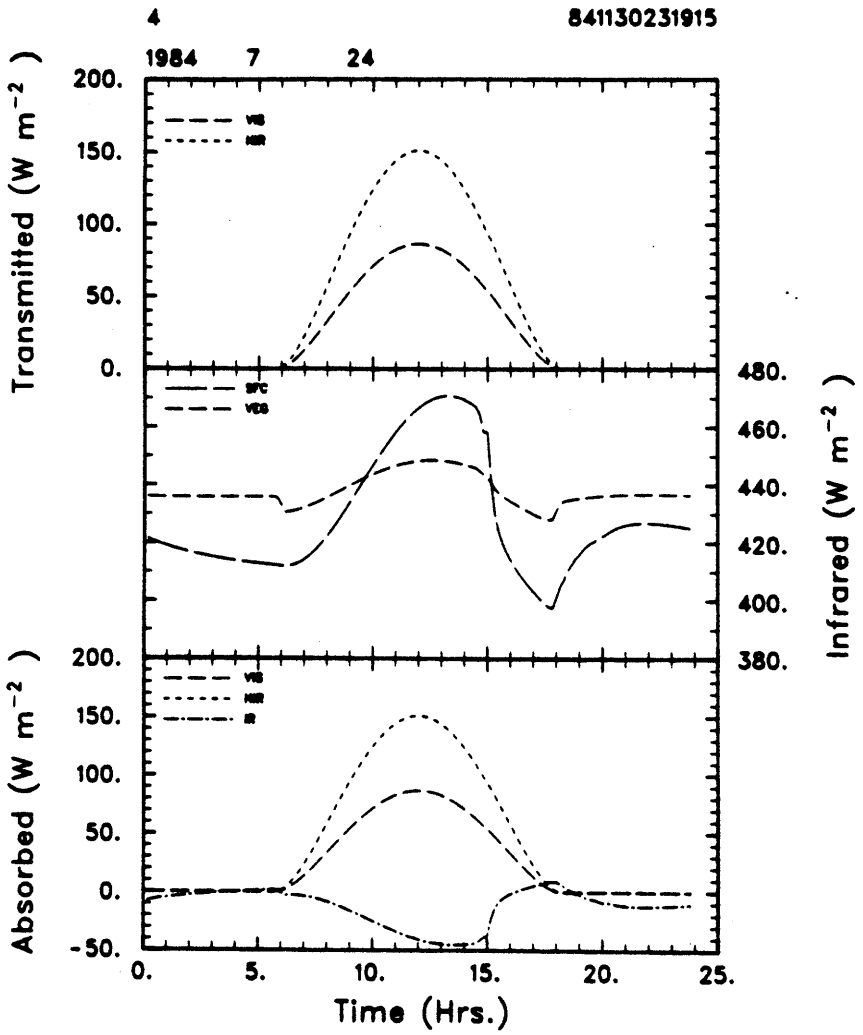

Figure 9.7: Surface radiative fluxes, canopy under cloudy sky

Finally, Figure 9.7 shows the radiative fluxes at the surface, under the canopy, in the case of cloudy skies. Again, the selective absorption of solar radiation by the canopy is clearly visible. The temperatures of the top soil layer and the canopy are relatively close, resulting in a very small infrared radiative cooling, especially at night.

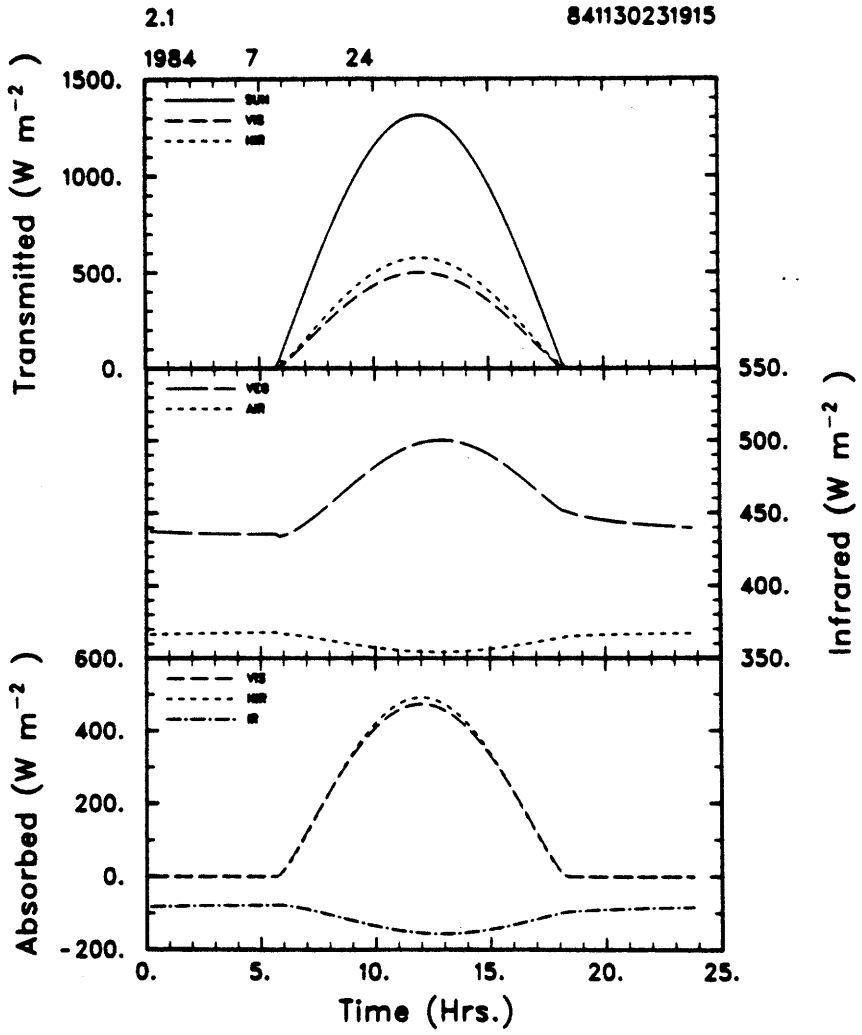

Figure 9.8: Radiative fluxes at the top of the canopy, under clear sky

The next two figures show the radiative fluxes at the level of the top of the canopy, for submodels 2 and 4, respectively.

The solar radiation fluxes transmitted to this level resemble those observed over bare ground (compare Figure 9.8 with Figure 9.4), since the interception by the canopy has not taken place yet. The net upward infrared flux from the soil/canopy system is about 10% less above the canopy than it was under it, however (compare with the middle frame of Figure 9.5).

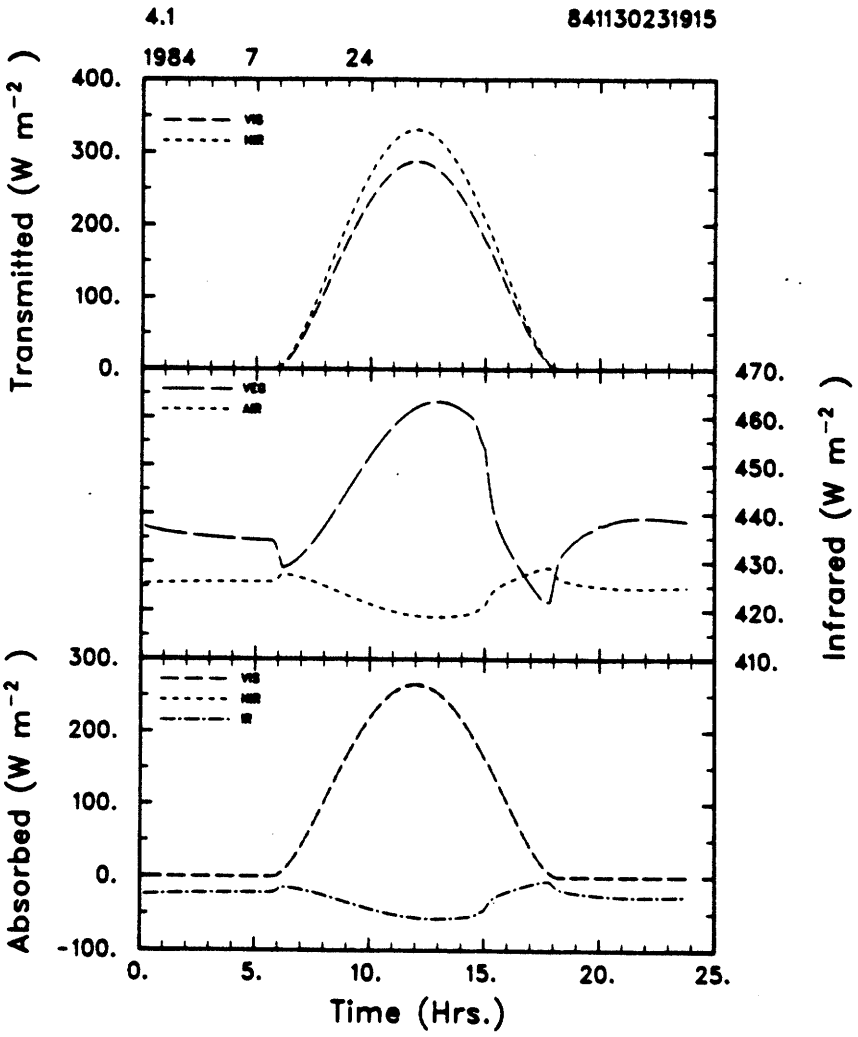

Figure 9.9: Radiative fluxes at the top of the canopy, under cloudy sky

Figure 9.9 shows the same radiation balance at the level of the top of the canopy under cloudy sky. The top frame can be compared with its correspondent in Figure 9.6, and the other frames with their equivalents in Figure 9.7.

9.4 Energy balance

The next 6 figures show the diurnal evolution of the energy balance at the soil surface and the top of the canopy. The negative of the ground heat flux has been plotted on these and all similar Figures. It is therefore positive when the deeper soil layer heat up the top soil layer (mostly at night), and the (negative) dip in the curve from approximately 7:00 am to 5:00 pm indicates that the lower soil layers heat up during the day.

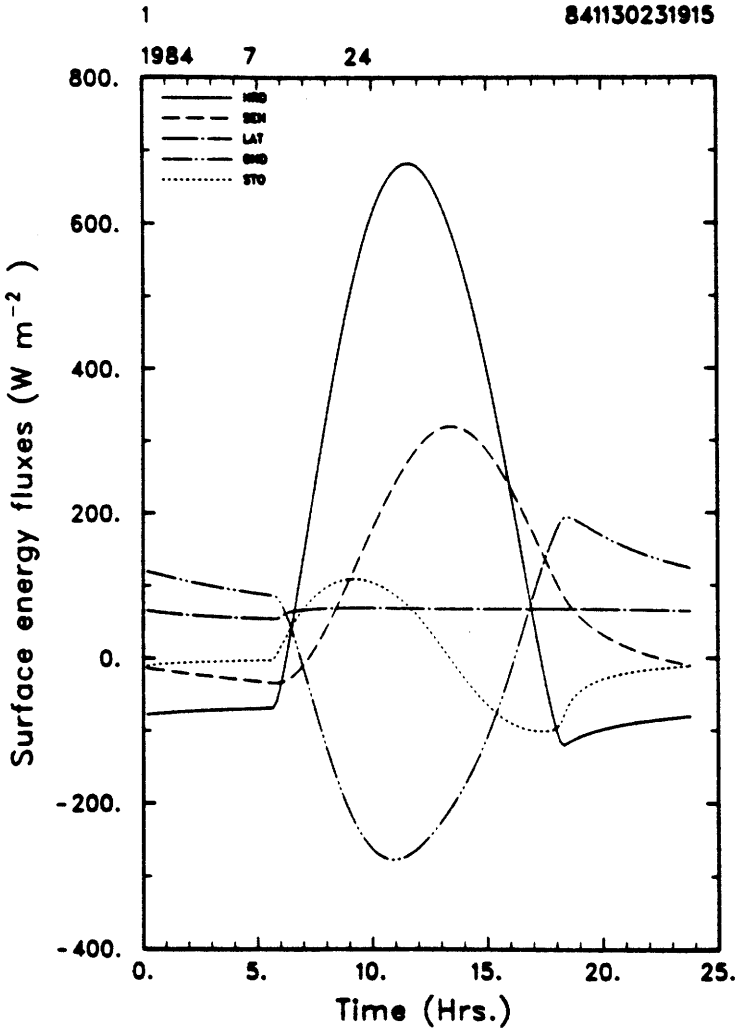

Figure 9.10: Energy balance, bare ground under clear sky

In the case of bare ground under clear sky (Figure 9.10), the energy balance is dominated by the high net radiation absorption (NRD: —), which is positive during the day and negative at night. This radiation is disposed of in sensible heat fluxes towards both the atmosphere (SEN: – –) and the ground (GND: – · · –). The latent heat flux (LAT: – · –) is completely controlled by the ability (or inability, in this case) of the top soil to supply moisture at the potential rate, and the storage term (STO: · · ·) shows the accumulation of heat in the top soil layer from 6:00 to 13:00; after that, the top soil starts cooling down.

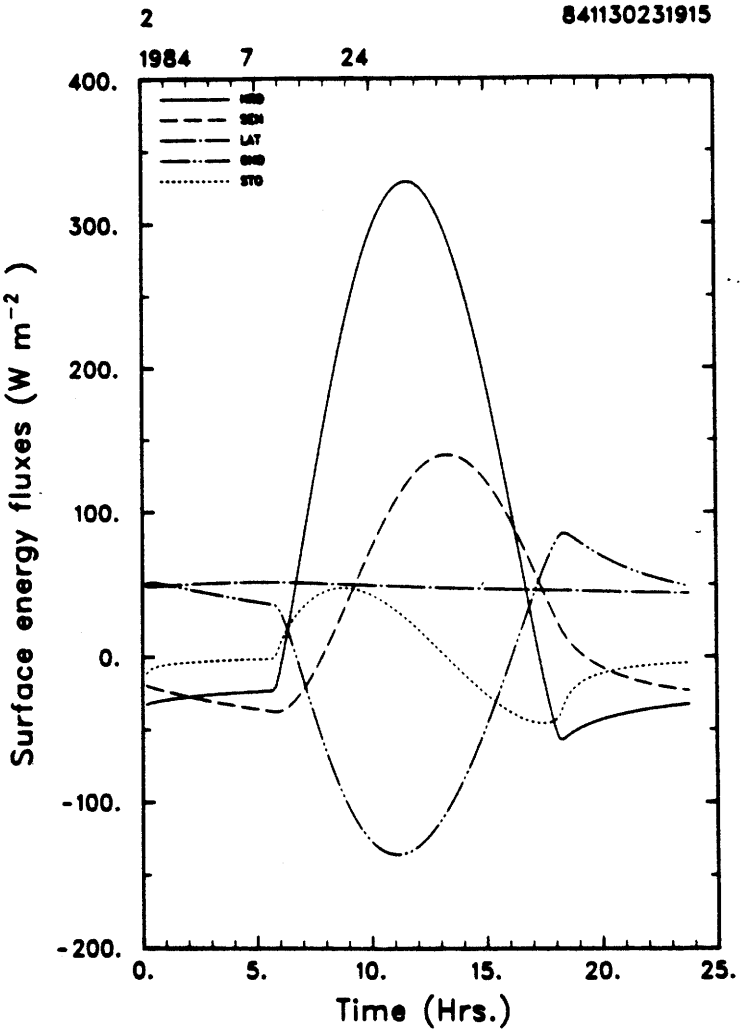

Figure 9.11: Energy balance, canopy under clear sky

When a canopy shields the surface from intense radiation (Figure 9.11), the net radiation balance at the soil surface is greatly diminished, but the relative roles of the various fluxes seem to be preserved: the latent heat flux is still very much controlled by the drying soil.

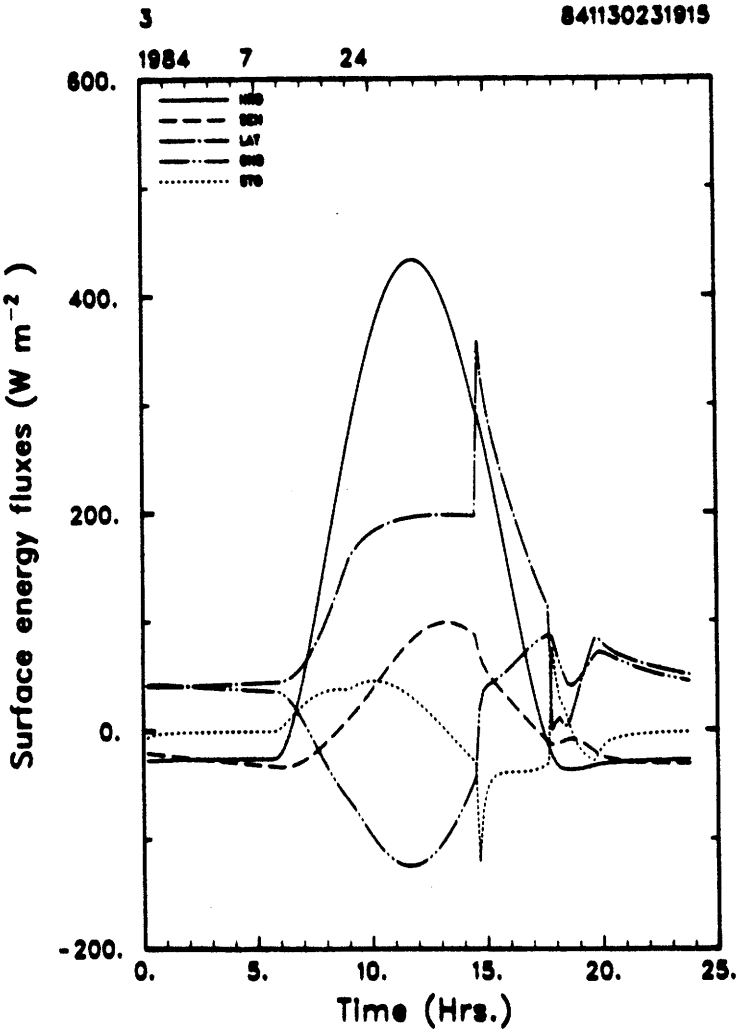

Figure 9.12: Energy balance, bare ground under cloudy sky

In the third submodel (Figure 9.12), the net radiation absorbed at the soil surface (NET: —) is reduced due to cloudiness. The latent heat flux (LAT: – · –) is allowed to play a much larger role, because the top soil has not dried up so much. Also, a peak of evaporation is visible when the precipitation starts at 14:30. During this rain event, the ground heat flux (GND: – · · –) provides part of the energy necessary for evaporating the water. The sensible heat flux and the storage term are much lower than under clear sky.

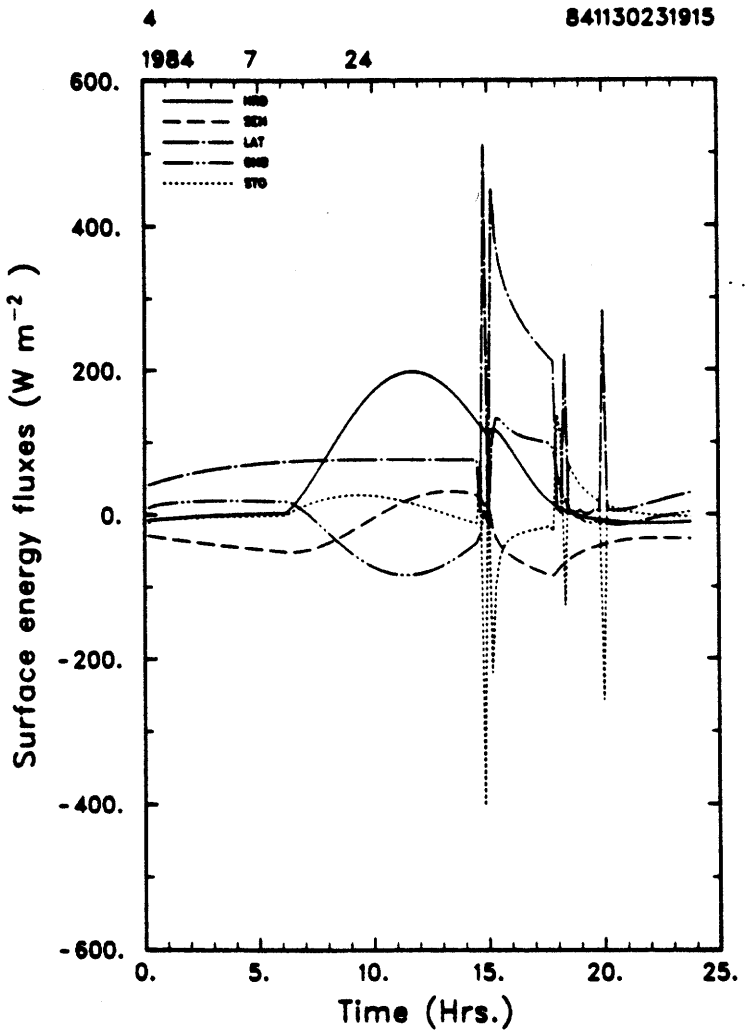

Figure 9.13: Energy balance, canopy under cloudy sky

Figure 9.13 shows the same information for the last submodel. The net radiation is even lower, since it is affected by both the cloud layer and the vegetation. A fairly large latent heat flux (LAT: –·–) takes place during the precipitation event, and requires sensible heat contributions from both the atmosphere (SEN: - - -) and the ground (GND: –···–), to supplement the radiation. The top soil layer also cools during that period. A couple of oscillations appear close to the start and after the end of the precipitation event; these result from readjustments in the model after instantaneous changes in the forcing function.

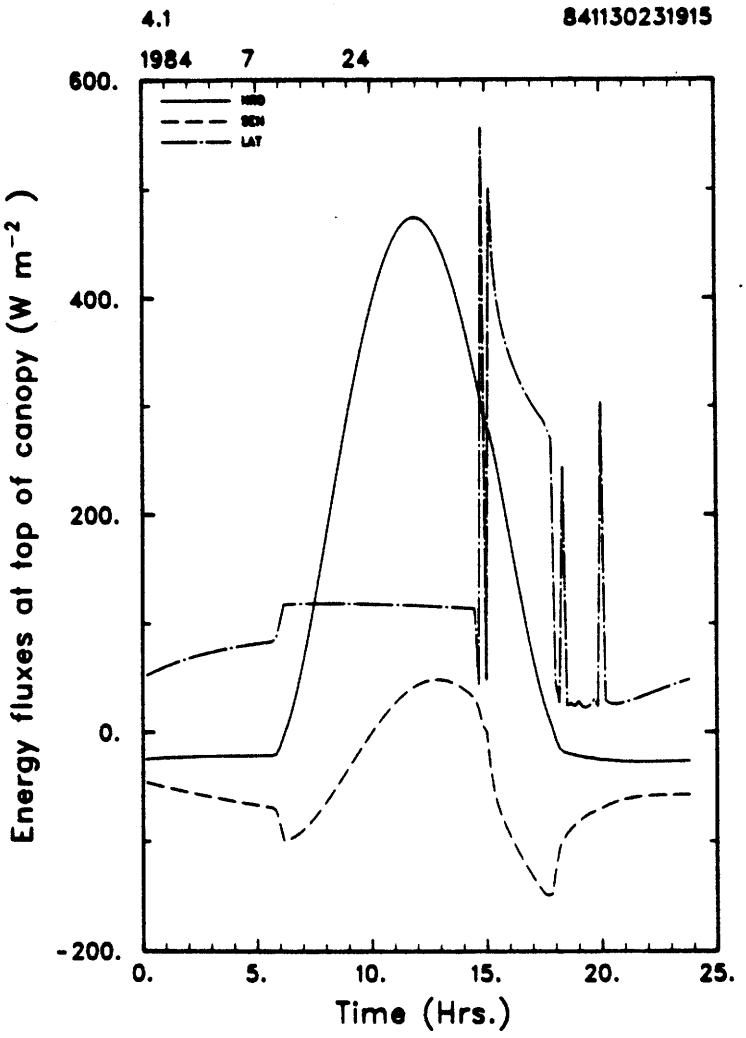

Figure 9.14: Energy balance at the top of the canopy, under cloudy sky

Figure 9.14 shows the energy balance at the level of the top of the canopy, for the last submodel. An increase in the latent heat flux is noticeable during the day (especially in the morning): this is due to the contribution of the transpiration from the canopy. During the afternoon, this effect is negligible compared to the increased evaporation from the soil, but also from the wet parts of the leaves in the canopy.

9.5 Water balance

Similar figures could be shown for the individual components of the water balance. To save space, only one graph will be shown, as an example.

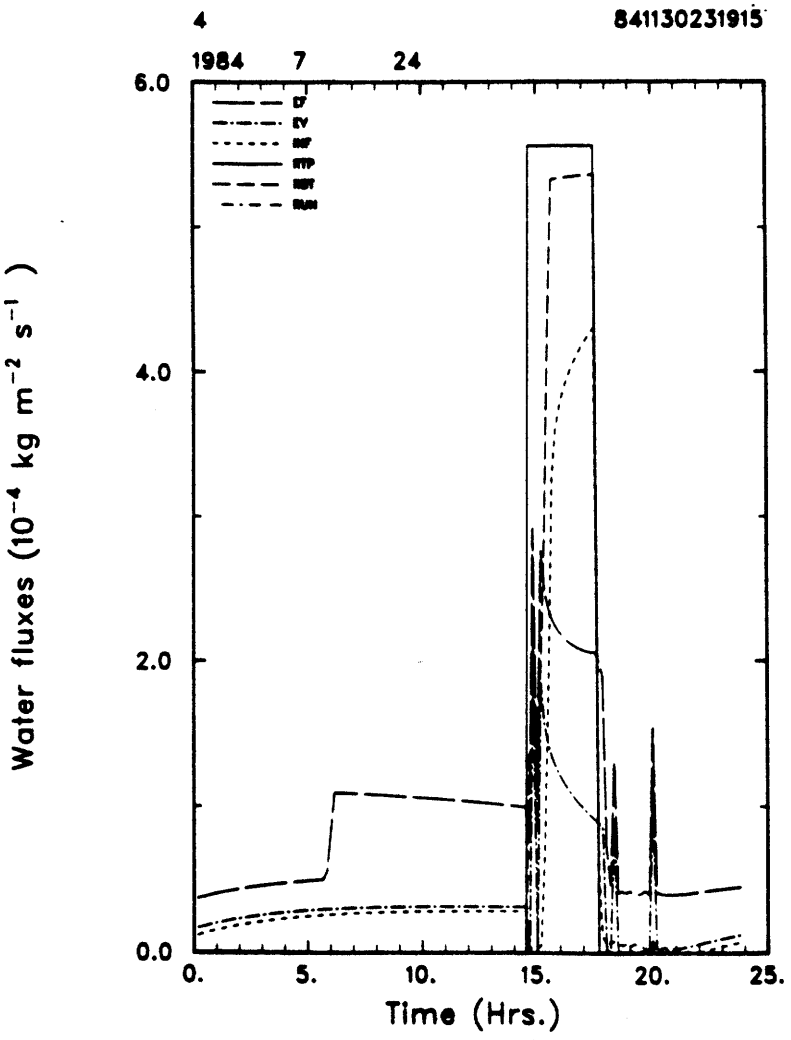

Figure 9.15: Water balance, canopy under cloudy sky

In Figure 9.15, the highest rectangular curve (RTP: —) represents the precipitation intensity, and the somewhat smaller quasi-rectangular curve (RBT: - - -) is the precipitation rate at the surface, under the canopy. For reference, $5.5\,10^{-4}\,\mathrm{kg\,m^{-2}\,s^{-1}}$ is about $2\,\mathrm{mm\,hr^{-1}}$. The difference between these curves represents the interception by the canopy. It is seen that the precipitation rate at the surface remains small during the first hour of the rain, while the canopy wets and stores water. When the capacity of the canopy to store water becomes saturated, the rate of dripping from the canopy to the soil increases sharply, but does not quite reach the precipitation rate above the canopy: the difference here is an indication of the rate of evaporation from the wet parts of the leaves. As long as the rain continues, the canopy keeps intercepting a fraction of the precipitation rate to make up for the evaporative losses.

The curves labeled EV (– · – ·) and EF (– –) represent the evaporation rate from the soil surface and the evapotranspiration from the soil and canopy, respectively. The difference between these curves shows the importance of the transpiration during the morning hours, and of the combined transpiration and evaporation during the precipitation event. The rate of infiltration into the soil (INF: · · ·) is also increasing soon after the water reaches the soil surface. No runoff was produced in this case.

9.6 Atmospheric humidity and temperature

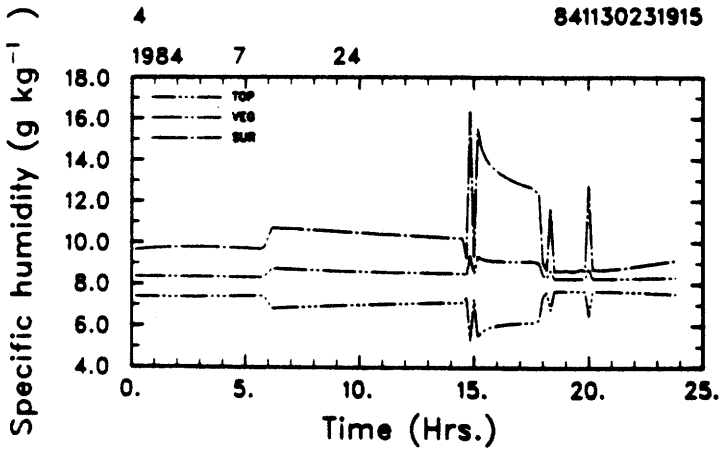

Figure 9.16: Specific humidity at three levels, submodel 4

Figure 9.16 shows the evolution of the specific humidity at three levels in the model atmosphere: the surface layer (0.10 m), the layer at the level of the top of the canopy (0.80 m), and the top model layer (3.0 m), for the same submodel as the previous figure. A limited diurnal signal is observable, but the major perturbation is occuring after the onset of the precipitation. In addition to increasing the surface specific humidity, the increased evapotranspiration rate produces a steeper gradient of specific humidity, and this, in turn, forces the specific humidity at the top of the model to decrease a little, especially during the precipitation event. This is not very realistic, and results from the no-storage condition imposed to solve the water diffusion equation in the atmosphere. If a small divergence in the vertical upward flux of water vapor was allowed, the profiles would not be as steep, and this peculiar behavior would not be present. The same phenomenon may occur with the air temperature, since no accumulation of sensible heat was allowed in the model's atmosphere.

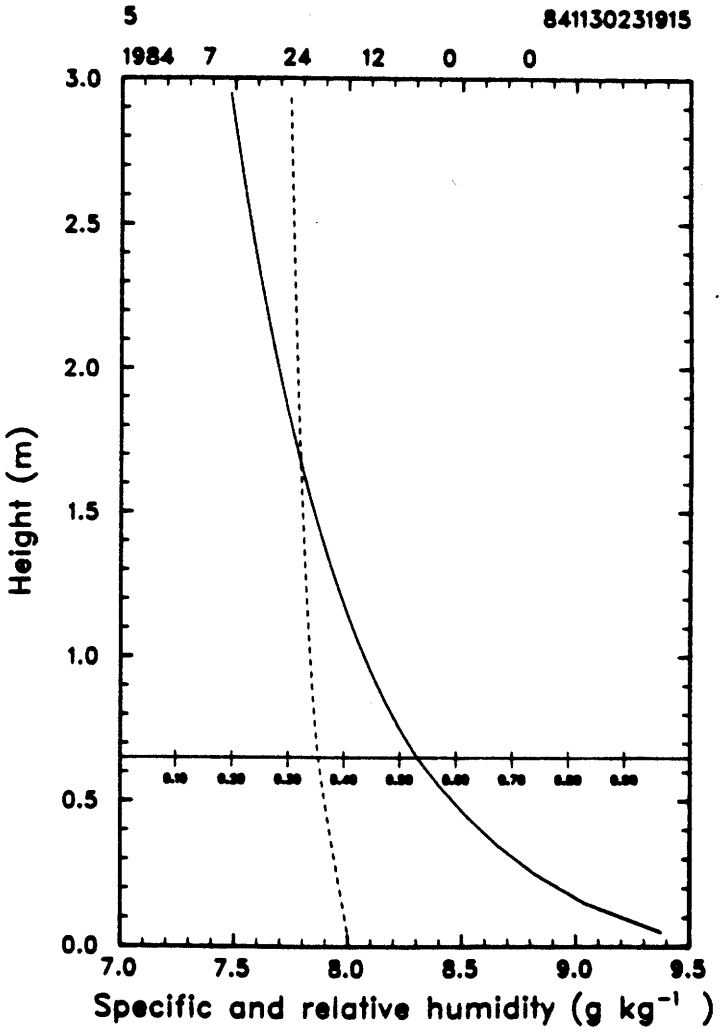

Figure 9.17: Mean atmospheric humidity profiles at noon

Figure 9.17 shows the weighted average of the four specific humidity profiles at noon (continuous line), as well as the relative humidity (broken line). The scale in the lower third of the figure is at the level of the top of the canopy and applies to the relative humidity.

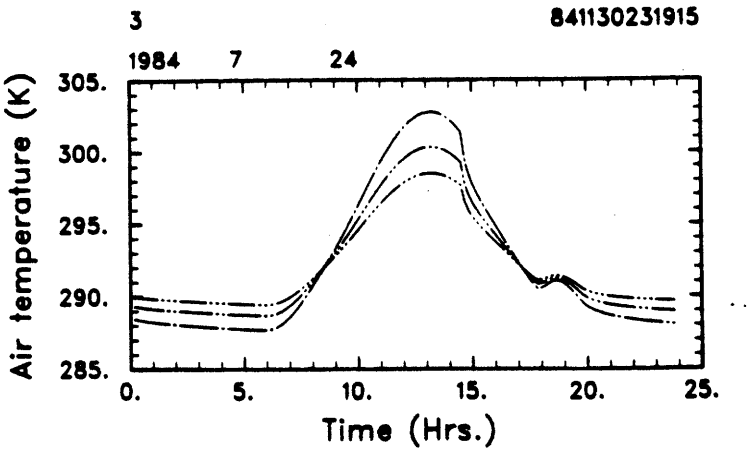

Figure 9.18: Air temperature at three levels, submodel 3

Similar graphs can be produced for the air temperature, and Figure 9.18 shows the diurnal temperature cycle over bare ground and under cloudy sky. The temperature inversion during the night is clearly visible, and the precipitation event is associated with a drop in temperature. The three curves ($-\cdot$, $-\cdot\cdot$, $-\cdot\cdot\cdot$) refer to the same three levels: 0.1, 0.8 and 3 m, respectively.

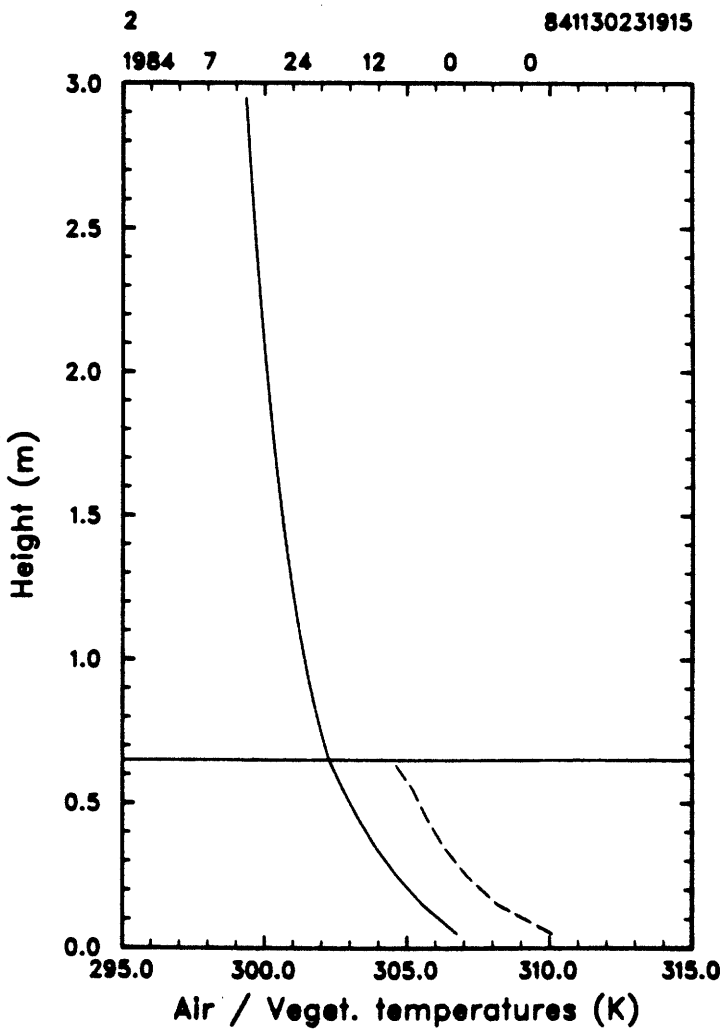

Figure 9.19: Air and vegetation temperature profiles, submodel 2

Figure 9.19 shows the air and vegetation temperature profiles at noon, under clear sky. In most cases, the vegetation temperature exceeds the air temperature during the day and the contrary happens at night.

9.7 Soil moisture and temperature

The upper and middle frames of Figure 9.20 are there for purely diagnostic purposes. They show the behavior of variables representing the top boundary condition and the source or sink term in the diffusion equation, respectively.

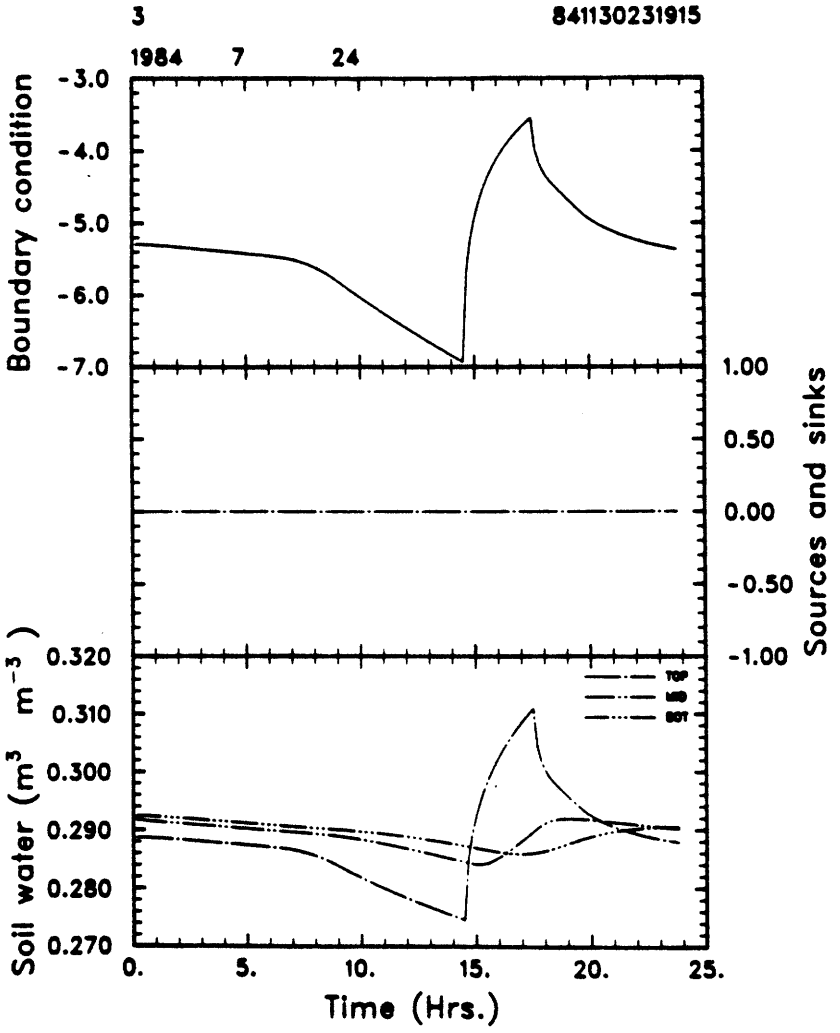

Figure 9.20: Soil water content, bare ground under cloudy sky

The lower frame is the most important: it is seen that the soil water content of the deeper levels continues to decrease slowly, under the influence of surface evaporation. The top soil layer dries up somewhat more rapidly during the day, and then wets sharply when the rain starts, although the precipitation event does not last long enough to it affect durably. The three depths are 1, 10 and 20 cm, respectively.

The familiar diurnal temperature waves in the soil are clearly visible in the lower frame of Figure 9.21. The top soil layer undergoes a much larger temperature range than the deeper layers, and the latter are out of phase with the surface, due to the time it takes the sensible heat to diffuse in the ground. The three curves refer again to depths of 1, 10 and 20 cm.

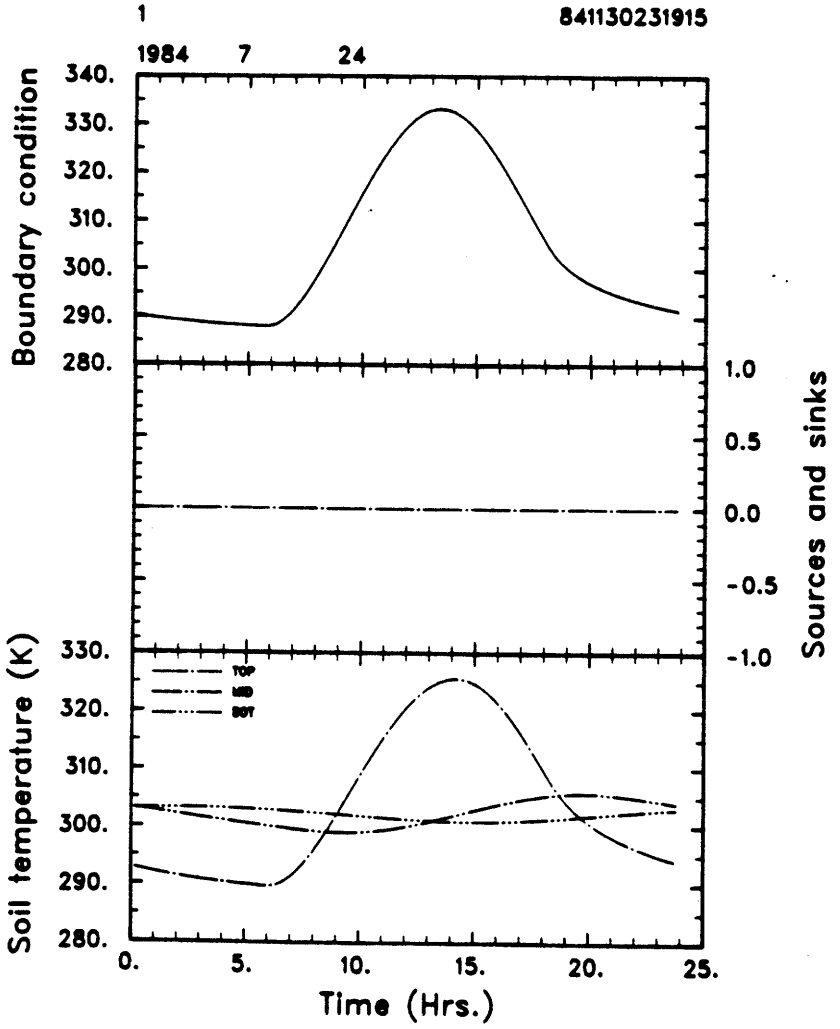

Figure 9.21: Soil temperature, bare ground under clear sky

9.8 Wetting and drying of the canopy

The unusual Figure 9.22 shows the progressive wetting of the canopy, after the onset of the precipitation. The fraction of each leaf which is wet is given here as a function of height (vertical axis) and time. Before the rain, all leaf layers are dry. As soon as the precipitation starts, the top of the canopy starts intercepting water and wets. The lower layers wet at a slower rate, since the dripping from above is less intense than the precipitation intensity above the canopy. Profiles have been drawn at 10 minutes interval,

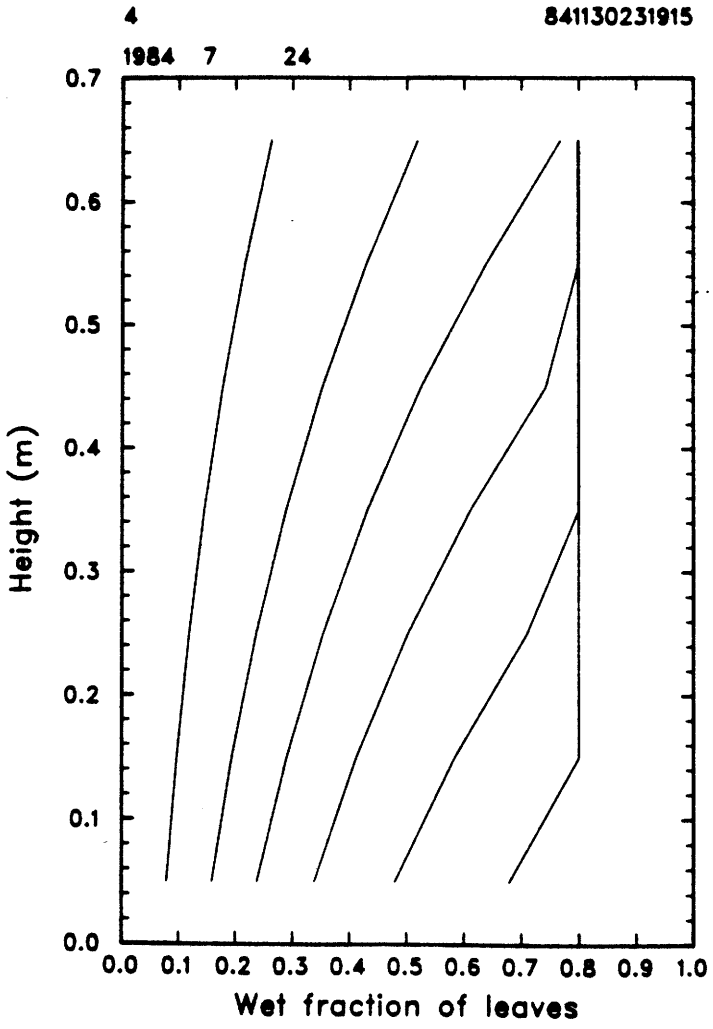

Figure 9.22: Wetting of the canopy, submodel 4

and it is seen that the whole canopy becomes saturated after slightly more than an hour. The fractional wet area does not exceed 0.8, since this was the maximum value imposed.

If the precipitation event is long enough, the whole canopy eventually wets, and it will remain wet until the end of the rain, except perhaps for extremely low precipitation intensities, if the evaporation rate from the wet parts of the leaves exceeds the interception rate.

As soon as the rain stops, the wet fractional area decreases due to evaporation. Figure 9.23 shows the evolution of this parameter after the end of the rain, and it can be seen

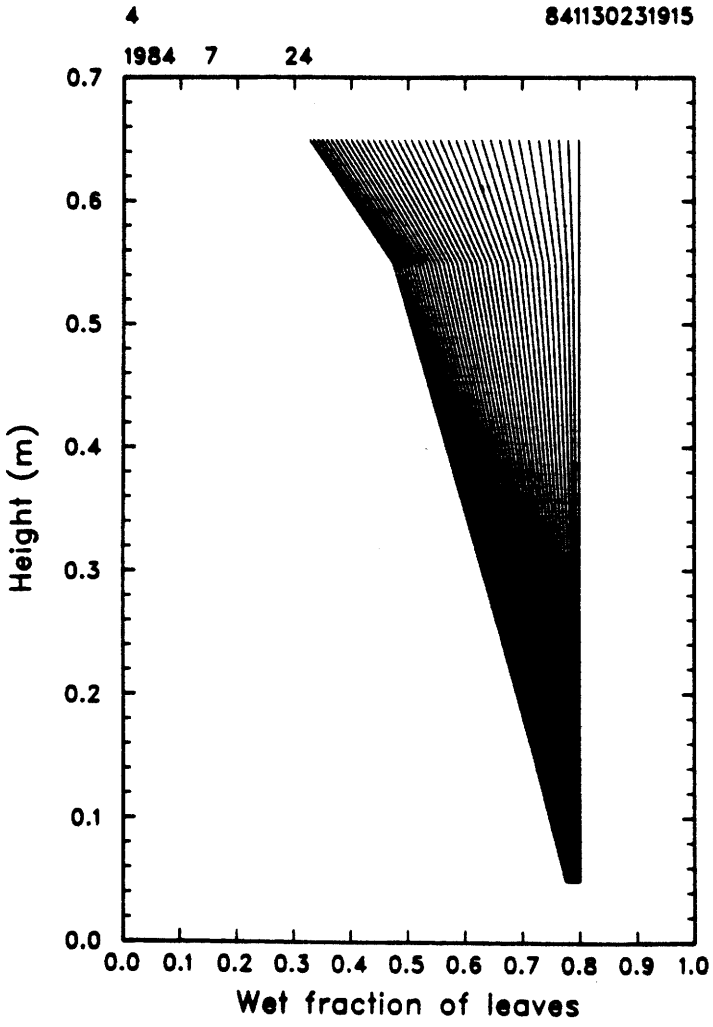

Figure 9.23: Drying of the canopy, submodel 4

that the canopy dries much more slowly than it wets. All profiles are again drawn at 10 minutes intervals, and the top layers dry faster than the lower ones, in part due to the higher wind speed and turbulence at these levels.

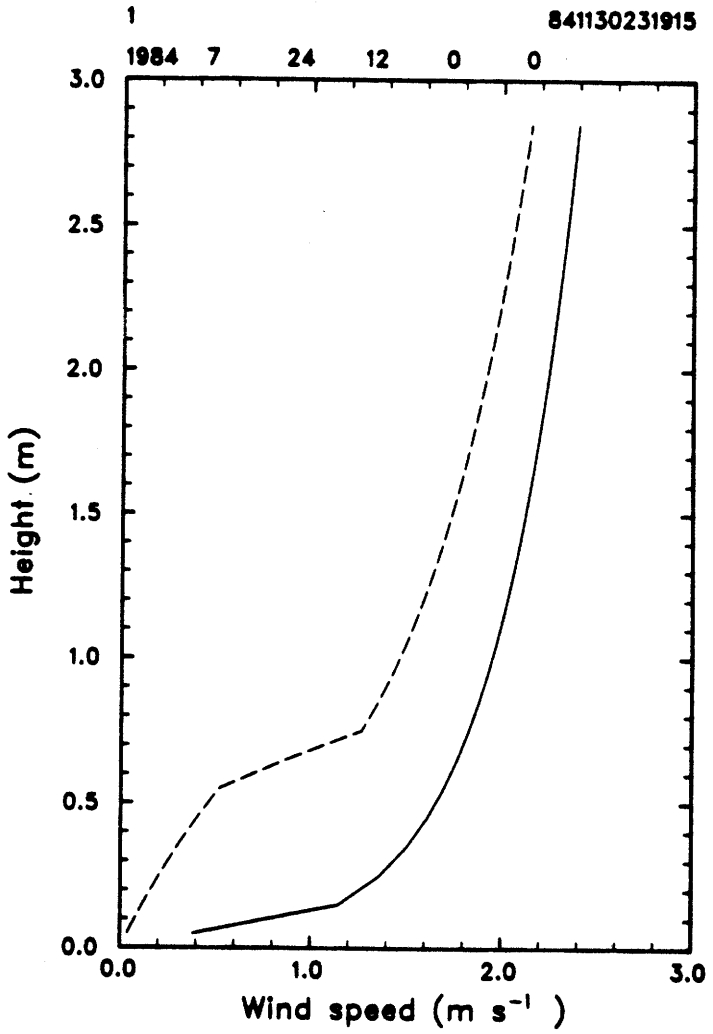

Figure 9.24: Wind profile, canopy and clear sky

The last figure shows the wind profiles, both outside (—) and inside (---) the canopy, at noon. The exponential decrease of wind speed in the canopy is clearly visible, as is the greater roughness of the vegetated areas, since the whole profile is to the left of the one predicted over bare ground.

Chapter 10: Comparing Different Runs

In addition to comparing the results from the four submodels of a particular run, it is also interesting to compare the results of different runs when only one (or a few) forcing parameters change. This is the purpose of this chapter. Clearly, each of these runs cannot be investigated with the same amount of detail as in the previous chapter, and only the most interesting results will be shown.

The first section below investigates the sensitivity of the model's response to a doubling of the vegetation leaf area index. Section 10.2 compares the reference run with another run where the soil is sand instead of loam, and Section 10.3 looks at a run in winter instead of summer. Section 10.4 is another winter run with the wind speed at the top of the model (a forced parameter) increased three-fold.

10.1 Differences in vegetation

The results discussed in the last chapter were relative to a rather low density vegetation. They are compared now with a similar run where the vegetation leaf area index is doubled to 3.2. All other parameters and forcings are kept the same. The figures shown below refer to the thicker canopy, and should be compared with those of the previous chapter.

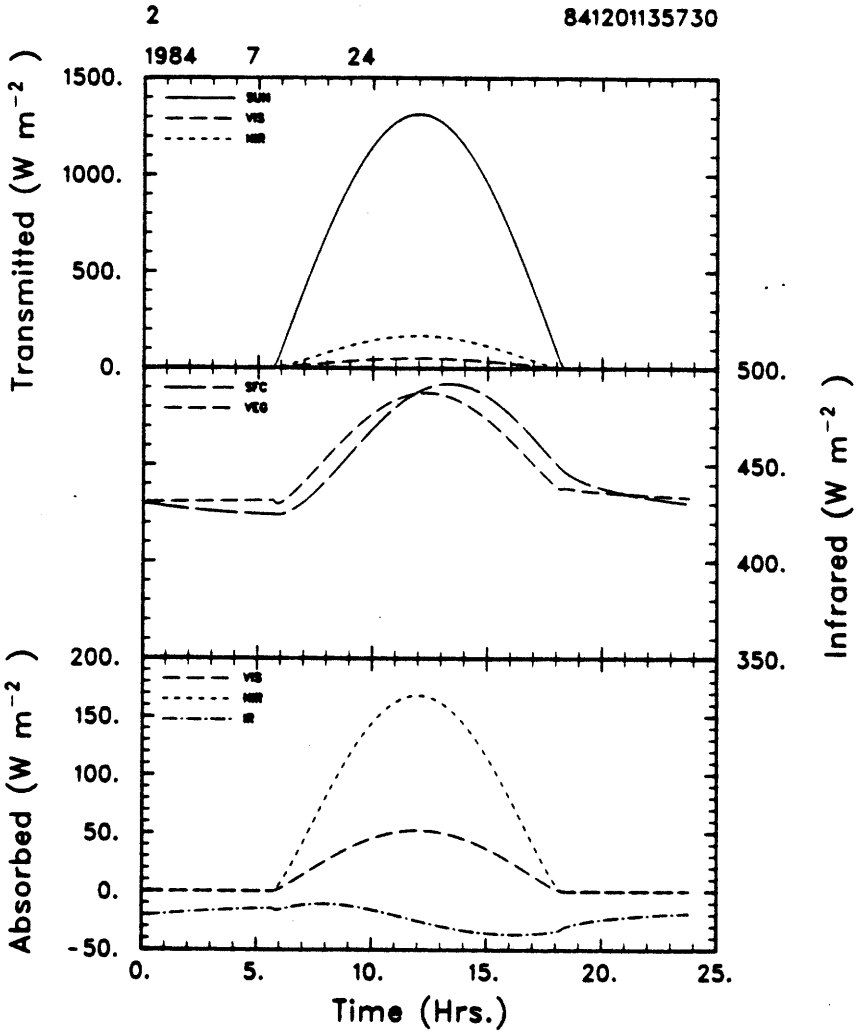

Figure 10.1: Surface radiative fluxes, canopy and clear sky

As can be expected, quite a few results are very similar for these two runs, especially for the sub-models 1 and 3, where there is no vegetation canopy. The following series of figures therefore concentrates on the other two submodels.

The leaf area index influences directly the canopy albedo, as explained in Chapter 4, and shown in Figures 9.2 and 4.2. No further comments are necessary here.

Figure 10.1 shows the radiation balance at the soil surface, under the deeper canopy. This figure should be compared with Figure 9.5 in the previous chapter. The first influence of the thicker canopy is to reduce further the amount of solar radiation at the surface,

as can be seen in the top and bottom parts of these frames. The difference in infrared is also notable: the emission from the soil surface has been reduced by some $50\,W\,m^{-2}$, and is now about the same as the (unchanged) downward radiation from the canopy. The diurnal "wave" of infrared emission by the soil surface is lagging behind the emission by the canopy by approximately an hour, while the two curves peak simultaneously over bare ground. The net infrared balance is still negative because of the lower emissivity of the soil.

The radiative fluxes at the top of the canopy under clear sky are not significantly different when the leaf area index is increased although the net infrared losses by the ecosystem are larger when the leaf area index is smaller, under clear sky.

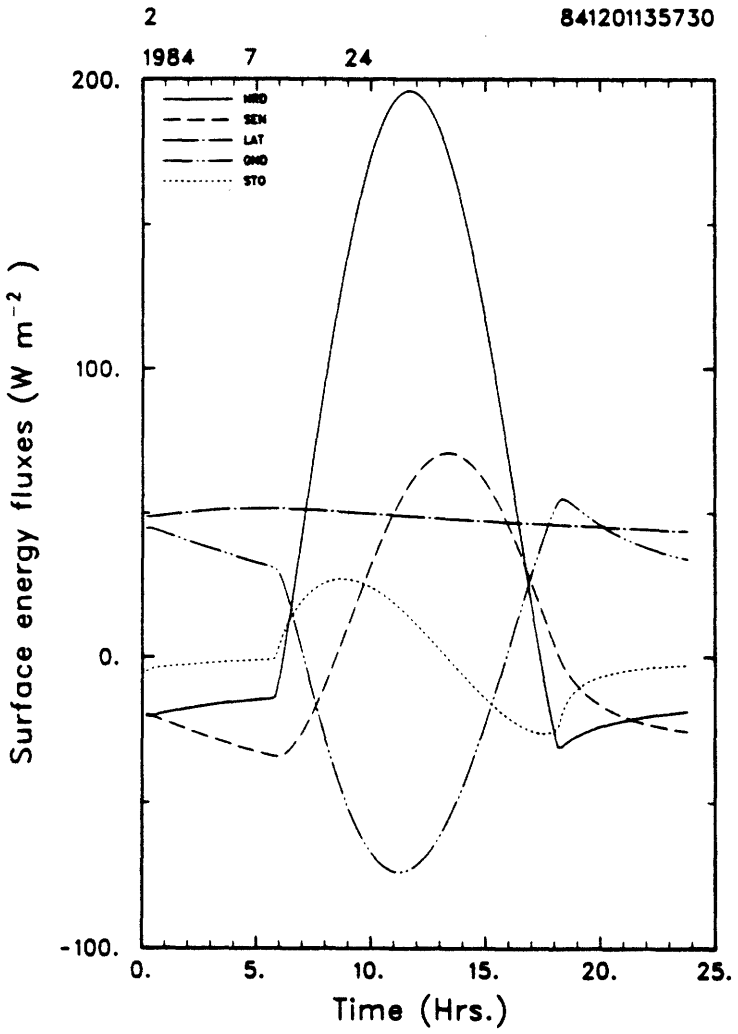

Figure 10.2: Surface energy fluxes, canopy and clear sky

The surface energy balance under the canopy (clear sky submodel) is also interesting (Figure 10.2): the net radiation (NRD: —) is decreased by some 40% by the thicker canopy (compare with Figure 9.8). The latent heat flux (LAT: – · –) from the soil surface to the atmosphere is not affected, since it is controlled by the soil in both cases, and the sensible heat flux (SEN: - -) wave presents a lesser amplitude. On the other hand, both the latent and the sensible heat fluxes at the top of the canopy (not shown on this figure) are increased due to the larger leaf area.

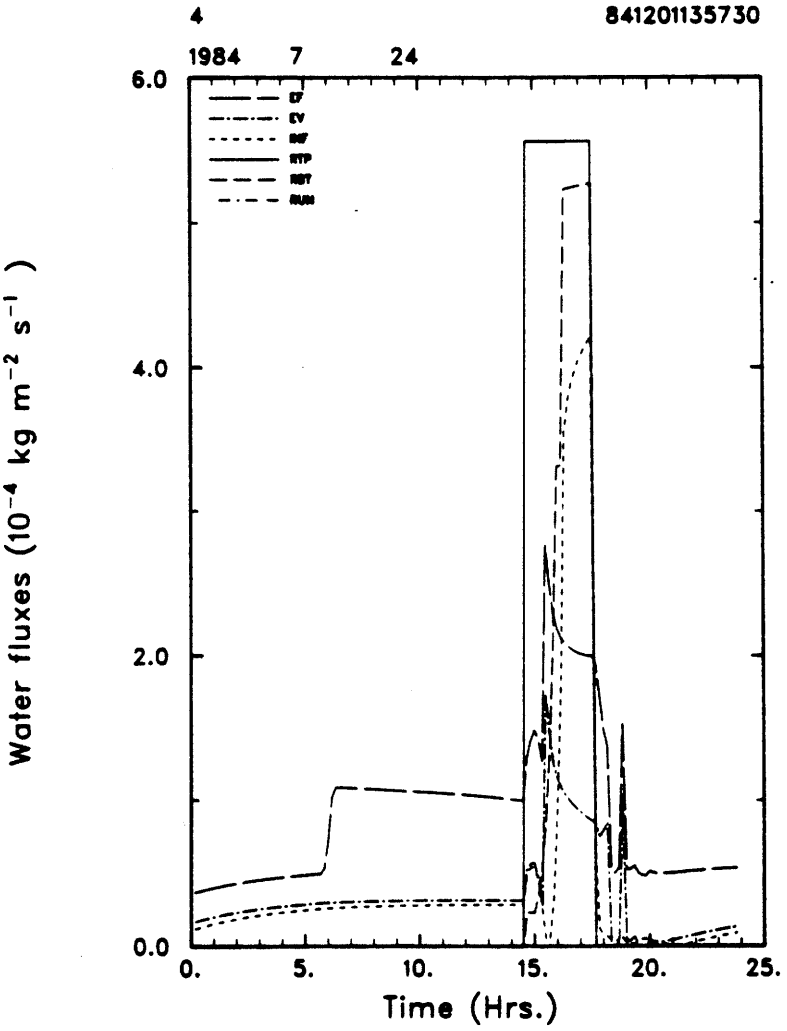

Figure 10.3: Water balance, canopy under cloudy sky

Figure 10.3, to be compared with Figure 9.15, shows the components of the water balance under the thicker canopy. The increased interception of the precipitation by the leaves is notable. The surface water balance also seems to readjust more easily to the precipitation forcing.

No changes of interest are observed in the profiles of atmospheric temperature or specific humidity. The same is true for the soil temperature and moisture profiles, although longer runs would be needed to detect a difference.

The temperature difference between the vegetation and the air is somewhat higher

when the leaf area index is larger, presumably because of its influence on the transfer of radiation in the canopy.

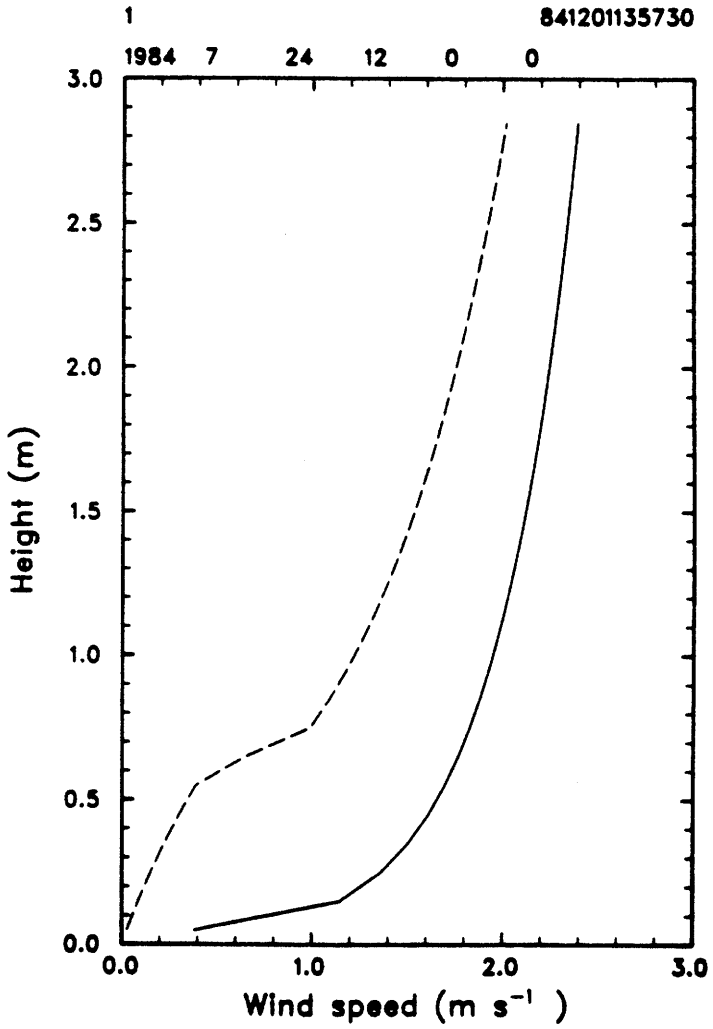

Figure 10.4: Wind profile, canopy and clear sky

The thicker canopy presents a higher roughness, and absorbs more momentum: Figure 10.4 shows the wind speed profiles inside (---) and outside (—) the denser canopy. It should be compared with Figure 9.24 at the end of the last chapter.

10.2 Differences in soil

All results presented so far were relative to a loam soil. The figures shown in this section are relative to a sandy soil. At the outset, this is expected to have an influence on the fluxes of water and energy at the soil surface, since the soil water and heat conductivities are very different for different soils. The initial soil moisture profiles on day 1 of each run were 0.33 for the loam and 0.24 for the sand respectively. These values were selected so that the evaporation rates allowed by each soil were initially the same.

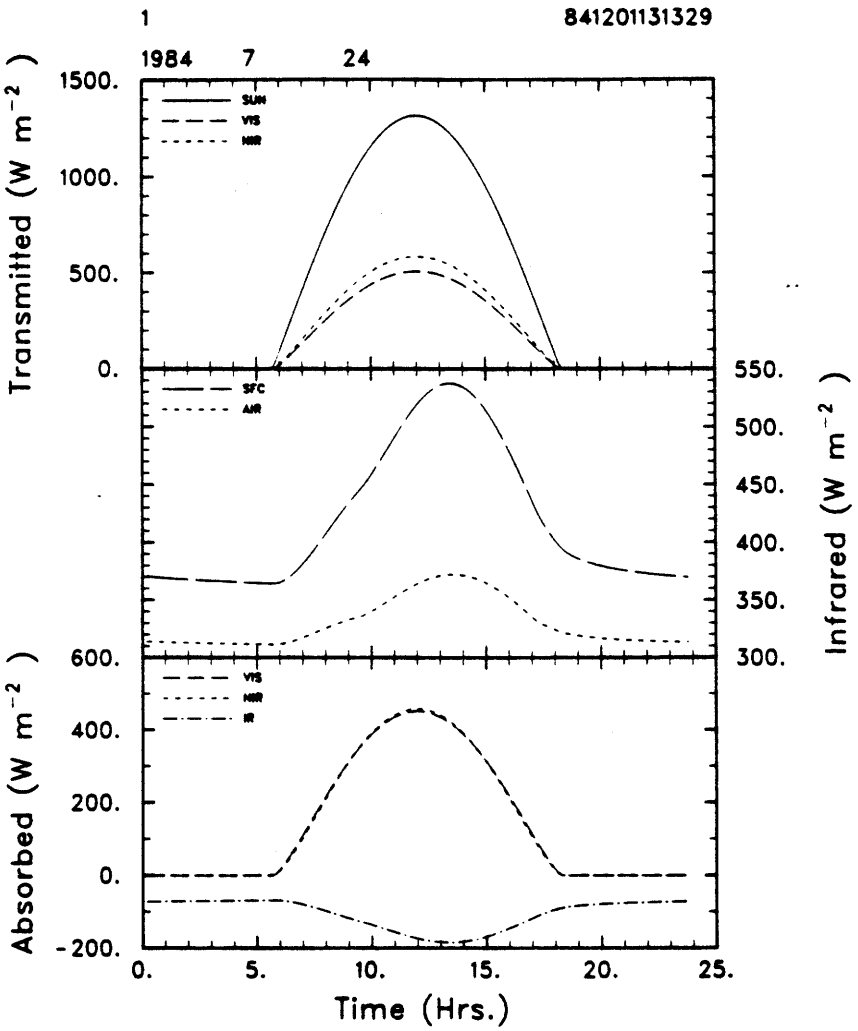

Figure 10.5: Surface radiative fluxes, bare ground and clear sky

Figure 10.5 shows the radiative fluxes at the soil surface, and should be compared to Figure 9.4. The only noticeable difference is in the level of infrared emission by the surface (SFC: --), which is about 20% lower for the sandy soil than for the loam soil. This indicates that the top soil layer is cooler. The reasons will become clear by looking at the next figure.

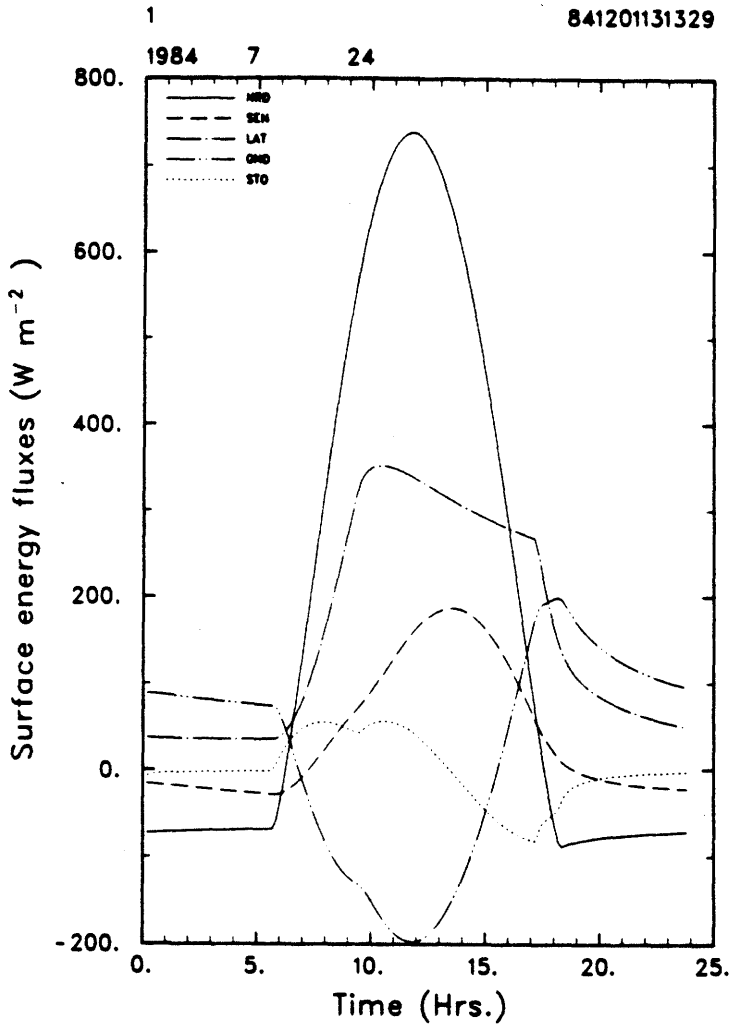

Figure 10.6: Surface energy fluxes, bare ground and clear sky

The energy fluxes at the surface of the sandy soil are displayed in Figure 10.6. Compared to the loam soil case (Figure 9.10), the latent heat flux (LAT: – · –) now plays a much more important role, as a result of the difference in hydraulic conductivity between the sand and the loam. It is remarkable that this occurs despite the fact that the volumetric soil moisture content in the top loam layer is still $0.25\,m^3\,m^{-3}$, while that of the top sand layer is not more than $0.17\,m^3\,m^{-3}$.

The actual evaporation rate is able to follow the potential rate from 6:00 to 10:00, but the soil again takes control until the sun sets. As a result of this increased latent heat flux,

the relative roles of the sensible heat fluxes, both to the atmosphere and to the ground are diminished. The storage term is also smaller in this case, and this explains why the top soil temperature does not raise as much as in the previous case.

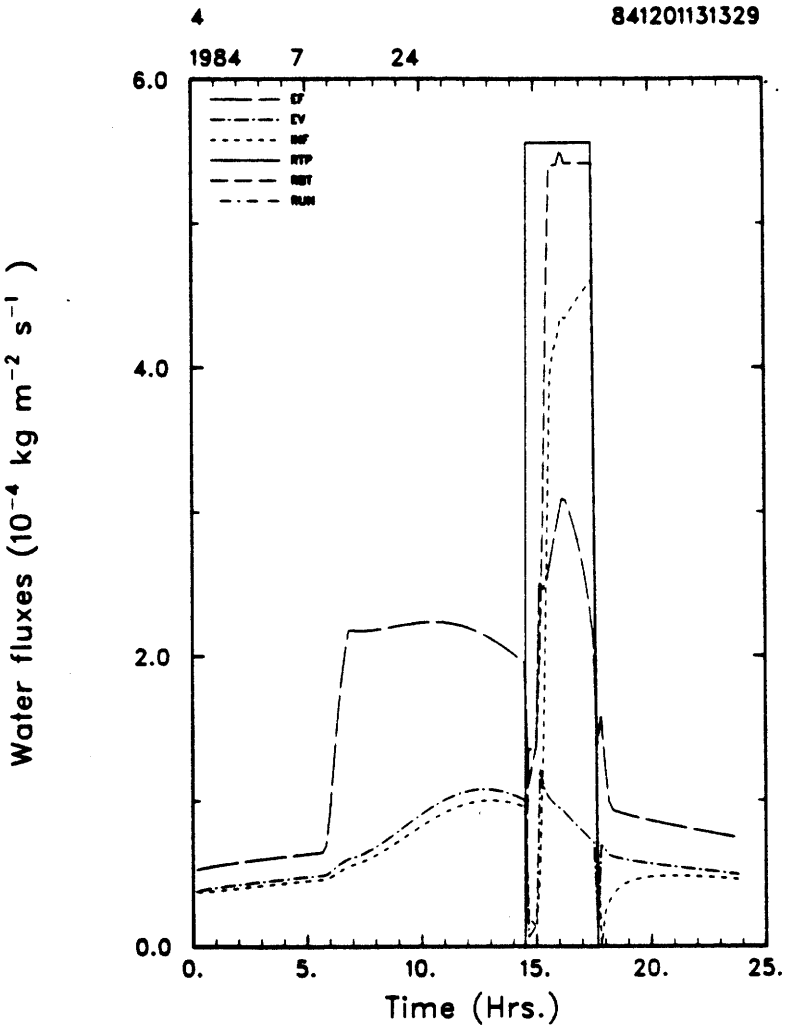

Figure 10.7: Water balance, canopy and cloudy sky

The wilting point of sand is almost three times lower than that of loam (Table 8.1): this indicates that it is easier for the root systems to extract water from a sand than it is from a loam, as can be observed in Figure 10.7, which shows a transpiration rate more than twice as large as the one in Figure 9.15.

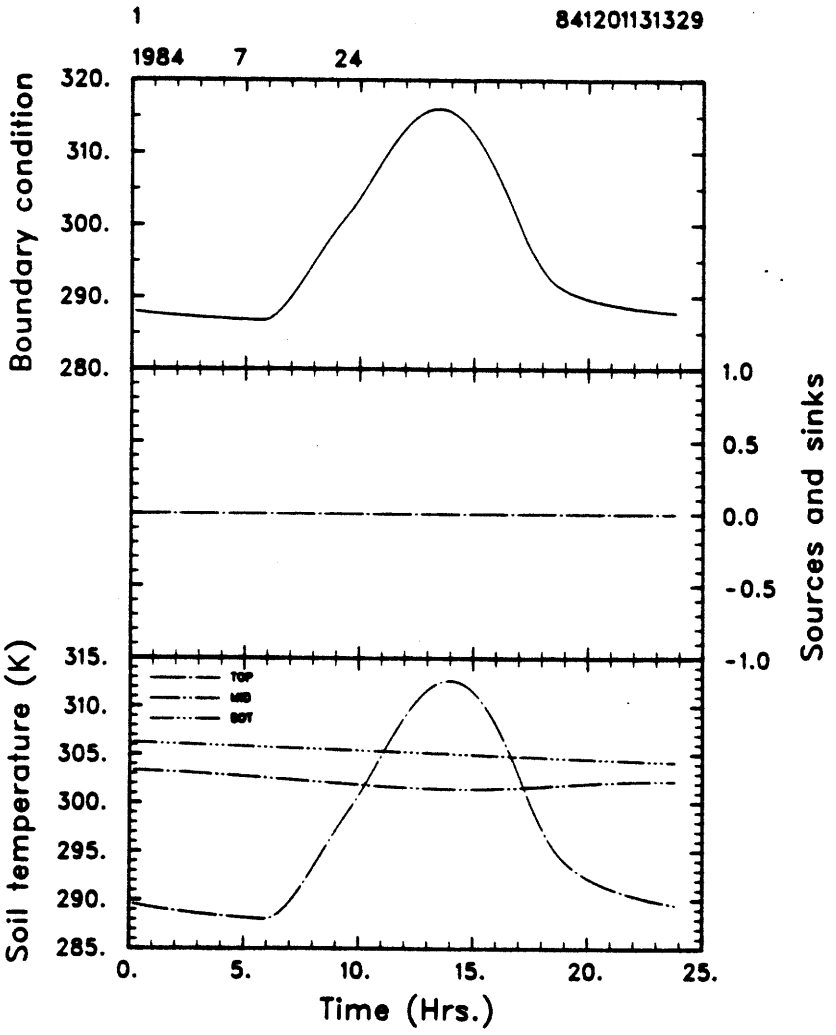

Figure 10.8: Soil temperature, bare ground and clear sky

Finally, Figure 10.8 shows the evolution of the top soil temperature for a sandy soil: although the night time temperatures are very similar (compare with Figure 9.21), the maximum is about 15 K less for sand than for loam, for the reasons explained above.

10.3 Differences in season

The next two runs involve a change of season, since they take place in January rather than in July. The seasonal cycle is never very pronounced in tropical regions. Referring to Figure 3.2, it is seen that the solar radiation forcing outside the atmosphere at 12° North is only 12% less in January than in July. As a result, no dramatic differences are expected at the outset. The soil type of both of these runs is sand, and comparisons must therefore be made with the previous run rather than the base run, as far as the sensitivity analyses are concerned.

The differences in the characteristics of the solar radiation between July 24 and January 24 are not large enough to produce significant differences in the surface albedo (through its dependency on the solar zenith angle) or in the fluxes transmitted to the surface.

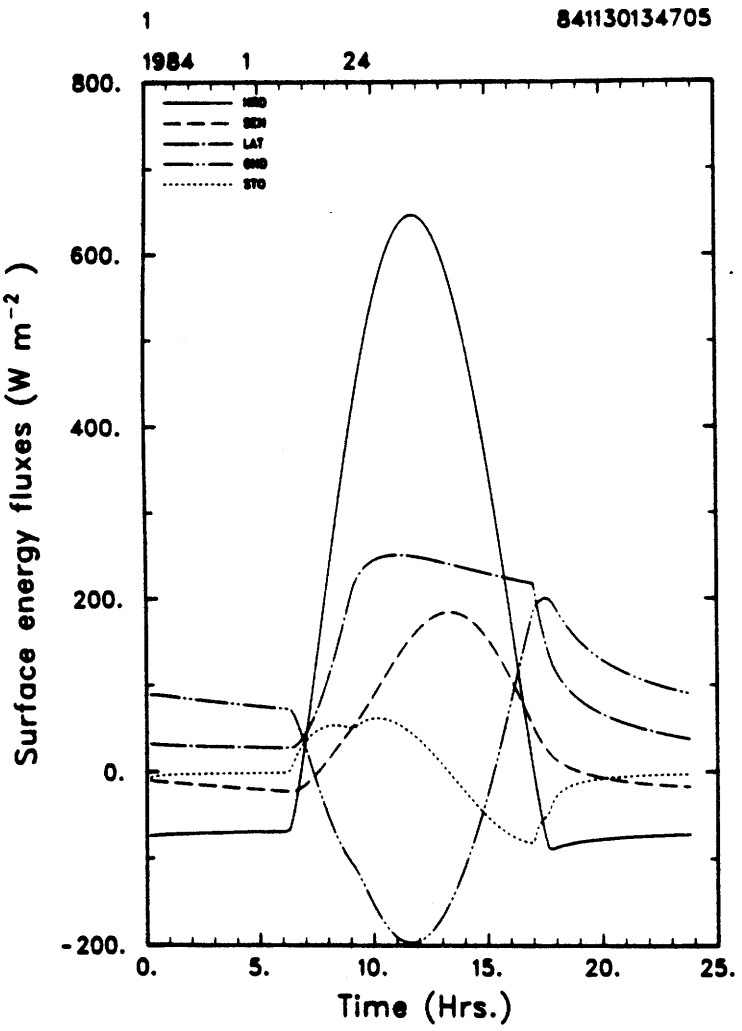

Figure 10.9: Surface energy fluxes, bare ground and clear sky

The first couple of interesting figures to compare is provided by Figures 10.6 and 10.9, showing the energy balance at the surface of a bare ground under clear sky, in summer and winter, respectively. First of all, the net radiation balance is reduced by about 15% in winter. The other fluxes are of the same order of magnitude than in the summer case (especially at night), but generally smaller during the day. The latent heat flux, for example, does not exceed 240 W m^{-2} at 10:00 in January, while it is of the order of 340 W m^{-2} in July, at the same time of the day.

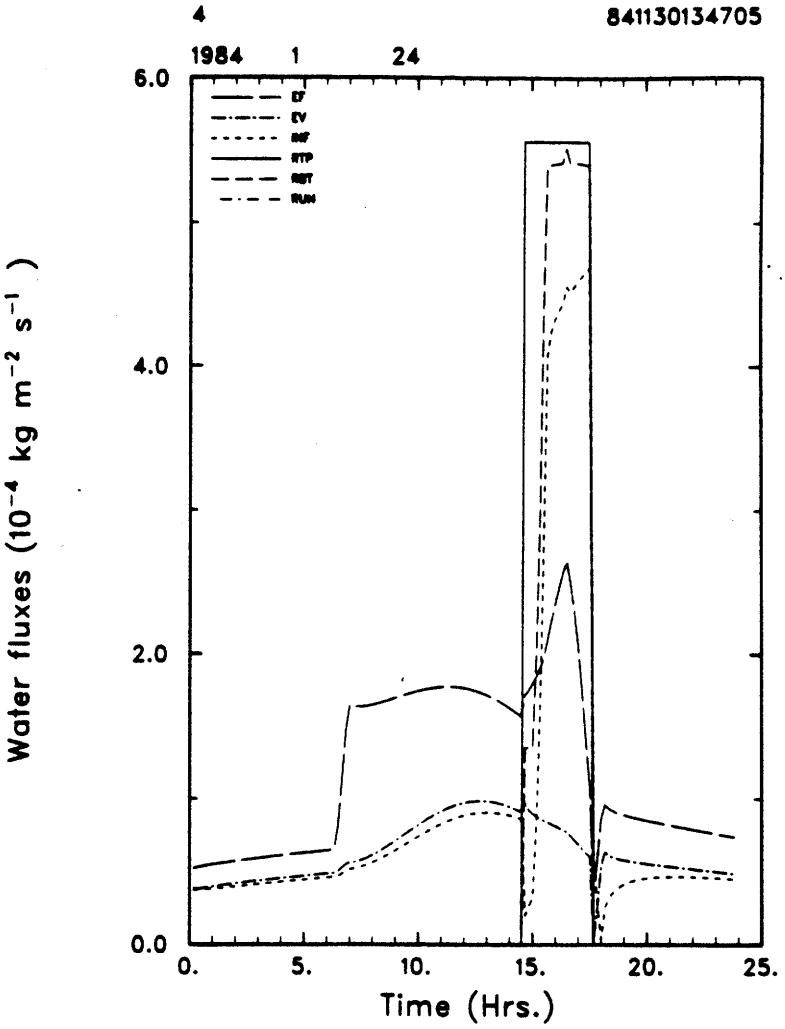

Figure 10.10: Water balance, canopy and cloudy sky

Figure 10.10 shows the usual water balance at the soil surface, under a canopy and cloudy skies: It can be compared with Figure 10.7 above. In the winter, the evapotranspiration rate is somewhat reduced.

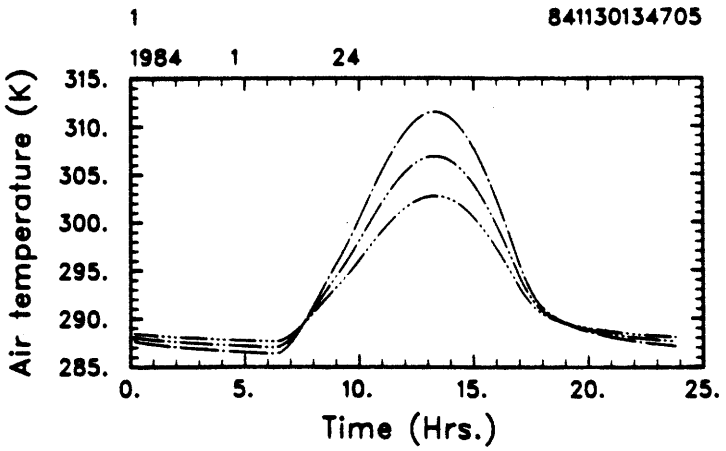

Figure 10.11: Air temperature, bare ground and clear sky

The air temperature is about 2 to 3 K lower in the winter than in the summer, in the first submodel (Figure 10.11). A similar drop of temperature is observable in the third submodel, and somewhat lower ones in the two vegetated submodels.

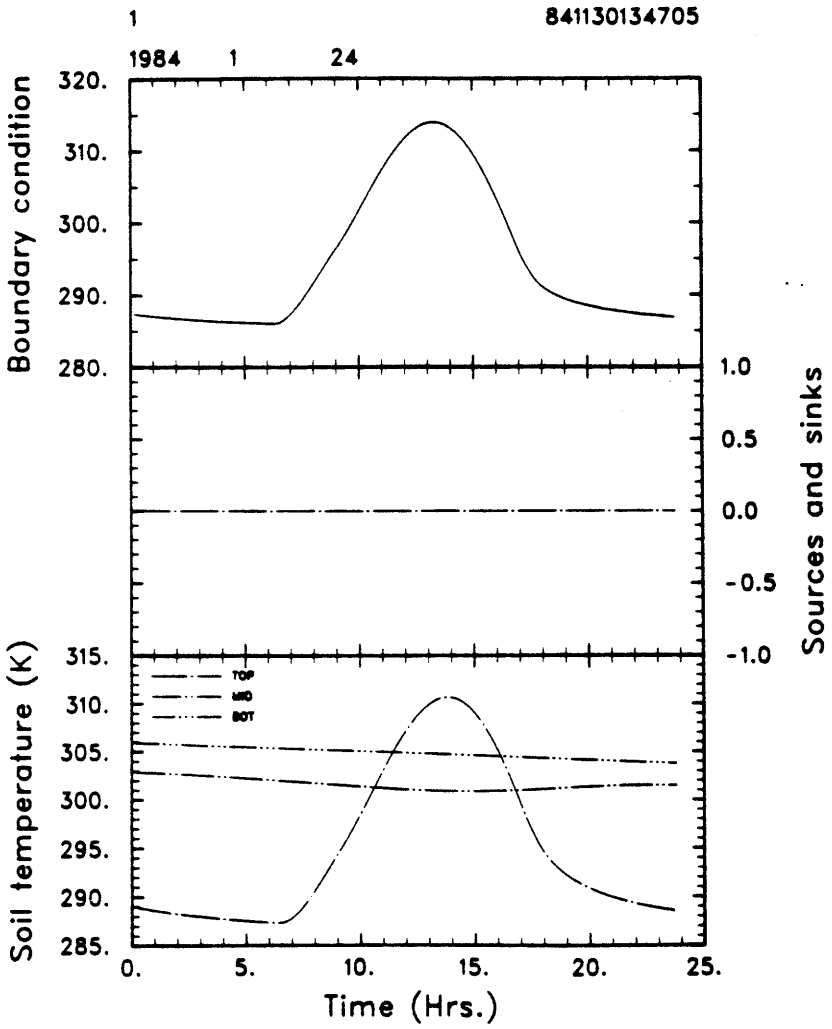

Figure 10.12: Soil temperature, bare ground and clear sky

Finally, Figure 10.12 shows that the top soil temperature is also 2 K lower than in the summer. It should be pointed out, though, that the longer time scales associated with soil diffusion processes may require more than a few days of integration to show appreciable differences.

10.4 Differences in wind speed

In Chapter 6, it was seen that both the sensible heat flux and the potential evaporation rate from the surface to the atmosphere depend directly on the wind speed at the top of the model (Equations (6.2) and (6.6)). Furthermore, the coefficients Ce_r and Ch_r, which enter these equations, also depend on the friction wind speed u_*, itself a function of the imposed wind speed, of the height at which it is imposed, and of the parameters d and z_0.

The displacement height d and the roughness coefficient z_0 are computed in the model, but the imposed wind speed and the anemometer height (10 m) at which it is imposed were selected somewhat arbitrarily. The purpose of this section is to identify which one of these parameters is the most important for u_*, and to see how the results of the model are affected by a change in this parameter.

Let $z_T = 10\,\mathrm{m}$, $u_T = 3\,\mathrm{m\,s^{-1}}$, $d = 0.1\,\mathrm{m}$, and $z_0 = 0.04\,\mathrm{m}$ be typical values of these coefficients. The following tables show the values of u_* for the indicated values of the dependent variables, where all other variables take on the above default values.

u_T	1.5	3.0	6.0
u_*	0.11	0.22	0.44

z_T	5.0	10.0	20.0
u_*	0.25	0.22	0.19

z_0	0.02	0.04	0.08
u_*	0.19	0.22	0.25

d	0.05	0.1	0.2
u_*	0.22	0.22	0.22

In these tables, the middle values are the defaults given above, and the left and right values are half and twice the default, respectively. This simple analysis of the functional dependency of the friction wind speed shows that u_* is most sensitive to the value of u_T,

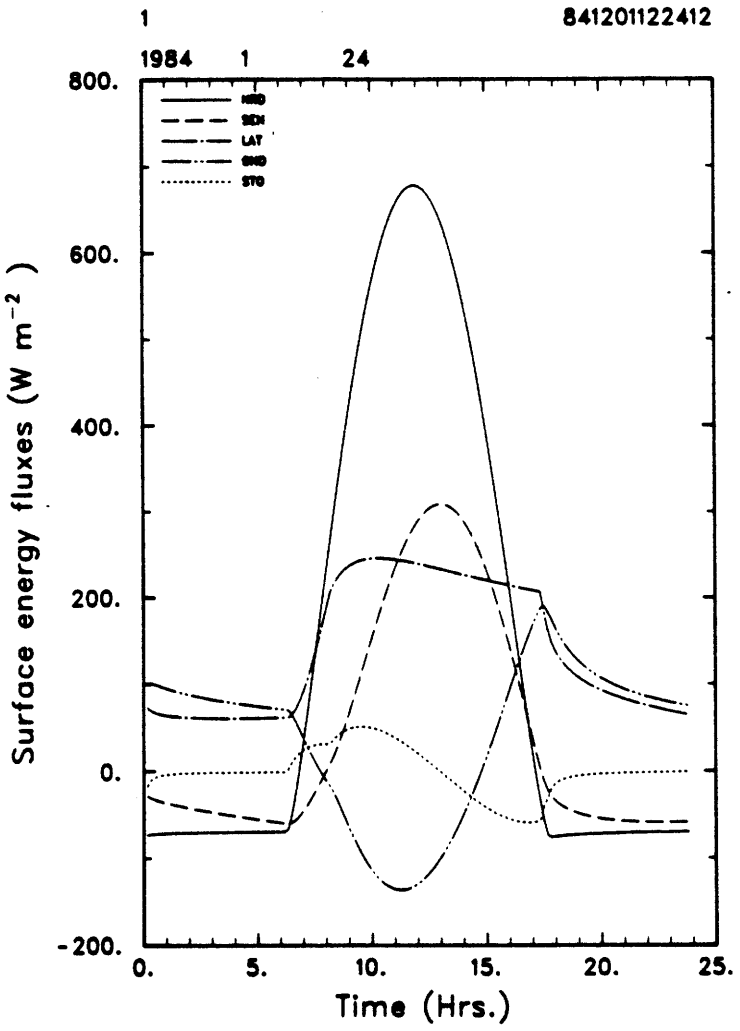

Figure 10.13: Surface energy fluxes, bare ground and clear sky

moderately sensitive to the values of z_T and z_0, and insensitive to d. Of all the dynamic parameters that affect the friction wind speed and therefore the surface fluxes of heat and water vapor, it is therefore the imposed wind speed which seems the dominant factor. To see the effect of an increased imposed wind speed on the model, an additional run was performed, where the wind speed at 10 m was 3 times larger than previously. The figures shown below are for such a case. The choice to make this experiment in January was made because strong dry winds are common in the Sahel in winter.

Figure 10.13 shows the fluxes of energy at the soil surface when the imposed wind

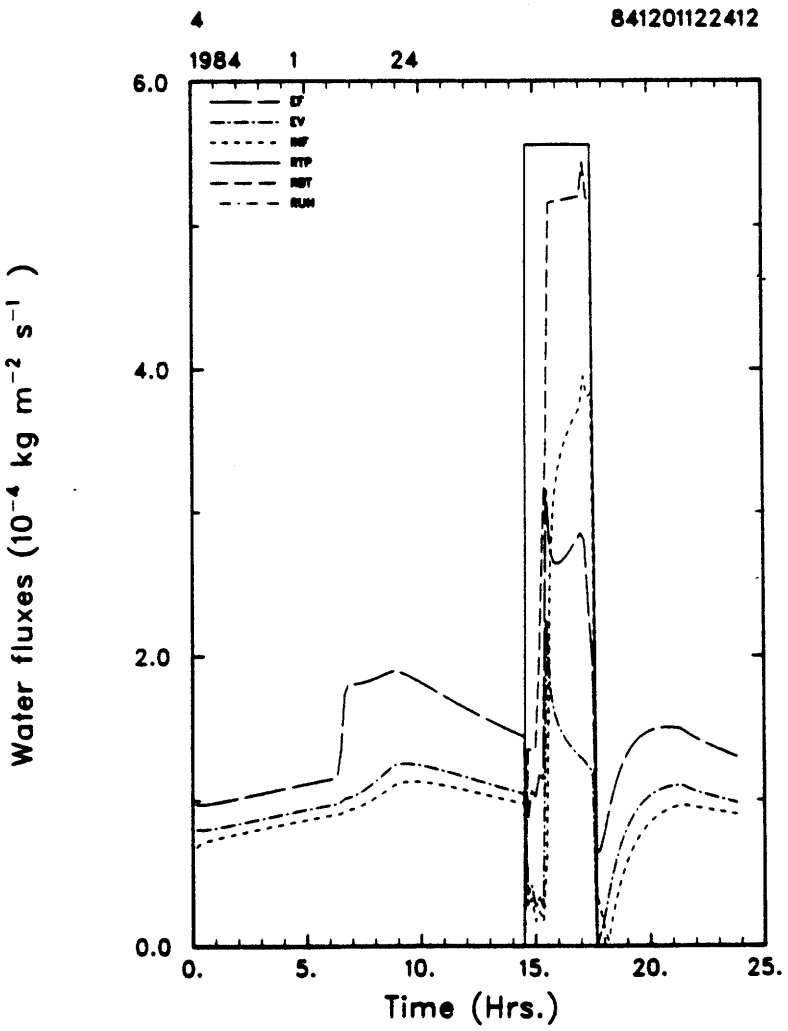

Figure 10.14: Water balance, canopy and cloudy sky

speed at 10 m is of the order of $9\,m\,s^{-1}$ instead of $3\,m\,s^{-1}$, as before. By comparing it with Figure 10.9, it appears that, to the extent that the evaporation rate is controlled by the soil, the actual latent heat flux is insensitive to the wind speed; but also that the resulting changes in the sensible heat flux to the atmosphere are compensated by the ground heat flux, and, to a lesser extent, by the storage term.

Figure 10.14, which displays the various terms of the surface water balance for submodel 4, suggests the following comments. First of all, the transpiration rate (the difference between EF: —— and EV: -·-·), especially in the morning, is decreased under

higher winds, because of the control the lower leaf temperature (not shown here) exerts on the stomates.

On the other hand, the evapotranspiration rate (EF: ——) is larger than before during the precipitation event, due to the more efficient evaporation of water from the wet parts of the leaves. This can be seen by observing that the difference between the forced precipitation rate (RTP: —) and the precipitation rate under the canopy (RBT: ---) is higher, after the canopy has been saturated, in the high winds case (above) than in a low wind case (Figure 10.10). As a result of increased losses through interception and evaporation, the infiltration rate (INF: ···) is decreased by almost 20%.

The temperature of the top soil in the first submodel (Figure 10.15) is decreased by some 5 K in the case of high winds, for the reasons explained above: a higher sensible heat flux must be compensated by a reduced ground heat flux and heat storage in the first layer.

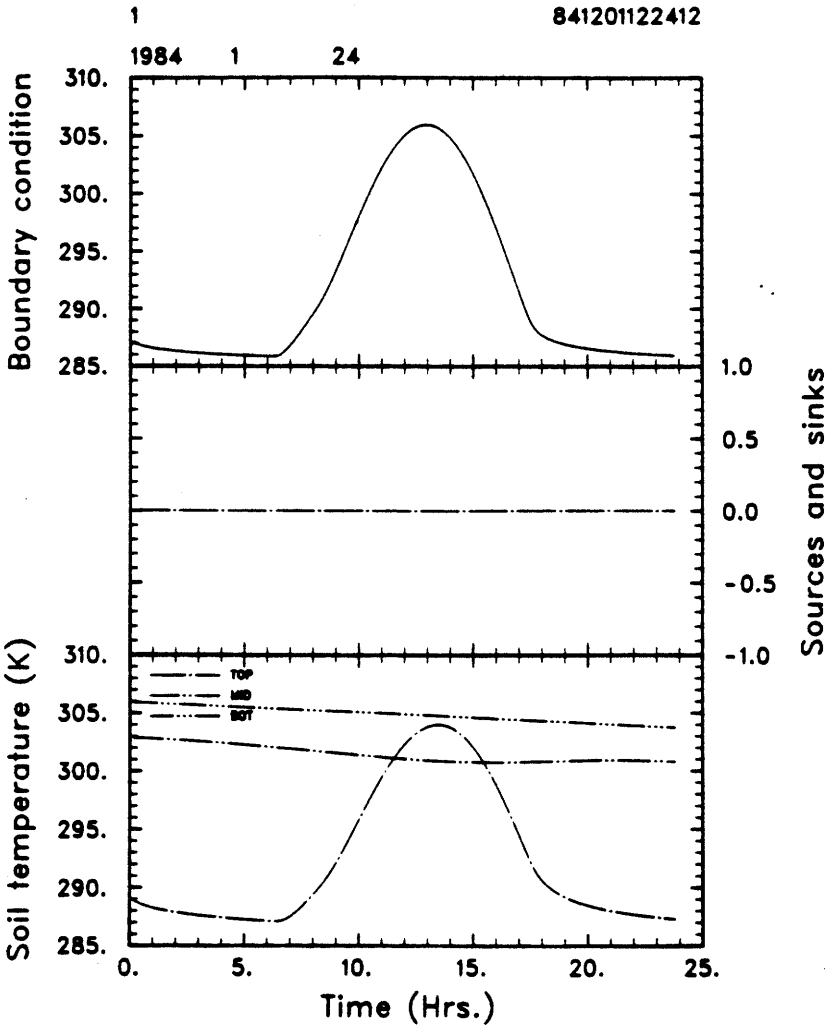

Figure 10.15: Soil temperature, bare ground and clear sky

Chapter 11: Discussion and Conclusions

A very detailed multi-layer one-dimensional model of the upper soil, vegetation, and lower atmosphere has been designed and implemented. The structure of the model was described in the first part of this dissertation, and the results of a selection of runs have been discussed in the second part. In this final chapter, I will discuss the problem of validating such a model, comment on how it could be improved, and suggest possible utilizations.

11.1 Validation of the model

The results discussed in the previous two chapters were generated from a computer model, i.e. from mathematical equations and initial conditions. Because all models are simplified representations of the real world, one must enquire to what extent these results are typical of what can be observed in the environment. This is the subject of this section.

The process of validation is naturally dependent on the objective pursued in building the model: a crop model to be used in the field should be simple to operate, designed for a particular crop, soil and climate, and accurate enough to be useful. A theoretical model like this one should emphasize generality in its design and promote physical understanding, rather than applicability to a particular situation.

A model may be evaluated from different points of view: nature of the underlying equations, internal consistency of the results, numerical accuracy and performance, and comparison of the results with independently obtained data. A full validation procedure for a complex model may take man-years of work (data collection and processing, design and implementation of numerical experiments, etc...), especially when the validating information is not routinely available, as is the case here. The following remarks are an attempt to cover these different approaches and to present supporting evidence when available.

This model is composed of a large number of equations. At one end of the spectrum are basic physical laws such as the conservation of mass or energy: these are known to be correct, and do not need to be validated. Next would be the diffusion equations, for example, which were derived from countless experiences in different fields of applied physics. For these, the estimation of the various diffusion coefficients proves to be the stumbling block. At a lower level of generality and confidence are different parameterizations which are believed to give acceptable results while simplifying the mathematical treatment. The relation between the soil water potential and the soil moisture content is one such relation. In all these cases, I have relied on the author of the parameterization in accepting his or her work.

In a few cases, I have made modifications to existing schemes, such as applying a correction to the wind profile inside a canopy to force it to converge to zero at the surface; or proposed new parameterizations, such as the formula to compute the infrared radiation exchange between different leaf layers. Unfortunately, no data was available to validate these procedures independently, prior to their inclusion in the model. The logic of the procedure and the overall performance of the model must serve as a justification for these special cases.

Another way to check a model is to ensure that independently produced partial results remain consistent with each other. This may require the computation of secondary

variables with known properties. For example, the atmospheric specific humidity and temperature can be combined to compute the relative humidity, which should remain within reasonable bounds (0 to 100%). This has been verified. Another internal check consists in making sure that the model does not violate conservation laws. Since the temperature of the air and leaves, for example, is computed iteratively from such an equation, it is known to be verified. In the case of the soil, the total water and energy content do not vary appreciably from one time step to another, compared to the surface fluxes of the same quantities.

Closely related is the issue of numerical accuracy and performance, as well as the sensitivity of the model to initial conditions. It turns out that some variables are more sensitive than others to initial conditions, and this is related to the characteristic space and time scales of the processes involved. Soil moisture, for example, had not quite reached a steady state after three days, while the profiles of atmospheric temperature and humidity showed no memory of initial conditions after three to six hours. This is expected from the turbulent processes in the atmosphere. The sensitivity of the model to initial conditions is expected to increase if additional processes that present hysteresis are included in the model.

Similarly, different processes in the model have different sensitivities to the size of the time step of integration. For example, a shorter time step may be required with sandy soils than for a loam, because the water moves so much more easily in sand. Higher precipitation rates, at least of the type used here (step functions) also required shorter time steps. Since the same time step is used for all processes in the model, the most demanding process was the deciding factor. However, since the purpose of the first few days of integration was solely to allow the model to relax from initial conditions, a longer time step (5 or 10 minutes) was usually chosen for this period. The time step should also be related to the spacing of the grid points, although no experimentation was made along these lines with the whole model.

Probably the ultimate test of validity is the comparison of the model results with observations of the actual ecosystems it is supposed to emulate. This presents two specific problems: the data may not be available, or it may not be of sufficient quality.

The greatest difficulty is to obtain significant observations for all or most of the parameters and variables, from the same site, at the appropriate space and time scale. Most of the atmospheric data routinely reported and accessible is related to the synoptic or climatological scales. Some agro-meteorological stations may collect relevant data, but this is much less accessible, and not necessarily in the right region: it is unfortunately the case that the tropical regions are poorly instrumented.

The situation is much worse when it comes to soil or biological data, probably because these disciplines do not enjoy the benefit of having an international organization such as the World Meteorological Organization, to evaluate and promote the use of standard procedures to observe the environment and report the data. For example, there is no universally accepted soil classification, although the Unesco and FAO have proposed a standard.

When observations are available, their quality must be questioned as they suffer from inherent and random errors introduced by the instruments themselves, the skills of the observers, or the reporting process. The influence of these errors may be reduced by averaging, either in space or in time, but the resulting data then becomes of lesser interest for the current purpose. Sometimes, excellent data is available in a format or unit unusable for this purpose: for example, global maps or data sets of vegetation do exist in terms of plant species, or biomass (in kg of carbon per square meter), but this is not easily converted in leaf area index.

With these limitations in mind, it remains important to try to compare the results with what is known of the environment. Since I am not aware of a single source of information that could be used to validate the many aspects of this model, I have assembled below a set of figures and data that support one or another aspect of the model results. The

variety of the sources, and the possible inhomogeneities this procedure introduces are unfortunate but unavoidable. I should also mention that all the comparisons mentioned here have all been made *after* the runs were executed: no tuning of the model to the data has been made whatsoever. The objective of the following comparisons is therefore not to try to demonstrate that the model results fit the observations, but, rather, that they are consistent with the limited available evidence.

1. The estimation of the level of solar radiation outside the atmosphere results directly from astronomical computations, and comparisons of results such as those shown in Figure 3.2 with published data (e.g. Sellers, 1965, p. 18) show, of course, an excellent agreement.
2. Budyko (1974) provides a number of maps and data on the various elements of the water and energy balances in different climatic zones. The comparisons with regional or global maps should be made in one of the two following ways: either the results of each submodel should be compared with data for actual places where the vegetation and cloudiness is known to approximate the extremes of the submodels, or the weighted averages of the results of the four submodels must be compared with the overall data for a region with known vegetation and cloudiness cover. Since these covers are often unknown, educated guesses must be made; and a couple of plausible guesses would provide a range of possible answers. It should also be remembered that the model produces instantaneous values, while most sources of climatic data report monthly mean values.

   Budyko (1974, p. 169) shows a global map of the June monthly mean sensible heat flux from the surface to the atmosphere. Although such data is not directly comparable to the model results for the 24^{th} of July, the following observations can be made: the monthly mean sensible heat flux at 12° North and 0° East in June is of the order $16\,W\,m^{-2}$. The meridional gradient is relatively large, however, and the June mean monthly sensible heat flux reaches $96\,W\,m^{-2}$ at 21° North, where the vegetation and

cloudiness covers are much reduced. Rough estimates of the daily average sensible heat fluxes from each of the four submodels of the base run are 83, 30, 13, and $-10\,W\,m^{-2}$, respectively. At that location and time, the last three submodels would have the largest weight, since it is the middle of the rainy and growing seasons. If both the vegetation and cloud covers were 0.7, the weighted average of these fluxes would be $11.6\,W\,m^{-2}$, and if both fractional covers were 0.6, the average flux would be $20\,W\,m^{-2}$. Of course, other combinations may actually have occured.

3. Similarly, Budyko's (1974, p. 165) map for the June monthly mean latent heat flux from the surface to the atmosphere is about $80\,W\,m^{-2}$. In this case, the meridional gradient is oriented in the other direction, since more northward locations actually evaporate less: the mean actual latent heat flux decreases to less than $16\,W\,m^{-2}$ at 20° North. The daily average latent heat fluxes from the four submodels of the base run are 75, 40, 100, and $87.5\,W\,m^{-2}$, respectively. If the same weights as before are applied to these fluxes, the 0.7 fractional cover yields an average latent heat flux of $79\,W\,m^{-2}$, and the 0.6 fractional cover an average of $77\,W\,m^{-2}$.
4. The submodels' daily mean global solar radiation levels, for the soil and canopy (when present) combined, are 110, 160, 85, and $115\,W\,m^{-2}$, respectively. The weighted averages of these values for fractional vegetation and cloud covers of 0.6 and 0.7 are both about $117\,W\,m^{-2}$, while the value of the radiation balance for June given by Budyko (1974, p. 159) is $96\,W\,m^{-2}$ ($112\,W\,m^{-2}$ at 20° North).
5. Lamb (1972, p. 522 ff.) provides a long table of surface climatological data for a number of stations around the Earth. Of course, these data items are monthly means, but some stations have standard deviations or ranges that give an idea of the variability. Fort Lamy (Chad) happens to be located at 12° North, 15° East, at an altitude of about 300 m. Unfortunately, the only data relevant for the current comparisons is the monthly mean temperature: in July, the mean temperature (average of maximum and minimum) is 300.7 K. The daily mean temperatures for each of the four submodels of

the base run, computed the same way, are 298.5, 300.5, 293.25, and 301.5 K, respectively. Assuming fractional covers of 0.6 and 0.7 as before gives mean temperatures of 298.8 and 299.3 K, respectively. By the way, the January monthly mean temperature for Fort-Lamy is 4 K less than in July, and the air temperature in the model was found to be 2 to 3 K less in winter than in summer.

6. On the other hand, the same data source shows that the monthly mean July temperature for Khartum, Sudan (15° North, 32° East at an altitude of 330 m) is 304 K, with a diurnal range of 13.5 K. The temperature ranges in the four submodels are 16, 3, 6.5 and 2 K, respectively. Of course, aside from being located slightly more northward than Fort-Lamy, Khartum is also a much more desertic environment. In the absence of specific data, the selection of particular values for the vegetation and cloud cover is open to question. Nevertheless, a vegetation cover of 0.2 and a cloud cover of 0.8 would give an average temperature range in the model of 10 K, for example. The large diurnal temperature variations observed over bare ground in the model results are also consistent with the data reported by Griffiths (1972, p. 21).
7. The amplitude of the daily waves of temperature in the soil, as well as their phase lag with respect to the top layer, are in general agreement with published data (Geiger, 1965, p. 56 ff.), or other theoretical estimations (Hillel, 1982, p. 169; or Oke, 1978, p. 40).
8. No data on soil moisture for the regions concerned was available for checking the model, but the rate of drying of submodel 1 (no vegetation and no cloudiness) compares favorably with that of a sandy loam as given by Hillel (1982, p. 242).

Again, the purpose of these comparisons was to suggest that the model behaves reasonably, not that the environment of Ouagadougou (Upper Volta) was successfully modeled. The fact that the model results are well within the range of observations is encouraging,

but much more detailed studies should be made to ensure that the matching holds or improves when more data is available for comparison or when the model is tuned to represent a particular place.

In order to validate more completely this model against observations, detailed data must be available on the nature, temperature and humidity of the soil, on the temperature and specific humidity of the air, on the radiative fluxes at the surface, and on the wind profile. The resolution of this data must be sufficient to resolve the diurnal cycle. Lysimeter data may be required to check the estimates of transpiration, and measurements of radiation fluxes at different levels in the canopy would also be needed. All this data should ideally come from the same site, and two or more such sites would be preferable to investigate the behavior of the model in different climatic regimes. It therefore appears that a well-instrumented agro-meteorological station would be the most likely place to test this model. It is of interest to note that the World Meteorological Organization is interested in collecting such data for the Sahelian region, and sponsors a research and training center in Niamey, Niger. This project has recently entered its operational phase.

11.2 Discussion of the model results

To my knowledge, this is the first model of this complexity ever built for the top soil, vegetation and lower atmosphere system. As was pointed out in Section 1.3, detailed models do exist for each of the components taken individually (lower atmosphere, canopy, root system, soil), but these are rarely integrated. And when they are, they usually make a number of simplifying assumptions about one or another component.

The model described in Part 1 has been subjected to sensitivity analyses in Part 2. There is obviously an almost infinite number of experiments that could be performed with such a model, and only a very limited number of them have been performed so far.

Although these results should be considered incomplete and preliminary, it has been shown that a reduction in leaf area index (amounting to a comparable reduction in the optical thickness of the vegetation canopy) by a factor 2 increased the transmission of solar radiation in the canopy and its absorption at the soil surface (as expected), but also increased the infrared losses, both by the surface, and by the vegetation and underlying surface combined, especially under clear sky. The canopy was also shown to introduce a lag of about an hour in the soil surface temperature signal.

Similarly, it was shown that a thicker canopy intercepts more precipitation (as expected), but that this, in turn, introduced longer delays before the water reached the surface, and increased the total loss of water through evaporation. The canopy also takes relatively more time to dry up after a rain event than to wet when the rain starts, and the temperature difference between the leaves and the air was shown to be larger in a thicker canopy.

No experiments were made in this direction, but it appears that the vertical distribution of the leaf area density (i.e. whether the leaves are concentrated at certain levels or distributed throughout) may alter the transfers of sensible and latent heat fluxes from the canopy to the air, and therefore the profiles of temperature and specific humidity. Investigations along these lines with this model could provide information on the ecological niches occupied by different plant and animal species.

The sensible heat flux above the thicker canopy was about 40% higher than above the thinner canopy, due to the increased roughness. It is interesting to note that a similar increase in the sensible heat flux was observed when the imposed wind speed at 10 m was increased by a factor 3, in the winter cases.

The importance of the nature of the soil was demonstrated by comparing the model's results for a loam and a sand. It turns out that the soil type exerts a strong influence on the surface energy balance in general, and the latent heat flux in particular. In this respect, the hydraulic conductivity is the most important factor, because its value is highly

dependent on the variable it controls, namely the soil moisture content, and it limits the actual rate of evaporation from the soil surface. The transpiration rate was also observed to be larger in a sand than in a loam soil, because it is easier for the roots to extract water from the sand.

The seasonal cycles are not very pronounced at 12° North, but the decreases observed in the various surface energy fluxes were found consistent with those actually observed at that latitude. It will be interesting to study the seasonal behavior of this model for more poleward locations, although the model should then also include additional processes such as snow deposition.

11.3 Suggestions for further work

This work could be expanded in a number of directions, some of which will be outlined here.

First of all, the model could be made more efficient numerically but otherwise retain its current structure and overall amount of detail. Improved numerical algorithms, combined with computer-specific optimization (vectorization) and longer integration time steps would make it possible to assess the characteristics of the model climate, that is, the statistical state to which the set of equations tends after a long period of integration. This, in turn, would allow the study of processes on a seasonal or interannual basis. In particular, it would be interesting to investigate the evolution of the microclimate at the end of climatic events, such as after a prolonged drought or a very wet period, or during a transition period between the two.

In a similar vein, the influence on the microclimate of a slow but continuous removal of the vegetation cover could be quantified. This would be of particular interest for understanding the process of desertification. It may be worth repeating here that although

this model does not include any human influence or interaction with the environment explicitly, these aspects can be easily included by manipulating the vegetation cover. The model could therefore be used to study the influence of overgrazing on the local microclimate. This information, coupled with data on the needs of specific plant species for seeding and establishment, could be used to assess the probability of survival for such species in the perturbed environment.

A second avenue of research and development would be to simplify the model greatly, or, rather, to derive from it another model simple enough to be incorporated in larger scale models, such as atmospheric general circulation models or meso-scale models. There is currently a growing interest in including more realistic vegetation processes in such models, because of the effect that these processes have on the balance of water and energy at the surface. Some experiments have been done at NCAR by Dickinson et al., and Mintz and his group (NASA) have also projects in this direction.

Attempting a better parameterization of surface processes could not only improve the accuracy of larger scale models, but should also allow the study of the influence on the regional climate of global processes, such as deforestation. Before such a coupling is implemented, however, the signals produced by this detailed model may have to be filtered through a low-pass filter, to remove undesirable transients.

Another use of a simplified model would be the study of very long time evolution of an ecosystem. Presumably, such a model would be relatively inexpensive to run, and its integration over years could be useful in studies of succession of vegetation.

A third possibility would be to couple this model with a radiative-convective model, so that the entire atmospheric column, or at least a large part of it, would be better represented. Short of that, a better parameterization of the boundary layer itself would provide already significant improvements (The logarithmic wind profile used here is derived under the assumption of neutral stability.)

At the other extreme, a convective cloud model that could interact with the surface would be of particular interest to study the influence of changes of surface vegetation cover on precipitation mechanisms, as was suggested by Charney (1975). This might provide some clues relative to the positive feedback mechanisms that maintain a drought, but perhaps also tell us something about the processes that ultimately break the drought.

Additional radiative and thermodynamic processes should be incorporated in such an expanded model, to account for the interaction between the vertical radiative flux divergence and the flow itself, or for other processes such as the phase changes of water.

This model could also be expanded in other directions. For example, one could include more biological processes and, in particular, design an interactive vegetation cover that would grow up and develop as a response to the changing microclimate. Alternatively, or in parallel to this, some of the major chemical cycles (CO_2 in particular), could be included. One could then investigate the influence of an increase in CO_2 on plant species as well as on the canopy. Each of these improvements would open new possibilities and applications.

Finally, one or another version of this model could be used for specific studies such as comparing the behavior of different drought indices under similar plant and microclimatological conditions, or trying to reconstruct the microclimate near the ground in different geological eras, based on the available evidence about the type and characteristics of the vegetation, as well as the known and estimated parameters of the macroclimate.

For almost thirty years now, satellites have been sent around the Earth and in space, and a large fraction of them carry sensors to measure radiation signals coming from the surface of this planet. The interpretation of these measurements is a major scientific challenge, and it has always been necessary to compare them with some form of "ground truth", i.e. data collected on the surface being observed from space. The collection of this data is not always feasible, and can sometimes be replaced by numerical computations with models that predict the characteristics of the reflected or emitted radiation from

the surface, given some information on the nature of the surface and on the general meteorological conditions. This is another area where surface models like this one could be of use.

Finally, after additional sensitivity analyses have been performed, more attention could be given to improve the realism of the model in its simulation of specific ecosystems. Scenarios can then be developed and evaluated, in terms of their influence on the local microclimate. More observations will be required to undertake such simulations. At this point, among the many data items that would be required, it seems that the leaf area index, together with the vegetation cover and height, would be the most needed to assess the influence of desertification on the microclimate with this model.

Appendix 1: List of Major Symbols and Units

Notes:

1. All symbols are defined in the text when they appear first in the discussion. This table lists only those symbols that may appear at different places, where the definition may not have been repeated.
2. It is intended that a given symbol has only one meaning throughout the entire text.
3. In the following table, "n-d" stands for non-dimensional, and the number between parentheses at the end of the description refers to the section number in which the symbol appears first.

Upper-case Roman characters

A_{ni} Absorbed visible solar radiation, in $\mathrm{W\,m^{-2}}$ (4.1)

A_{vi} Absorbed near-infrared solar radiation, in $\mathrm{W\,m^{-2}}$ (4.1)

A_{oz} Ozone absorption coefficient, n-d (3.2)

A_{H_2O} Water vapor absorption coefficient, n-d (3.2)

C Fractional cloud cover, n-d (2.4)

E Evaporation rate, in $\mathrm{kg\,m^{-2}\,s^{-1}}$ (6.1)

G_h Ground heat flux, in $\mathrm{W\,m^{-2}}$ (6.2)

G_w Infiltration rate, in $\mathrm{kg\,m^{-2}\,s^{-1}}$ (6.1)

H Sensible heat flux, in $\mathrm{W\,m^{-2}}$ (6.2)

H_v Scale height for water vapor, in m (3.2)

I^d Downward infrared radiation flux density, in $\mathrm{W\,m^{-2}}$ (4.3)

I^u Upward infrared radiation flux density, in $\mathrm{W\,m^{-2}}$ (4.3)

L Latent heat of vaporization, in $\mathrm{J\,kg^{-1}}$ (6.2)

$L(z)$ Leaf area index above a level z, in $\mathrm{m^2\,m^{-2}}$ (2.2)

LAD Leaf Area Density, in $\mathrm{m^2\,m^{-3}}$ (2.2)

LAI Leaf Area Index, in $\mathrm{m^2\,m^{-2}}$ (2.2)

M Magnification factor, n-d (3.2)

P Precipitation rate, in $\mathrm{kg\,m^{-2}\,s^{-1}}$ (6.1)

R_f Runoff rate, in $\mathrm{kg\,m^{-2}\,s^{-1}}$ (6.1)

R_0 Solar radiation flux density, in $\mathrm{W\,m^{-2}}$ (3.1)

R_d Gas constant for dry air, 287.04 $\mathrm{J\,kg^{-1}\,K^{-1}}$ (3.2)

R_n Net radiation balance at the surface, in $\mathrm{W\,m^{-2}}$ (6.2)

R_v Gas constant for water vapor, 461.50 $\mathrm{J\,kg^{-1}\,K^{-1}}$ (3.2)

S_0 Solar constant, 1367 $\mathrm{W\,m^{-2}}$ (3.1)

S_h Storage of heat in the top soil layer, in $\mathrm{W\,m^{-2}}$ (6.2)

S_w Storage of water in the top soil layer, in $\mathrm{kg\,m^{-2}\,s^{-1}}$ (6.1)

T_a Air temperature, in K (3.2)

T_s Soil surface temperature, in K (4.3)

T_{n1} Transmitted near-infrared solar radiation flux density under clear skies, in $\mathrm{W\,m^{-2}}$ (3.4)

T_{n2} Transmitted near-infrared solar radiation flux density under cloudy skies, in $\mathrm{W\,m^{-2}}$ (3.5)

T_{v1} Transmitted visible solar radiation flux density under clear skies, in $\mathrm{W\,m^{-2}}$ (3.4)

T_{v2} Transmitted visible solar radiation flux density under cloudy skies, in $\mathrm{W\,m^{-2}}$ (3.5)

V Fractional vegetation cover, n-d (2.4)

Z Solar zenith angle, in rad (3.1)

Lower-case Roman characters

d Displacement height, in m (5.1)

e_a Surface water vapor pressure, in Pa (3.2)

h_v Height of the canopy, in m (2.2)

k von Karman constant, 0.4, n-d (5.1)

u Wind speed, in $\mathrm{m\,s^{-1}}$ (5.1)

u_* Friction speed, in $\mathrm{m\,s^{-1}}$ (5.1)

z Altitude in the atmosphere, or depth in the soil, in m (3.2)

z_0 Roughness height, in m (5.1)

Greek characters

α_c Vegetation canopy albedo, n-d (4.2)

α_s Surface albedo, n-d (3.4)

ϵ_a Atmospheric emissivity, n-d (4.3)

ϵ_s Surface emissivity, n-d (4.3)

θ Volumetric soil water content, in $\mathrm{m^3\,m^{-3}}$ (4.1)

μ_0 Cosine of the solar zenith angle, n-d (3.1)

ν Kinematic viscosity of the air, in $\mathrm{m^2\,s^{-1}}$ (6.1)

ρ_v Atmospheric water vapor density, in $\mathrm{kg\,m^{-3}}$ (3.2)

ρ_{vs} Surface value of the atmospheric water vapor density, in $\mathrm{kg\,m^{-3}}$ (3.2)

σ Stefan-Boltzmann constant, $5.66961\,10^{-8}\,\mathrm{W\,m^{-2}\,K^{-4}}$ (4.3)

ψ Soil water potential, in m (8.1)

ϕ Latitude, in rad (3.1)

Bibliography

BERGER, A. L. (1978) Long-term Variations of Daily Insolation and Quaternary Climatic Changes, *Journal of the Atmospheric Sciences*, **35**, (12), 2362–2367.

BRUTSAERT, W. H. (1982) *Evaporation into the Atmosphere*, D. Reidel Publishing Company, 299 pp.

CAMPBELL, G. S. (1974) A Simple Method for Determining Unsaturated Conductivity from Moisture Retention Data, *Soil Science*, **117**, (6), 311–314.

CHARNEY, J. (1975) Dynamics of Deserts and Droughts in the Sahel, in *The Physical Basis of Climate and Climate Modeling*, GARP Publications Series, No. **16**, WMO, Geneva, 171–176.

CLAPP, R. B. and G. M. HORNBERGER (1978) Empirical Equations for Some Soil Hydraulic Properties, *Water Resources Research*, **14**, (4), 601–604.

CONDIT, H. R. (1970) The Spectral Reflectance of American Soils, *Photogrammetric Engineering*, **36**, 955–966.

DE VRIES, D. A. (1963) Thermal Properties of Soils, in *Heat and Mass Transfer in the Biosphere, Part 1, Transfer Processes in the Plant Environment*, edited by D. A. de Vries and N. H. Afgan, Wiley, 5–28.

DE VRIES, D. A. (1975) Heat Transfer in Soils, in *Physics of Plant Environment*, edited by W. R. Van Wijk, North-Holland, 210–235.

DICKINSON, R. E., J. JÄGER, W. WASHINGTON, and R. WOLSKI (1981) *Boundary Subroutine for the NCAR Global Climate Model*, National Center for Atmospheric Research, Technical Note TN-173+IA, 75 pp.

DICKINSON, R. E. (1983) Land Surface Processes and Climate - Surface Albedos and Energy Balance, *Advances in Geophysics*, **25**, 305–353.

DICKINSON, R. E. (1984) Modeling Evapotranspiration for Three - Dimensional Global Climate Models, in *Climate Processes and Climate Sensitivity*, edited by J. E. Hansen and T. Takahashi, Geophysical Monograph **29**, American Geophysical Union, Washington D.C.

DICKINSON, R. E. and B. HANSON (1984) Vegetation - Albedo Feedbacks, in *Climate Processes and Climate Sensitivity*, edited by J. E. Hansen and T. Takahashi, Geophysical Monograph **29**, American Geophysical Union, Washington D.C.

DUFOUR, L. and J. VAN MIEGHEM (1975) *Thermodynamique de l'Atmosphère*, Institut Royal Météorologique de Belgique, 278 pp.

EAGLESON, P. S. (1970) *Dynamic Hydrology*, McGraw Hill, 462 pp.

EL-BAZ, F. (1983) A Geological Perspective of the Desert, in *Origin and Evolution of Deserts*, edited by S. G. Wells and D. R. Haragan, University of New Mexico Press, 163–183.

FEDERER, C. A. (1979) A Soil-Plant-Atmosphere Model for Transpiration and Availability of Soil Water, *Water Resources Research*, **15**, (3), 555–562.

FEDERER, C. A. (1982) Transpirational Supply and Demand: Plant, Soil, and Atmospheric Effects Evaluated by Simulation, *Water Resources Research*, **18**, (2), 355–362.

GERALD, C. F. (1978) *Applied Numerical Analysis*, Addison-Wesley, 518 pp.

GRIFFITHS, J. F. (1972) General Introduction, in *Climates of Africa*, Volume **10**, World Survey of Climatology, Elsevier, 604 pp.

HILLEL, D. (1982) *Introduction to Soil Physics*, Academic Press, 365 pp.

HOUGHTON, J. T. (1977) *The Physics of Atmospheres*, Cambridge University Press, 203 pp.

IDSO, S. B., R. JACKSON, R. REGINATO, B. KIMBALL, B. and F. NAKAYAMA (1975) The Dependence of Bare Soil Albedo on Soil Water Content, *Journal of Applied Meteorology*, **14**, (2), 109–113.

JONES, H. G. (1983) *Plants and Microclimate*, Cambridge University Press, 323 pp.

KIMBALL, B. A.; R. D. JACKSON; R. J. REGINATO, F. S. NAKAYAMA and S. B. IDSO (1976) Comparison of Field-Measured and Calculated Soil-Heat Fluxes, *Soil Science Society of America Journal*, **40**, 18–25.

KNAPP, C. L., T. L. STOFFEL and S. D. WHITAKER (1980) *Insolation Data Manual*, Solar Energy Research Institute, SP-755-789, 281 pp.

LACIS, A. A. and J. E. HANSEN (1974) A Parameterization for the Absorption of Solar Radiation in the Earth's Atmosphere, *Journal of the Atmospheric Sciences*, **31**, (1), 118–133.

LAMB, H. H. (1972) *Climate: Present, Past and Future*, Vol. **1**, Methuen, 613 pp.

MILLER, D. H. (1977) *Water at the Surface of the Earth*, International Geophysics Series, **21**, Academic Press, 557 pp.

MILLY, P. C. D. and P. S. EAGLESON (1980) *The Coupled Transport of Water and Heat in a Vertical Soil Column under Atmospheric Excitation*, Report No. 258, Ralph Parsons Laboratory for Water Resources and Hydrodynamics, Department of Civil Engineering, MIT.

MILLY, P. C. D. and P. S. EAGLESON (1982) *Parameterization of Moisture and Heat Fluxes across the Land Surface for Use in Atmospheric General Circulation Models*, Report No. 279, Ralph Parsons Laboratory for Hydrology and Water Resource Systems, Department of Civil Engineering, MIT.

MUNN, R. E. (1966) *Descriptive Micrometeorology*, Academic Press, 245 pp.

NĚMEC, J. (1983) The Concept of Runoff in the Global Water Budget, in *Variations in the Global Water Budget*, edited by A. Street-Perrott, M. Beran and R. Ratcliffe, D. Reidel, 479–488.

OKE, T. R. (1978) *Boundary Layer Climates*, Methuen, 372 pp.

PALTRIDGE, G. W. and C. M. R. PLATT (1977) *Radiative Processes in Meteorology and Climatology*, Developments in Atmospheric Sciences, **5**, Elsevier, 318 pp.

PHILIP, J. R. (1957a) The Theory of Infiltration: 1. The Infiltration Equation and its Solution, *Soil Science*, **83**, 345–357.

PHILIP, J. R. (1957b) The Theory of Infiltration: 2. The Profile of Infinity, *Soil Science*, **83**, 435–448.

PHILIP, J. R. (1957c) The Theory of Infiltration: 3. Moisture Profiles and Relation to Experiment, *Soil Science*, **83**, 345–357.

PHILIP, J. R. (1975) Water Movement in Soil, in *Heat and Mass Transfer in the Biosphere, Part 1, Transfer Processes in the Plant Environment*, edited by D. A. de Vries and N. H. Afgan, Wiley, 29–47.

ROSS, J. (1975) Radiative Transfer in Plant Communities, in *Vegetation and the Atmosphere*, Vol. **1**, edited by J. L. Monteith, Academic Press.

SCHNEIDER, S. H. and R. E. DICKINSON (1974) Climate Modeling, *Reviews of Geophysics and Space Physics*, **12**, (3), 447–493.

SEGINER, I. (1974) Aerodynamic Roughness of Vegetated Surfaces, *Boundary-Layer Meteorology*, **5**, 383–393.

SELLERS, P. J. and J. G. LOCKWOOD (1981a) A Computer Simulation of the Effects of Differing Crop Types on the Water Balance of Small Catchments Over Long Time Periods, *Quarterly Journal of the Royal Meteorological Society*, **107**, 395–414.

SELLERS, P. J. and J. G. LOCKWOOD (1981b) A Numerical Simulation of the Effects of Changing Vegetation Type on Surface Hydroclimatology, *Climatic Change*, **3**, 121–136.

SELLERS, W. D. (1965) *Physical Climatology*, The University of Chicago Press, 272 pp.

SUTTON, O. G. (1953) *Micrometeorology*, McGraw Hill, 333 pp.

THOM, A. S. (1971) Momentum absorption by Vegetation, *Quarterly Journal of the Royal Meteorological Society*, **97**, 414–428.

THOM, A. S. (1972) Momentum, Mass and Heat Exchange of Vegetation, *Quarterly Journal of the Royal Meteorological Society*, **98**, 124–134.

UNITED NATIONS (1977) *Desertification: Its Causes and Consequences*, Pergamon Press, 448 pp.

VERSTRAETE, M. M. (1983) Another Look at the Concept of Desertification, in *Origin and Evolution of Deserts*, edited by S. G. Wells and D. R. Haragan, University of New Mexico Press, 213–228.

WARREN, A. and J. K. MAIZELS (1977) Ecological Change and Desertification, in *Desertification: Its Causes and Consequences*, edited by the United Nations, Pergamon Press, 169–260.

WELLS, S. G. and D. R. HARAGAN (Editors) (1983) *Origin and Evolution of Deserts*, University of New Mexico Press, 228 pp.